Radiative Transfer

Skript zu Vorlesung S3137 **Strahlungstransport**,
Universität Bern, Sommersemester 2005,

Christian Mätzler

Institut für Angewandte Physik,
Sidlerstrasse 5, 3012 Bern
Schweiz

Email: matzler@iap.unibe.ch
http://www.iapmw.unibe.ch/

These lecture notes on radiative transfer, starting with an overview on scattering and absorption of electromagnetic waves, are based on lectures given at the Institute of Applied Physics, University of Bern in 2000 and 2005. Accompanying are computer programs in the numeric computation and visualisation software MATLAB. The codes and the manuscript are available from the internet address given above.

Contents

Part 1:
Scattering and Absorption of Electromagnetic Waves (Chapters 1 to 6)

Part 2:
Radiative Transfer (Chapters 7 to 13)

Historical Overview....3

1 Introduction to Scattering and Absorption....7
1.1 Electromagnetic waves in matter....7
1.2 Effective medium and mixing formulas....8

2 Scattering and Absorption by Single Particles....13
2.1 Cross sections and scattering amplitude....13
2.2 Forward-Scattering Theorem....15
2.3 Efficiencies....15
2.4 Scattering Matrix....15
2.5 Polarisation....17

3. Approximate Scattering and Absorption Models....18
3.1 Rayleigh scattering and absorption by spheres....18
3.2 Rayleigh scattering and absorption by ellipsoids....20
3.3 Born Approximation....21
3.4 Geometrical Optics....25

4 Lorenz-Mie Scattering and Absorption by Spheres....31
4.1 The scattered field....31
4.2 Mie Coefficients....31
4.3 Mie Efficiencies....34
4.4 The internal field....34
4.5 Computation of Q_a, based on the internal fields....35
4.6 Examples and tests....37
4.7 Extinction Paradox....40
4.8 Lorenz-Mie scattering without diffraction....41
4.9 Comparison of Mie results with approximations....46

5 On Scattering and Absorption by Non-Spherical Particles....51

6 Scattering and Absorption by a Cloud of Particles....52
6.1 The particle cloud....52
6.2 Size distributions....52
6.3 Scattering and absorption by clouds....53

7 Introduction to Radiative Transfer....54
7.1 Radiance and related quantities....54
7.2 Radiation in thermal equilibrium....56
7.3 Radiation in Local Thermodynamic Equilibrium: Kirchhoff's Law....57

8 The Radiative Transfer Equation....59
8.1 Radiative transfer without absorption and scattering....59
8.2 Absorbing medium....60
8.3 Including absorption, emission and scattering....61
8.4 Formal solution: integral form of the RTE....62
8.5 The Flux Equation....63
8.6 Plane-parallel medium....64

9 Solutions Without Scattering 65
9.1 Note on spectroscopy 65
9.2 Layers at constant temperature 65
9.3 Effective mean temperature 66
9.4 Linear temperature profile in an exponentially decreasing atmosphere 66

10 Standard Problems for Scattering 73
10.1 Scattering at a half-space 73
10.2 Scattering in and transmission through a layer 75
10.3 Distinction between direct and scattered radiation 76
10.4 Axial symmetry 76

11 Single Scattering 78
11.1 The radiative transfer equation and its solution 78
11.2 Scattering and transmission functions 79
11.3 Reflectivity and transmissivity 79
11.4 Successive orders of scattering 83

12 Exact Multiple Scattering 84
12.1 Exact solution of Standard Problem 1 for isotropic scattering 84
12.2 Exact solution of Standard Problem 2 for isotropic scattering 87
12.3 Discussion 89
12.4 Appendix: Derivation of Equation (12.2) 89

13 Approximate Solutions for Multiple Scattering 91
13.1 A simple snowpack/cloud reflectance and transmittance model from microwaves to ultraviolet: The ice-lamella pack 91
13.2 Comparison of lamella pack with spherical scatterers 99

Literature 100

Historical Overview

Radiative transfer is a valuable tool for **astronomy** and **astrophysics**, for **remote sensing** of the earth surface atmosphere and ocean, but also for the assessment of the **light and heat** transport in the natural (climatology, hydrology, meteorology), human (e.g. architecture, medicine) and technical environment. When looking at the history we realise that radiometry and radiative transfer are rooted in the oldest human disciplines. Radiative transfer describes the **emission, propagation, scattering and absorption of radiation**. Since almost everything that we know about the universe has been brought to men by radiation, radiative transfer is as old as vision.

The basis of today's knowledge on emission and absorption of **thermal** (or quasi-thermal), electromagnetic radiation was laid by Josef von **Fraunhofer** (1787-1826), Robert **Bunsen** (1811-1899), Gustav Robert **Kirchhoff** (1824-1887), and others at and before the time when James Clark **Maxwell** (1831-1879) stated that magnetism, electricity, and light are different manifestations of the same fundamental laws. Application of the first and second laws of thermodynamics let Kirchhoff formulate his law of radiation in 1860, stating in today's language, that under local thermodynamic equilibrium the emissivity of a given object is equal to its absorptivity.

James Clark Maxwell

Josef von Frauenhofer

Gustav Kirchhoff (left) and Robert Bunsen (right)

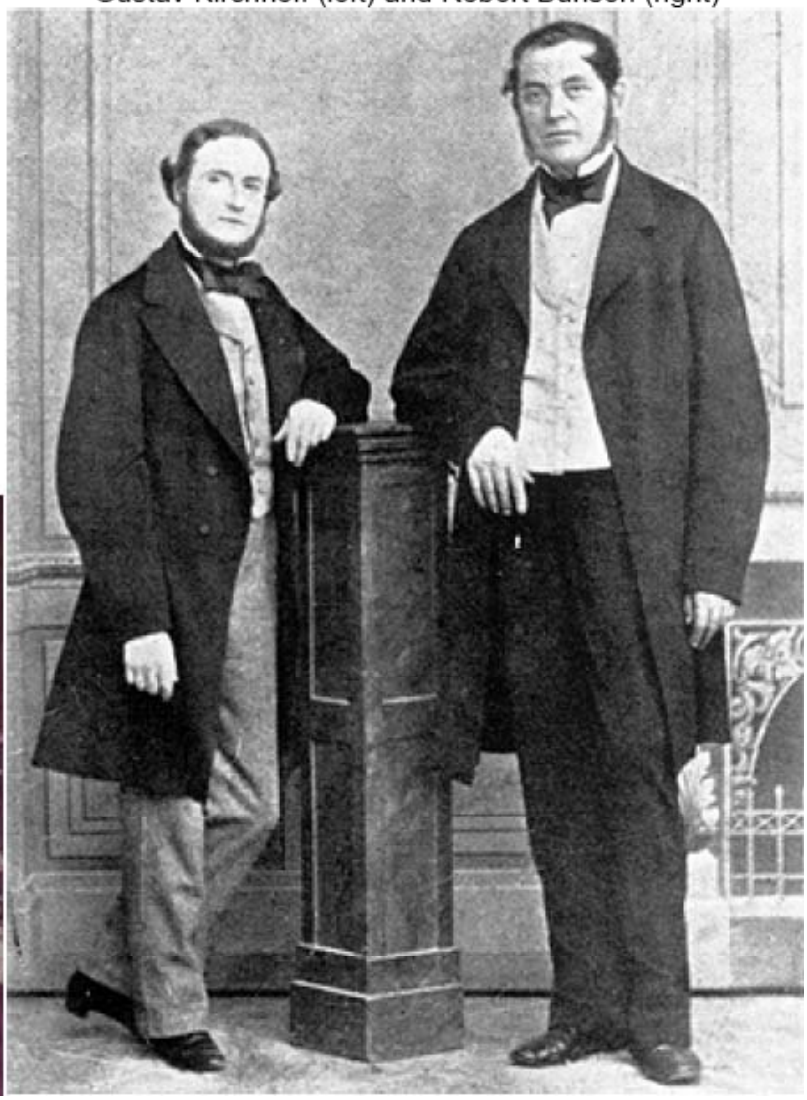

Even before the **Planck** function was found in 1900 (Max Planck, 1858-1947), radiative transfer and spectroscopy enabled the identification of atoms in the solar atmosphere. Experimental rules of Bunsen revealed properties of low and high optical thickness:

Rule 1 : A hot and opaque solid, liquid or highly compressed gas emits a continuous spectrum.
Rule 2 : A hot, transparent gas produces an emission spectrum with bright lines. The number and colours of these lines depend on which elements are present in the gas, constituting signatures of these elements.
Rule 3 : If a continuous spectrum passes through a transparent gas at a lower temperature, the gas generates dark absorption lines, whose number and colours depend on the elements in the gas.

What was missing at that time was the understanding of the spectral line positions, strengths and widths. The driving questions led to the fast and successful development of **quantum theory** in the early 20th Century.

Hendrik Christoffel van de Hulst

Subrahmanyan Chandrasekhar

The term, **light rays**, originated from the observation that light propagates radially from the source along straight lines. This applies to **homogeneous media**. More complex is the situation if the medium is **inhomogeneous** (or heterogeneous). Then radiation suffers **refraction, reflection, diffraction and scattering**; the phenomena were already investigated by Willebrord **Snell** (1591-1626) and Augustin **Fresnel** (1788-1827). The Fresnel equations, describing the reflection of polarised radiation at a plane, are a basic law to describe surface emissivity in a simple situation. Scattering by reflecting spheres was described by Alfred **Clebsch** in 1863. Light scattering by refractive spheres was described by Ludvig V. **Lorenz** in 1890. Better known is the work on the same topic carried out by Gustav **Mie** (1867-1957) in 1908. Microwave radiometer observations of precipitating clouds can be explained by Lorenz-Mie scattering and absorption. Scattering of radiation by particles, which are small with respect to the wavelength, is named after Baron Rayleigh, John William Strutt (1842-1919). **Rayleigh** scattering of radar waves by raindrops has become a standard in radar meteorology to relate rain rate with radar intensity. Rayleigh scattering has also been used in microwave radiometry to describe the emission of clouds and snow.
Multiple scattering of radiation in a cloudy atmosphere was first described by Sir Arthur **Schuster** (1851-1934) in 1905. Technical applications in the paper and paint industry followed (Kubelka and Munk, 1931). However it was mainly in the field of astrophysics that radiative transfer methods made substantial progress. Two important contributors were

Subrahmanyan **Chandrasekhar** (1910-1995) and Hendrik Christoffel **van de Hulst** (1918-2000), both working for some time at the Yerkes Observatory of the University of Chicago. They developed mathematical methods in the 1940's to describe radiative transfer in stellar and planetary atmospheres under the assumption that the refractive index of the medium is equal to one. Although not necessary, this assumption was used in the majority of works on this topic. Chandrasekhar's collected papers on radiative transfer were published in book form in 1950, and van de Hulst's work led to a book dealing with scattering by small particles in 1957 and a second one on multiple scattering in 1980. Approximate solutions of the radiative transfer equation for multiple scattering are named after Sir Arthur **Eddington** (1884-1944), see Joseph et al. (1976), Meador and Weaver (1980) and Thomas and Stamnes (1999).

More general treatments were required when it was realised that strong refractive effects occur for radiation in conductive media, especially at frequencies near the plasma frequency. A formulation of radiative transfer, including the inhomogeneity and anisotropy of the propagating medium, was presented by George **Bekefi** (1925-1995) in 1960 in his textbook on radiation processes in plasmas, introducing the *ray-refractive index*. Refractive treatments were also applied to radiative transfer in natural waters (Mobley, 1994). They appeared to be so relevant that they were formulated in the ***fundamental theorem of radiometry*** (Wyatt, 1978). The theorem was already formulated by David **Hilbert** (1862-1943) in 1912, and even Kirchhoff was aware of it because it follows from Snell's law.

Invisible radiation at **infrared** wavelengths was known at the time of Kirchhoff. This radiation was called **dark rays**. **Microwaves** at still longer wavelengths have been known since the validation of Maxwell's electromagnetic wave theory by Heinrich Hertz (1857-1894) in 1888. The pioneer in the development of **microwave radiometry** was Robert Henry **Dicke** (1916-1997), a brilliant physicist in theoretical and in experimental work. The radiometer type named after him was a great invention in 1944 to measure the low power levels associated with thermal microwave radiation (Dicke, 1946). A first radiometer operated at the MIT in Massachusetts at a wavelength of 1.25 cm; this is close to the 22 GHz water-vapour line. From theoretical work by John H. **Van Vleck** (1899-1980) in 1942, Dicke realised that the enhanced radiation was due to emission by **water vapour**. He and others went to Florida with three radiometers (at wavelengths of 1.0, 1.25 and 1.5 cm) to measure the rather weak atmospheric absorption in this frequency range for the first time (Dicke et al. 1946). In this work they introduced the concepts of **antenna temperature** T_A, of the **mean atmospheric temperature** T_m relevant for the observed radiation, and the **tipping-curve** method. Dicke also measured the surface temperature of the moon and of the sun. Later he played a key role in the discovery of the **cosmic background** radiation.

Before microwave radiometry was exploited for the investigation of the earth, emphasis was put on extra-terrestrial objects, leading to the evolution of **radio astronomy** (Kraus, 1966). But even radio astronomers had to deal with the terrestrial atmosphere to identify the nature of their signals. Therefore they paved the way in spectroscopy and radiative transfer.

Special interest in terrestrial applications of microwaves was based on the capability to **penetrate clouds and smoke**. Shortly before, during and after World War II, the priority in the advancements of microwave methods was given to **radar**. This active technique is excellent for locating and ranging remote objects, but it is limited in radiometric accuracy. In contrast to radars, radiometers are passive devices, meaning that they receive radiation, only. Their virtue is high radiometric accuracy, but the ranging capability of radiometers is either inexistent or indirect, for instance by using stereo techniques or knowledge on spectral properties of the medium to be sensed. It is evident that the properties of radars and radiometers are complementary.

The interaction of electromagnetic waves with **matter** is mainly described by the **dielectric**, **magnetic and geometric** properties. A classic textbook on this topic is "Dielectrics and Waves" by von Hippel (1954) who introduced and compared different approaches from **microscopic and macroscopic** views, from the physics and electrical engineering standpoints, using historical, theoretical and experimental aspects. Of special importance are the dielectric properties of **water** and of aqueous solutions with the concept of **relaxation** phenomena. A leading scientist was **Peter Debye** (1884–1966) who wrote a treatise on

polar molecules (Debye, 1929). He received the Nobel Prize in 1936 for achievements in molecular studies.
Another topic is the description of **heterogeneous** media in terms of an effective dielectric constant and of other **effective-medium** properties (Sihvola, 1999). The topic is important because many natural media are inherently heterogeneous, but, for sufficiently fine structure, may be treated as if they were homogeneous.
Spectroscopy and the understanding of spectral lines evolved from **quantum theory** (see e.g. **Microwave Spectroscopy** of molecular gases by Townes and Schawlow, 1955).
A treatise on **microwave remote sensing**, including important aspects of radiative transfer was written by Ulaby, Moore and Fung (1982, 1982, 1986). More specialised books were dedicated to theoretical aspects (e.g. of microwave remote sensing: Tsang et al. 1985) or to special applications, like microwave radiometry of the atmosphere (Janssen, 1993).
Modern work on radiative transfer and scattering includes **numerical methods**, see e.g. Tsang et al. (2000) and the lecture Notes of Warnick (2005).

1 Introduction to Scattering and Absorption

1.1 Electromagnetic waves in matter

Although homogeneity is not exactly met in a world of atoms and molecules or in granular media, in a physical sense the homogeneity requirement only means that any structural feature of the medium must be much finer than the wavelength λ of a sensing wave. The microscopic behaviour is reflected by bulk properties, and they are contained in the constitutive relations between the electromagnetic fields. These relations apply to linear media and are shown below. For most situations of interest, the media behave linearly. The fields, i.e. the electric field **E**, the displacement field **D**, the magnetic field **H**, and the magnetic induction field **B**, are governed by Maxwell's Equations. For homogeneous and isotropic media (away from sources), and for **time-harmonic** fields with time factor $\exp(-i\omega t)$, where t is time and ω is the **angular frequency**, **Maxwell's Equations** can be written as

$$\nabla \times \mathbf{H} = \frac{\partial \mathbf{D}}{\partial t} + \mathbf{j} = -i\omega\mathbf{D}; \quad \text{where} \quad \nabla \cdot \mathbf{D} = \rho_e = 0 \tag{1.1}$$

$$\nabla \times \mathbf{E} = -\frac{\partial \mathbf{B}}{\partial t} = i\omega\mathbf{B}; \quad \text{where} \quad \nabla \cdot \mathbf{B} = 0 \tag{1.2}$$

with the **constitutive relations**

$$\mathbf{D} = \varepsilon\varepsilon_0\mathbf{E} \quad \text{and} \quad \mathbf{B} = \mu\mu_0\mathbf{H} \tag{1.3}$$

where ∇ is the **nabla operator**, ε is the (relative) **dielectric constant** (also called relative electric permittivity), ε_0=8.854·10^{-12}As/V/m the **vacuum permittivity**, μ the **relative magnetic permeability** and μ_0=4π·10^{-7}Vs/A/m the **vacuum permeability**. Furthermore, in **chiral** or **bi-isotropic** media, also the electric and magnetic fields are linearly related (Sihvola, 1999). For simplicity, let us assume isotropic media obeying (1.3). Eliminating the **D**, **B**, **H** fields from (1.1) to (1.3) leads to the vector-wave equation in the unbounded homogenous medium for **E**:

$$c^2\Delta\mathbf{E} = -\omega^2\mathbf{E} \tag{1.4}$$

Here Δ is the **Laplace operator**, and c is the phase velocity in the medium, determined by

$$c = \frac{c_0}{n}\ ; \quad c_0 = \frac{1}{\sqrt{\varepsilon_0\mu_0}} \tag{1.5}$$

where c_0 is the speed of light in vacuum. The refractive index n follows from

$$n = \sqrt{\varepsilon\mu} \tag{1.6}$$

or simply $n = \sqrt{\varepsilon}$, for the frequent situation of non-magnetic materials (μ=1). For a plane wave $\mathbf{E}\propto\exp(ikx-i\omega t)$ propagating along path x with wave number k, the Laplace -operated electric field is $\Delta\mathbf{E} = \frac{\partial^2\mathbf{E}}{\partial x^2} = -k^2\mathbf{E}$. Insertion in the wave equation leads to the dispersion relation

$$k = \pm n\frac{\omega}{c_0} \tag{1.7}$$

Since the x direction is arbitrary, the dispersion relation holds for all directions, and it is independent of polarisation. In a medium with losses, the quantities are complex ($k = k' + ik''$, $n = n' + in''$, $\varepsilon = \varepsilon' + i\varepsilon''$), and they depend on **frequency** $\nu = \omega/2\pi$. The current density **j** excited in a conducting medium by the electric field **E** is given by Ohm's Law $\mathbf{j}=\sigma\mathbf{E}$ where σ is the conductivity**.** In our notation **j** is expressed as a displacement current, $-i\omega\mathbf{D}$, in Equations (1.1-3), with the complex dielectric constant $\varepsilon = \varepsilon' + i\varepsilon''$ whose imaginary part ε'' is given by

$$\varepsilon'' = \frac{\sigma}{\varepsilon_0\omega} \tag{1.8}$$

Therefore conductivity and imaginary permittivity are different representations of the same effect. In our **convention**, the imaginary parts of *n*, ε and μ are positive for lossy media (negative values of the opposite convention often used by electrical engineers are obtained by the transformation to $j=-i$ for the imaginary unit). The losses are responsible for wave attenuation, and if scattering is absent, the attenuation is due to absorption. Since the wave intensity is proportional to $|\mathbf{E}|^2$, its spatial variation is an exponential decay $\propto \exp(-2k''x)$, and *k*" is the imaginary part of *k*. The damping coefficient 2*k*" is the **absorption coefficient** γ_a, and by (1.7), it is related to the imaginary refractive index *n*".

$$\gamma_a = 2k'' = \frac{2n''\omega}{c_0} \tag{1.9}$$

Finally, Equation (1.6) gives the relationship with the dielectric constant. For μ=1

$$\gamma_a = \frac{4\pi}{\lambda_0}\sqrt{\frac{\varepsilon'}{2}\left(\sqrt{1+\frac{\varepsilon''^2}{\varepsilon'^2}}-1\right)} \cong \frac{\varepsilon''\omega}{\sqrt{\varepsilon'}c_0} = \frac{2\pi\varepsilon''}{\sqrt{\varepsilon'}\lambda_0} \tag{1.10}$$

where λ_0 is the vacuum wavelength, and the approximate expression is valid for small dielectric loss (ε"<<ε').

The medium descriptors *n*, ε and μ depend on **frequency** (or wavelength), and on the **physical state** and **chemical composition**, see von Hippel (1954) and the **lecture** on **microwave physics**, especially the section on the **interaction with matter** by N. Kämpfer, http://www.iapmw.unibe.ch/teaching/vorlesungen/mikrowellenphysik/.

1.2 Effective medium and mixing formulas

Particles that are small with respect to a sensing wavelength are invisible, or they may appear as point-like scatterers without any structure. Effective-medium theories use this property of radiation to determine effective mean values, $\varepsilon(\mathbf{r})$ and $\mu(\mathbf{r})$, for **heterogeneous** or **granular** media with structures much smaller than the wavelength. The effective-medium properties are expressed by **mixing formulas** (Sihvola, 1999). The topic is important because the theory allows significant simplifications without losing the physical basis. Here we will discuss one of the most important mixing rules:

The **effective** dielectric constant ε of a heterogeneous medium is defined on the basis of fields (**D** and **E**) averaged over a volume sufficiently large to smear out the heterogeneity, but still small with respect to the wavelength. The averaging is expressed by brackets < >. Let us assume a **host medium** of dielectric constant ε_1 with **embedded particles** of dielectric constant ε_2 and **volume fraction** f. Then the following equations can be set up:

$$\begin{aligned} &< D >= \varepsilon\varepsilon_0 < E > \\ &< D >= (1-f) < D_1 > + f < D_2 > \\ &< E >= (1-f) < E_1 > + f < E_2 > \\ &< D_i >= \varepsilon_i\varepsilon_0 < E_i >; \quad i = 1,2 \end{aligned} \tag{1.11}$$

In addition we need a relationship between the electrical field strengths in the particle and in the host medium. Let us assume a proportionality:

$$< E_2 >= K < E_1 >; \tag{1.12}$$

The set of equations leads to an expression for the effective ε:

$$\varepsilon = \frac{(1-f)\varepsilon_1 + f\varepsilon_2 K}{1-f+fK} \tag{1.13}$$

By inserting the electrostatic *K* factor for spheres (see Section 3):

$$K = \frac{3\varepsilon_1}{\varepsilon_2 + 2\varepsilon_1} \tag{1.14}$$

we get the **Maxwell-Garnett** (1904) mixing formula.

$$\varepsilon = \varepsilon_1 \left(1 + 3f \frac{\varepsilon_2 - \varepsilon_1}{\varepsilon_2 + 2\varepsilon_1 - f(\varepsilon_2 - \varepsilon_1)} \right) \tag{1.15}$$

Equation (1.13) can be regarded as a generalised form of (1.15). In general *K* has to be determined either experimentally or theoretically.
At this point let us consider two extreme situations. This will lead to **bounds** for the mixing formula: Let the particles be **plane-parallel** slabs (Figure 1.1).

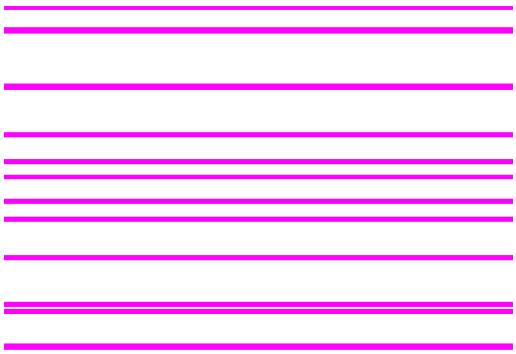

Figure 1.1: Plane-parallel slabs.

In **Case 1**, the slabs are **parallel** to the **E** field, and in **Case 2**, they are **perpendicular**. Let us recall from **electrodynamics**, that the following **boundary conditions** apply to the **E** and **D** fields at **interfaces** between different media: The parallel components of **E** and the perpendicular components of **D** are continuous. Furthermore, in each component, the fields are homogeneous.

Case 1: D and **E** are parallel to the boundaries. Thus $\mathbf{E}_2=\mathbf{E}_1$, and thus K=1. This means that

$$\varepsilon = (1-f)\varepsilon_1 + f\varepsilon_2 \tag{1.16}$$

Case 2: D and **E** are perpendicular to the boundaries. Thus $\mathbf{D}_2=\mathbf{D}_1$, and thus $K=\varepsilon_1/\varepsilon_2$. Then

$$\varepsilon = \frac{\varepsilon_1\varepsilon_2}{\varepsilon_2 - f(\varepsilon_2 - \varepsilon_1)} \quad \text{or} \quad \frac{1}{\varepsilon} = \frac{1-f}{\varepsilon_1} + \frac{f}{\varepsilon_2} \tag{1.17}$$

Whereas Case 1 corresponds to 2 capacitors connected in parallel, Case 2 corresponds to 2 capacitors connected in series. Let us consider two examples: (a) ε_1=1 and ε_2=2, and (b) ε_1=1 and ε_2=10. The mixing formulas (1.15) - (1.17) are plotted in Figures 1.2a and b. The figures show that in Case 2, ε is smaller than in Case 1, and Maxwell-Garnett formula is in between. The differences increase with increasing contrast $\varepsilon_2/\varepsilon_1$. The two formulas (1.16) and (1.17) are extreme limits.

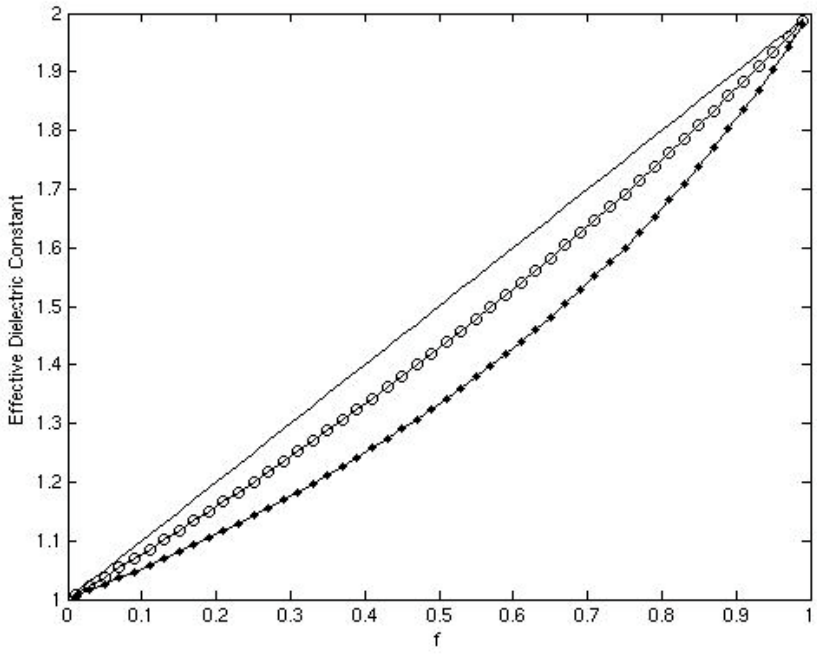

Figure 1.2a:
Effective dielectric constant versus volume fraction *f* for a medium with ε_1=1, ε_2=2, according to Equations (1.15), circles, (1.16), solid line, and (1.17) pointed line.

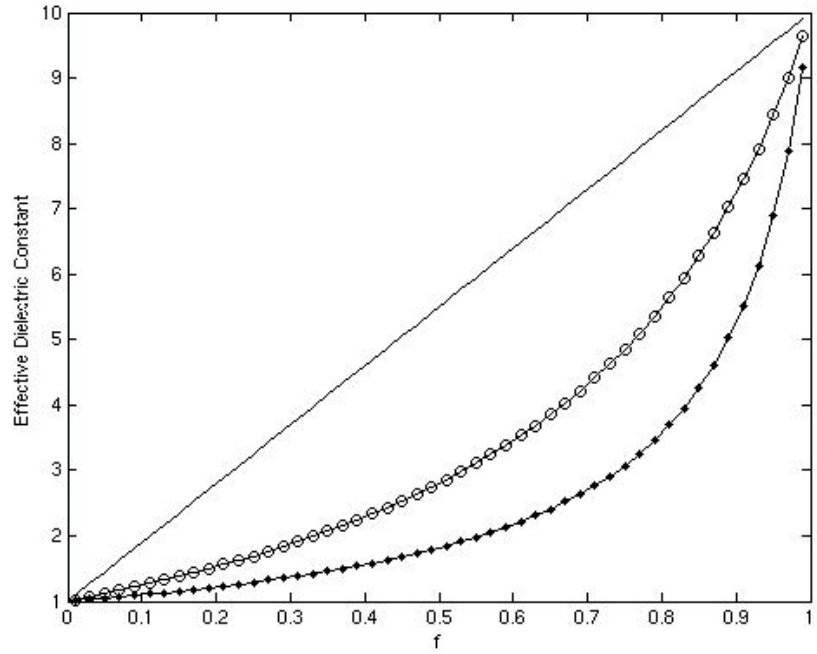

Figure 1.2b:
Same as Fig. 1.2.a, but with ε_1=1, ε_2=10.

To compare the mixing formulas with **experimental data** we consider dry snow as a mixture of ice particles (ε_2=3.185) in air (ε_1=1) in Figure 1.3.

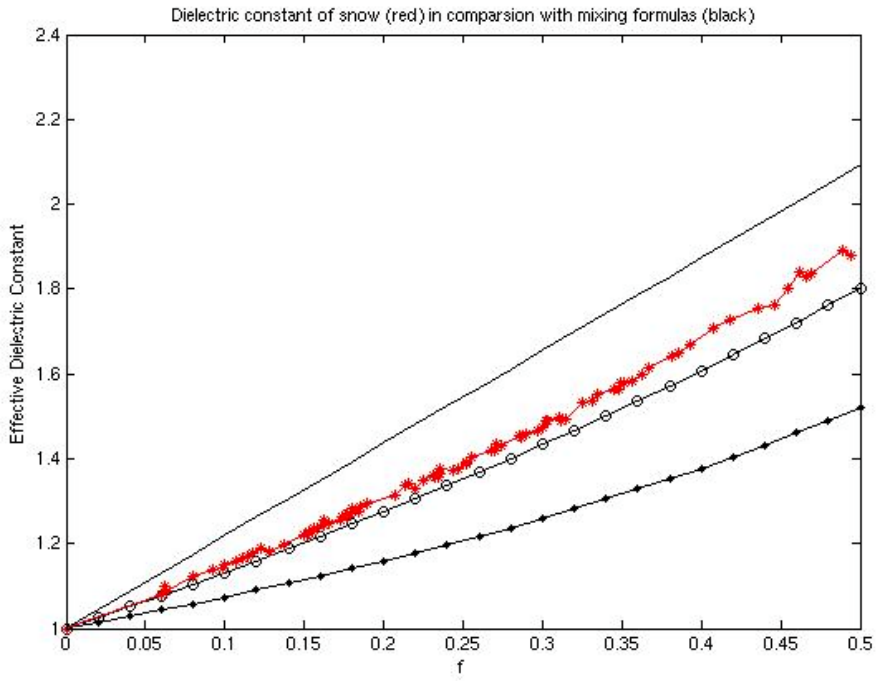

Figure 1.3: Dielectric constant of **dry snow** (*) at 1 GHz versus ice-volume fraction in comparison with Equations (1.15) (o), (1.16) (solid line) and (1.17) (pointed line).

Exercise

Compute and discuss the absorption coefficient versus frequency in logarithmic frequency scale from ν=1 to 1000 GHz for an effective medium consisting of water (for *f*=0.01 and *f*=0.9) embedded in ice for Equations (1.15) to (1.17), assuming a real dielectric constant of **ice** ($\varepsilon_1 = 3.17$) and a **Debye relaxation spectrum** for the complex dielectric constant (ε_2) of **water**, according to

$$\varepsilon_2 = \varepsilon_\infty + \frac{\varepsilon_s - \varepsilon_\infty}{1 - i\nu/\nu_0} \tag{1.18}$$

where $\nu_0 = 8.8$ GHz is the relaxation frequency at 0C, and the static and infinite-frequency dielectric constants of water at 0C are, respectively, $\varepsilon_s = 88$ and $\varepsilon_\infty = 4.9$.

Solution:

a) Generalisation of the three situations according to Wiener (1910):

$$K = \frac{\varepsilon_1(1+u)}{\varepsilon_2 + \varepsilon_1 u} \tag{1.19}$$

where u is a free parameter, called **Formzahl**. Case 1: u=∞, Case 2: u=0, Case MG: u=2. The tree situations can be described by the **Wiener Mixing Formula**

$$\frac{\varepsilon - \varepsilon_1}{\varepsilon + u\varepsilon_1} = f\frac{\varepsilon_2 - \varepsilon_1}{\varepsilon_2 + u\varepsilon_1} \tag{1.20}$$

which is identical with (1.13) for *K* given by (1.19).

b) The effective dielectric constant ε also follows a Debye Relaxation spectrum:

$$\varepsilon = \varepsilon_{m\infty} + \frac{\varepsilon_{ms} - \varepsilon_{m\infty}}{1 - i\nu/\nu_{m0}} \tag{1.21}$$

where the Debye parameters are given by (1.22):

$$\varepsilon_{ms} = \varepsilon_1 \frac{\varepsilon_s + u\varepsilon_1 + uf(\varepsilon_s - \varepsilon_1)}{\varepsilon_s + u\varepsilon_1 - f(\varepsilon_s - \varepsilon_1)};\ \varepsilon_{m\infty} = \varepsilon_1 \frac{\varepsilon_\infty + u\varepsilon_1 + uf(\varepsilon_\infty - \varepsilon_1)}{\varepsilon_\infty + u\varepsilon_1 - f(\varepsilon_\infty - \varepsilon_1)};\ \nu_{m0} = \nu_0 \frac{\varepsilon_s(1-f) + \varepsilon_1(u-f)}{\varepsilon_\infty(1-f) + \varepsilon_1(u-f)} \tag{1.22}$$

Comment: This result is a behaviour of bilinear transformations in the complex plane where circles transform to circles again (Cole Diagrams).

c) Computing and plotting the absorption coefficient γ_a using MATLAB function "mixspectra":

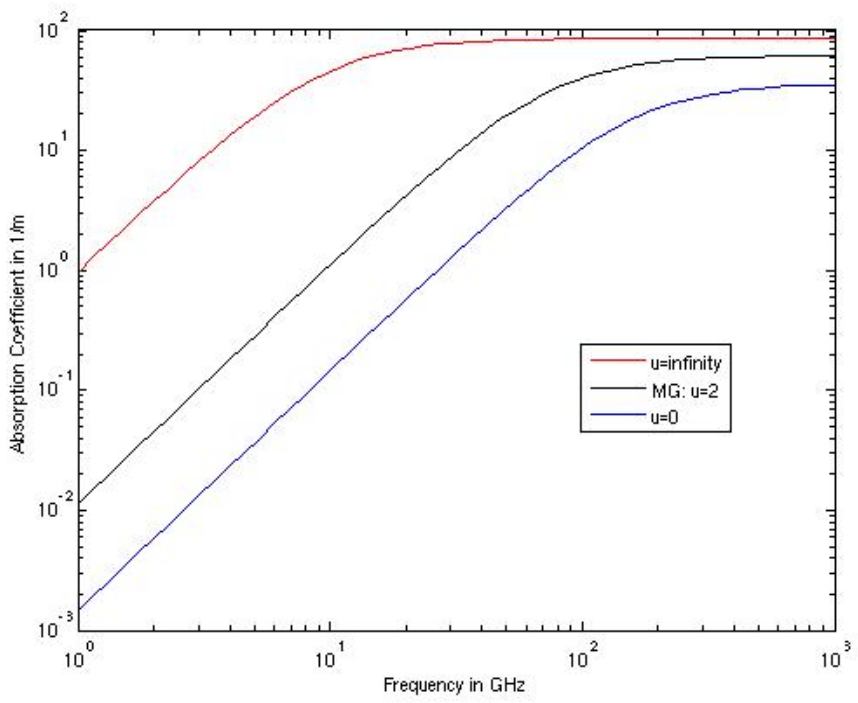

Figure Ex1a:
Absorption coefficient versus frequency for a medium consisting of water particles with volume fraction f=0.01 in a host of ice for three different shapes using the Formzahl *u* of Wiener.

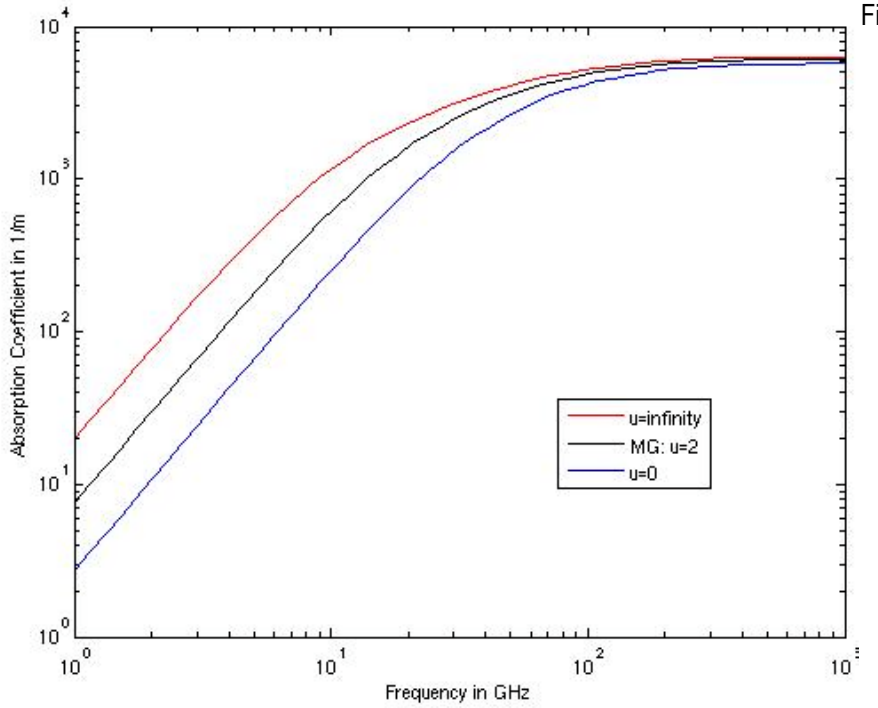

Figure Ex1b: Same as Ex1a, but for f=0.9.

Note that the shape effects are more accentuated at low frequencies. The transition from the frequency-square to a frequency-independent behaviour of the absorption coefficient occurs at the relaxation frequency ν_{m0} of the mixture.

2 Scattering and Absorption by Single Particles

This section follows Chapter 2 of Ishimaru (1978). Scattering is a result of a local disturbance of the propagating incident wave. In vacuum, such a disturbance (scatterer) can be an **atom**, a **molecule**, or an **extended particle** consisting of a dielectric or magnetic material. Here we will assume that the scatterer is a dielectric particle described by a spatially variable dielectric constant $\varepsilon(\mathbf{r})=\varepsilon'+i\varepsilon''$. Similar scattering and absorption properties are found for magnetic scatterers with a relative magnetic permeability $\mu(\mathbf{r})=\mu'+i\mu''$. The type of scattering to be considered is elastic scattering, a linear process that keeps the angular frequency ω constant (apart from possible Doppler effects for moving objects).

2.1 Cross sections and scattering amplitude

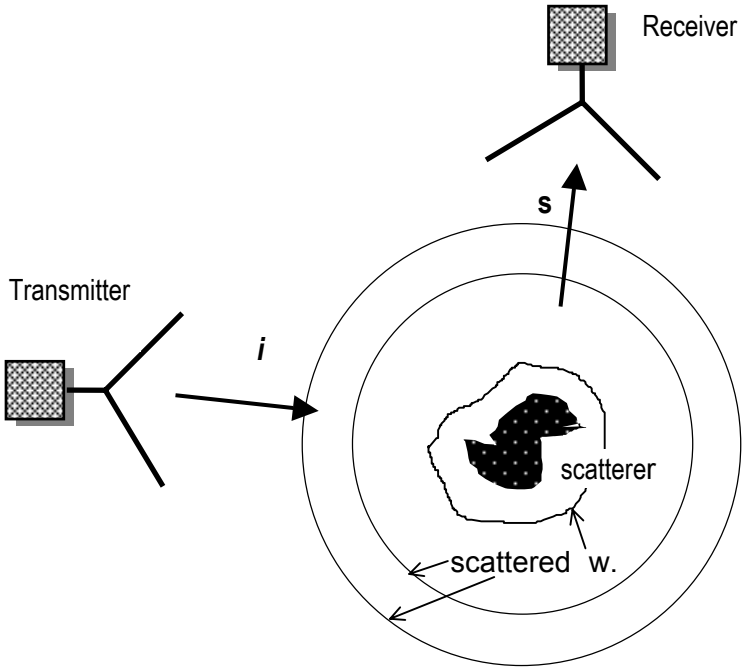

Figure 2.1: Illustration of scattering experiments.

Here the scatterer is a cloud

A scattering particle is illuminated by radiation from an incident plane electromagnetic wave whose electric field at position **r** and time *t* is the real part of the complex phasor

$$\mathbf{E}_i = \mathbf{E}_{i0}\exp(\mathrm{i}\mathbf{k}\cdot\mathbf{r}\text{-}\mathrm{i}\omega t).$$

Here ω is the **angular frequency**, and $k = \omega/c = 2\pi/\lambda$ is the **wave number** where λ is the **wavelength**, c is the speed of light, and **k**=*k***i** is the **wave vector** of the **i**ncident wave.
Part of the radiation is absorbed by the particle, another part is scattered in various directions. At a sufficiently large distance *R* from the centre of the scatterer, the scattered field $\mathbf{E}_s$ at position $\mathbf{r} = \mathbf{s}R$ is a spherical wave:

$$\mathbf{E}_s(\mathbf{r}) = \mathbf{f}(\mathbf{s},\mathbf{i})\left|\mathbf{E}_i\right|\frac{\exp(ikR - i\omega t)}{R} \tag{2.1}$$

Here the vector $\mathbf{f}(\mathbf{s},\mathbf{i})$ is called **scattering amplitude**, **i** and **s** are unit vectors in the directions of the incident and scattered wave, respectively. The scattering amplitude describes the directional dependence of the scattering process (sometimes the amplitude of the incident wave is set to $\left|\mathbf{E}_i\right| = 1$ which means that the electric field is normalised). The dimension of **f** is length (m).
Ishimaru (1978, p.10-17) developed an electrodynamics expression for **f** for a dielectric scatterer with volume V_s in vacuum:

$$\mathbf{f}(\mathbf{s},\mathbf{i}) = \frac{k^2}{4\pi\left|\mathbf{E}_i\right|}\int_{V_s}\left\{-\mathbf{s}\times\left[\mathbf{s}\times\mathbf{E}(\mathbf{r}')\right]\right\}\cdot\left\{\varepsilon(\mathbf{r}')-1\right\}\exp(-ik\mathbf{r}'\cdot\mathbf{s})dV' \tag{2.2}$$

The exponential term in the integral is a far-field phase correction of the spherical wave in (2.1) for points excited away from the scattering centre. The integral requires knowledge on the electric field $\mathbf{E}(\mathbf{r}')$ inside the scatterer. A problem is to find this internal field. For the moment we assume this problem to be solved.
The **incident** and **scattered intensities** I_i and I_s (power per unit area) are proportional to the squared absolute value of the respective electric fields, namely:

$$I_{i,s} = \frac{\left|\mathbf{E}_{i,s}\right|^2}{2Z_0} \qquad \text{where } Z_0 = \sqrt{\frac{\mu_0}{\varepsilon_0}} = 277\Omega \qquad \text{vacuum impedance} \tag{2.3}$$

where μ_0 and ε_0 are the vacuum permeability and permittivity, respectively. Thus we get

$$I_s = I_i\frac{\left|\mathbf{f}\right|^2}{R^2} \tag{2.4}$$

The nominator $\left|\mathbf{f}\right|^2 = \sigma_d$ (dimension of an area) is called the **differential scattering cross section** σ_d. Here, we will use the **bistatic scattering cross section** σ_{bi}, defined by

$$\sigma_{bi} = 4\pi\sigma_d = 4\pi\left|\mathbf{f}(\mathbf{s},\mathbf{i})\right|^2 \tag{2.5}$$

The total-scattered power P_s is the integral of I_s over a closed surface *A* around the scatterer. Let us choose a spherical surface *A* of radius *R*; then the integral becomes

$$P_s = \int_A I_s dA = \int_{4\pi} I_s R^2 d\Omega = I_i\int_{4\pi}\sigma_d d\Omega = I_i\sigma_s \tag{2.6}$$

The last quantity σ_s is the **scattering cross section** which can also be expressed by

$$\sigma_s = \frac{P_s}{I_i} = \frac{1}{4\pi}\int_{4\pi}\sigma_{bi}d\Omega \tag{2.7}$$

In this form σ_s appears as the **angular average** of σ_{bi}. In analogy to σ_s the **absorption cross section** σ_a is the ratio of the power P_a absorbed by the particle to the incident intensity:

$$\sigma_a = \frac{P_a}{I_i} \tag{2.8}$$

A formal expression for P_a, again requiring the internal **E** field, was given by Ishimaru (1978)

$$P_a = 0.5\varepsilon_0\omega \int_V \varepsilon''(\mathbf{r}')\left|\mathbf{E}(\mathbf{r}')\right|^2 dV' \tag{2.9}$$

This power is just the Ohmic loss due to the electrical current density $\mathbf{j}=\sigma\mathbf{E}$ excited in the particle. Inserting (2.9) and (2.3) in (2.8) gives

$$\sigma_a = \frac{\omega}{c}\int_V \varepsilon''(\mathbf{r}')\left|K(\mathbf{r}')\right|^2 dV' \qquad \text{where} \left|K(\mathbf{r}')\right|^2 = \left|\frac{\mathbf{E}(\mathbf{r}')}{\mathbf{E}_i}\right|^2 \tag{2.10}$$

The total cross section, also called **extinction cross section**, is the sum

$$\sigma_e = \sigma_s + \sigma_a \tag{2.11}$$

As we will see below there exists another expression that allows to determine the extinction cross section. For completeness we also define the radar cross section (backscatter) by

$$\sigma_b = 4\pi\left|\mathbf{f}(-\mathbf{i},\mathbf{i})\right|^2 \tag{2.12}$$

2.2 Forward-Scattering Theorem

See also Ishimaru (1978, p. 14-15), van de Hulst (1957, p. 30-31).
The extinction cross section represents the total power loss from the incident wave. This loss is related to the behaviour of the scattered wave in the forward direction (incident direction), and this relationship is expressed by the **forward-scattering theorem**, also called **optical theorem** or **extinction theorem**. It says that the scattering amplitude in the direction **s=i** is related to σ_e by

$$\sigma_e = 2\lambda\frac{\mathbf{E}_i}{\left|\mathbf{E}_i\right|}\cdot \mathrm{Im}\left[\mathbf{f}(\mathbf{i},\mathbf{i})\right] \tag{2.13}$$

The application of (2.13) requires the scattering amplitude to be known with sufficient accuracy. For approximations found by geometrical optics or Rayleigh scattering, the application of the theorem leads to incorrect results.

2.3 Efficiencies

Often it is convenient to use non-dimensional quantities to express the various interactions. This is achieved by dividing the cross sections by the geometrical cross section σ_g of the scatterer. The resulting quantities are called efficiencies Q_i:

$$Q_a = \frac{\sigma_a}{\sigma_g};\ Q_b = \frac{\sigma_b}{\sigma_g};\ Q_{bi} = \frac{\sigma_{bi}}{\sigma_g};\ Q_e = \frac{\sigma_e}{\sigma_g};\ \ Q_s = \frac{\sigma_s}{\sigma_g} \tag{2.14}$$

These absorption, backscatter, bistatic, extinction and scattering efficiencies, respectively, are not limited to numbers smaller than 1. Under certain conditions a particle can absorb or scatter more radiative power than the power which crosses an area equal to σ_g.

2.4 Scattering Matrix

The incident and scattered fields, $\mathbf{E}_i$ and $\mathbf{E}_s$ or $\mathbf{f}$, are vectors with a rather complex relationship (2.2). Nevertheless it is a linear one (2.1), thus it can be described by an **amplitude-scattering matrix**. As a convention the incident direction is the $\mathbf{x}_3$ direction of a Cartesian coordinate system (x_1,x_2,x_3), and scattering takes place in the ($\mathbf{x}_2$,$\mathbf{x}_3$) plane, thus scattering is from a direction (unit vector) **i**=(0,0,1) to **s**=(0,s_2,s_3), with $s_2 = \sin\vartheta$ and $s_3 = \cos\vartheta$, where ϑ is the **scattering angle**. The incident electric field $\mathbf{E}_i$ makes a **polarisation angle** φ with respect to the scattering plane, having components perpendicular $\perp$ and parallel $\parallel$ to this plane and thus to $\mathbf{x}_2$, see following figure (Note that other conventions exist as well):

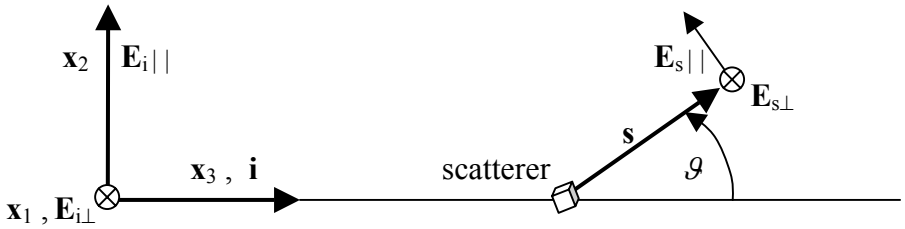

Figure 2.2: Scattering geometry with scattering in ($\mathbf{x}_2$,$\mathbf{x}_3$) plane showing parallel and perpendicular components of the incident and scattered electric fields.

According to Figure 2.2 the direction of the perpendicular $\mathbf{E}_{i\perp}$ component does not change by the scattering process. However the parallel component changes from $\mathbf{E}_{i||} = (0, E_{i||}, 0)$ to a scattered component of the form $\mathbf{E}_{s||} = (0, E_{s||}\cos\vartheta, E_{s||}\sin\vartheta)$.

The relationship between $\mathbf{E}_s$ and $\mathbf{E}_i$ is described by a (2x2) **scattering matrix F**, consisting of elements f_{ij}, *i, j*=1,2:

$$\mathbf{E}_s(\mathbf{r}) = \mathbf{F}(\mathbf{s},\mathbf{i}) \cdot \mathbf{E}_i(0) \frac{\exp(ikR)}{R} \tag{2.15a}$$

where the fields are now split into the perpendicular and parallel components:

$$\begin{pmatrix} E_{s\perp}(\mathbf{r}) \\ E_{s||}(\mathbf{r}) \end{pmatrix} = \begin{pmatrix} f_{11} & f_{12} \\ f_{21} & f_{22} \end{pmatrix} \cdot \begin{pmatrix} E_{i\perp}(0) \\ E_{i||}(0) \end{pmatrix} \frac{\exp(ikR)}{R} \tag{2.15b}$$

For comparison between the conventions of Ishimaru (1978) and van de Hulst (1957), see Table 2.1 below.

Dielectric scatterer in a vacuum	**Convention of Ishimaru (1978)** p.10–14, 33-36	**Conv. of van de Hulst (1957)** p. 12, 29, 34, 35, 125
Incident wave at scatterer **r**=0: oscillating **E**-field with unit amplitude	$\mathbf{E}_i(\mathbf{r}=0) = \begin{pmatrix} E_{i\perp} \\ E_{i||} \end{pmatrix} = \mathbf{e}_i \cdot \exp(-i\omega t);$ $\lvert\mathbf{e}_i\rvert = 1, \mathbf{e}_i = \begin{pmatrix} e_{i\perp} \\ e_{i||} \end{pmatrix} = \begin{pmatrix} \sin\varphi \\ \cos\varphi \end{pmatrix}$	$\mathbf{E}_0 = \begin{pmatrix} E_{r0} \\ E_{l0} \end{pmatrix} = \mathbf{e}_0 \cdot \exp(j\omega t);$ $\lvert\mathbf{e}_0\rvert = 1,\ \mathbf{e}_0 = \begin{pmatrix} e_{r0} \\ e_{l0} \end{pmatrix} = \begin{pmatrix} \sin\varphi \\ \cos\varphi \end{pmatrix}$
Scattered wave: **E**- field at distance *R* Relations between quantities: *j*=–*i* f_{11}=iS_1/k, f_{22}=iS_2/k f_{21}=iS_3/k, f_{12}=iS_4/k	$\mathbf{E}_s = \begin{pmatrix} E_{s\perp} \\ E_{s||} \end{pmatrix} = \mathbf{f}(\mathbf{s},\mathbf{i}) \frac{\exp(ikR - i\omega t)}{R}$ $\mathbf{f}(\mathbf{s},\mathbf{i}) = \begin{pmatrix} f_\perp \\ f_{||} \end{pmatrix} = \mathbf{F} \cdot \begin{pmatrix} e_{i\perp} \\ e_{i||} \end{pmatrix}$ $\mathbf{F} = \begin{pmatrix} f_{11} & f_{12} \\ f_{21} & f_{22} \end{pmatrix}$	Scalar: $u = S(\vartheta,\varphi) \frac{\exp(-jkR + j\omega t)}{jkR}$ Vector*: $\mathbf{E}_s = \begin{pmatrix} E_r \\ E_l \end{pmatrix} =$ $\begin{pmatrix} S_1 & S_4 \\ S_3 & S_2 \end{pmatrix} \cdot \begin{pmatrix} e_{r0} \\ e_{l0} \end{pmatrix} \frac{\exp(j\omega t - jkR)}{jkR}$
Forward-scattering theorem	$\sigma_e \equiv \sigma_t = (4\pi/k)\mathrm{Im}[\mathbf{f}(\mathbf{i},\mathbf{i})] \cdot \mathbf{e}_i$	$C_e = (4\pi/k^2)\mathrm{Re}[S(0)]$
Differential scattering cross section	$\sigma_d = \lvert\mathbf{f}(\mathbf{s},\mathbf{i})\rvert^2$	$\frac{r^2 I_{sca}}{I_0} = \frac{F}{k^2} = \frac{\lvert S\rvert^2}{k^2}$
Scattering cross section	$\sigma_s = \int_{4\pi} \sigma_d \, d\Omega$	$C_{sca} = \frac{1}{k^2} \int_{4\pi} F d\Omega$

Table 2.1: Comparison of conventions used to describe elastic scattering. Note * that the sequence of the components by van de Hulst has been inverted to adapt to the one of Ishimaru. The original relationship is equivalent, but reads

$$\begin{pmatrix} E_l \\ E_r \end{pmatrix} = \begin{pmatrix} S_2 & S_3 \\ S_4 & S_1 \end{pmatrix} \cdot \begin{pmatrix} e_{l0} \\ e_{r0} \end{pmatrix} \frac{\exp(j\omega t - jkr)}{jkr} \tag{2.15c}$$

Furthermore Bohren and Huffman (1983), in short BH, use this convention with j = –i:

$$\begin{pmatrix} E_{||s} \\ E_{\perp s} \end{pmatrix} = \begin{pmatrix} S_2 & S_3 \\ S_4 & S_1 \end{pmatrix} \cdot \begin{pmatrix} E_{||i} \\ E_{\perp i} \end{pmatrix} \frac{\exp(ikr)}{-ikr} \tag{2.15d}$$

2.5 Polarisation

So far we have assumed a fully coherent wave $\mathbf{E}_i = \mathbf{E}_{i0}\exp(i\mathbf{k}\cdot\mathbf{r}-i\omega t)$. Such a wave is totally **polarised**. Radiation, however, consists of waves at different frequencies ω, often covering a wide spectrum and including different polarisations. Scattering and other processes may depend on ω. Therefore one has to investigate the frequency dependence by focussing on quasi-monochromatic radiation (within a narrow frequency interval). This radiation can be described as before, but with the amplitude $\mathbf{E}_{i0}$ and an additional phase to fluctuate slowly with time. The quantities of interest are then specified by **time averages** describing the **mean intensity** and **polarisation**. The polarisation state of the radiation is expressed by four different intensities, called **Stokes Parameters**, collected in an intensity vector **I** = (I,Q,U,V). An **alternative Stokes Vector I** is defined by **I** = (I_1,I_2,U,V). The temporal averages (where $2Z_0$ has been neglected for simplicity) are expressed by $\langle\ \rangle$

$$I_1 = \left\langle |E_\perp|^2 \right\rangle;\ I_2 = \left\langle |E_{||}|^2 \right\rangle;\ U = \left\langle 2\,\mathrm{Re}(E_\perp E_{||}^*) \right\rangle;\ V = \left\langle 2\,\mathrm{Im}(E_\perp E_{||}^*) \right\rangle \tag{2.16}$$

The total intensity is given by the sum $I=I_1+I_2$, the difference is called $Q=I_1-I_2$, and the **degree of polarisation** ($0 \le \rho_p \le 1$) is given by

$$\rho_p = \frac{\sqrt{Q^2+U^2+V^2}}{I} \tag{2.17}$$

The scattering matrix for the electric field can be transformed to a scattering matrix for the Stokes parameters. A scatterer transforms the alternative Stokes Vector $\mathbf{I}_i$ (I_1,I_2,U,V) of the incident radiation to the one of scattered radiation $\mathbf{I}_s$ by a linear process according to

$$\mathbf{I}_s = \mathbf{M}\cdot\mathbf{I}_i \tag{2.18}$$

where the **Müller Matrix M** is given by (Ishimaru, p. 35):

$$\mathbf{M} = \begin{pmatrix} |f_{11}|^2 & |f_{12}|^2 & \mathrm{Re}(f_{11}f_{12}^*) & -\mathrm{Im}(f_{11}f_{12}^*) \\ |f_{21}|^2 & |f_{22}|^2 & \mathrm{Re}(f_{21}f_{22}^*) & -\mathrm{Im}(f_{21}f_{22}^*) \\ 2\,\mathrm{Re}(f_{11}f_{21}) & 2\,\mathrm{Re}(f_{12}f_{22}^*) & \mathrm{Re}(f_{11}f_{22}^*+f_{12}f_{21}^*) & -\mathrm{Im}(f_{11}f_{22}^*-f_{12}f_{21}^*) \\ 2\,\mathrm{Im}(f_{11}f_{21}) & 2\,\mathrm{Im}(f_{12}f_{22}^*) & \mathrm{Im}(f_{11}f_{22}^*+f_{12}f_{21}^*) & \mathrm{Re}(f_{11}f_{22}^*-f_{12}f_{21}^*) \end{pmatrix} \tag{2.19}$$

Note that the 16 elements of **M** are not independent. For properties of **M** for scatterers with special symmetries, see van de Hulst (1957), Chapter 5. For general descriptions of polarisation, see Bohren and Huffman (1983), p. 44-56, and Kraus (1966).

3. Approximate Scattering and Absorption Models

A number of approximate descriptions of scattering and absorption exist. The most important models are presented here. The common assumption is that the scatterers with a dielectric constant ε are situated in free space with dielectric constant of 1 (else, if the propagating medium has a dielectric constant different from 1, then ε may be regarded as the ratio of the dielectric constant of the scatterer to the one of the surrounding medium).

3.1 Rayleigh scattering and absorption by spheres

The scatterer is a small sphere. Rayleigh scattering is an approximate solution of the scattering for particles much smaller than the wavelength. For a sphere of radius a, we require that the **size parameter** x is sufficiently small:

$$x = \frac{\text{circumference}}{\text{wavelength}} = \frac{2\pi a}{\lambda} = ka << 1 \tag{3.1}$$

This means that the phase of the electric field inside the particle is everywhere the same as in the electrostatic situation, and the exponential function in (2.2) $\rightarrow$1 because the argument $\rightarrow$0. The internal field is obtained from the electrostatic solution (Eder 1967; BH 1983):

$$\mathbf{E}(\mathbf{r}') = \frac{3}{\varepsilon + 2}\mathbf{E}_i \tag{3.2}$$

This is a homogeneous field ($\mathbf{E} < \mathbf{E}_i$ for ε>1) and parallel to the incident electric field.

Scattering amplitude

Inserting (3.2) in Equation (2.2), and noting that the scatterer volume is $V_s = 4\pi a^3/3$, the scattering amplitude becomes

$$\mathbf{f}(\mathbf{s},\mathbf{i}) = a^3 k^2 \frac{\varepsilon - 1}{\varepsilon + 2}\{-\mathbf{s} \times [\mathbf{s} \times \mathbf{e}_i]\} \tag{3.3a}$$

where $\mathbf{e}_i$ is the unit vector describing the direction of the incident electric field. Equation (3.3) can also be regarded as the scattering amplitude from an electric dipole with **dipole moment** $\mathbf{p} = \alpha\varepsilon_0\mathbf{e}_i$ for a unit-amplitude incident field and **polarisability** $\alpha = 4\pi a^3 \frac{\varepsilon - 1}{\varepsilon + 2}$ of the sphere:

$$\mathbf{f}(\mathbf{s},\mathbf{i}) = \frac{k^2}{4\pi\varepsilon_0}\{-\mathbf{s} \times [\mathbf{s} \times \mathbf{p}]\} \tag{3.3b}$$

This simple expression is valid for all kinds of small particles.

Cross sections and efficiencies

If we denote the angle between incident electric field and the scattering direction by χ, we get for the bistatic scattering cross section

$$\sigma_{bi} = 4\pi|\mathbf{f}(\chi)|^2 = 4\pi a^6 k^4 \left|\frac{\varepsilon - 1}{\varepsilon + 2}\right|^2 \sin^2\chi \tag{3.4}$$

The scattering cross section requires the integral of (3.4) over all scattering directions:

$$\sigma_s = \int_{4\pi} |\mathbf{f}(\chi)|^2 d\Omega = 2a^6 k^4 \left|\frac{\varepsilon - 1}{\varepsilon + 2}\right|^2 \int_0^{2\pi} d\phi \int_0^{\pi} \sin^2\chi \cdot \sin\chi d\chi = \frac{8\pi}{3} a^6 k^4 \left|\frac{\varepsilon - 1}{\varepsilon + 2}\right|^2 \tag{3.5}$$

and the scattering efficiency becomes:

$$Q_s = \frac{\sigma_s}{\pi a^2} = \frac{8}{3}(ak)^4 \left|\frac{\varepsilon-1}{\varepsilon+2}\right|^2 = \frac{8}{3}x^4\left|\frac{\varepsilon-1}{\varepsilon+2}\right|^2 \tag{3.6}$$

Due to the high power of x the Rayleigh scattering rapidly diverges to unrealistically large values when x approaches or exceeds 1.

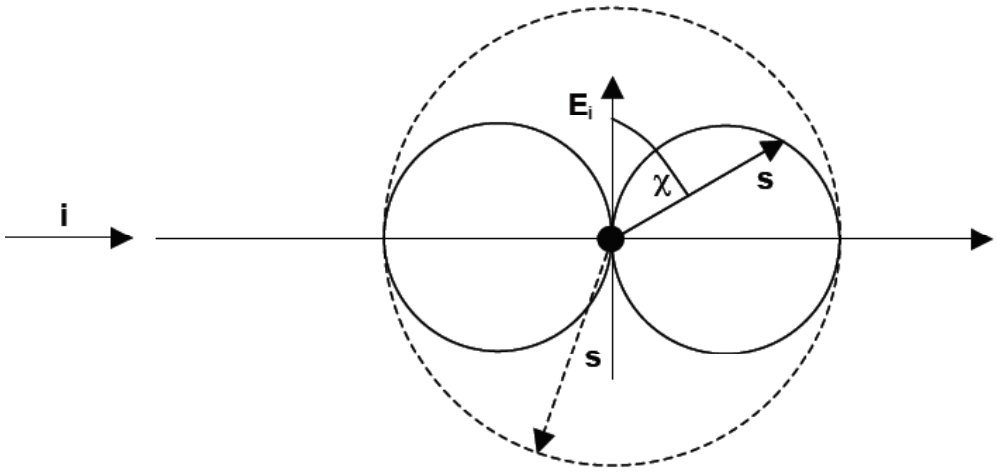

Figure 3.1: Dipole radiation pattern for Rayleigh scattering: solid lines for parallel, dashed line for perpendicular field. The length of the vectors in **s** direction are proportional to the scattered field strength.

The absorption cross section requires the integral of Equation (2.10):

$$\sigma_a = \frac{\omega}{c}\int_V \varepsilon''(\mathbf{r}')\left|K(\mathbf{r}')\right|^2 dV' = \frac{12\pi a^3 k}{\left|\varepsilon+2\right|^2}\varepsilon''; \text{ then } Q_a = \frac{12ak}{\left|\varepsilon+2\right|^2}\varepsilon'' = 12x\frac{\varepsilon''}{\left|\varepsilon+2\right|^2} \tag{3.7}$$

Application of the forward-scattering theorem to the expression (3.3) gives

$$\sigma_e = 2\lambda\mathbf{e}_i\cdot\mathrm{Im}\mathbf{f}(\mathbf{i},\mathbf{i}) = 2\lambda a^3k^2\,\mathrm{Im}\left(\frac{\varepsilon-1}{\varepsilon+2}\right) = 4\pi a^3 k\,\mathrm{Im}\left(\frac{\varepsilon-1}{\varepsilon+2}\right) = \frac{12\pi a^3 k\varepsilon''}{\left|\varepsilon+2\right|^2} \tag{3.8}$$

which is identical to the expression (3.7) for the absorption cross section. Equation (3.8) is inaccurate due to the approximate nature of the Rayleigh-scatter formula. In fact, since x<<1 is required, the term x^4 appears to be negligible with respect to the term proportional to *x*. An exception occurs for low-loss materials ($\varepsilon''\to 0$) if $x\varepsilon'' < x^4$. A better result for the extinction cross section is obtained from the sum of (3.6) and (3.7).

The backscattering cross section σ_b (or radar cross section) is determined from σ_{bi} for **s**=–**i**:

$$\sigma_b = 4\pi\left|\mathbf{f}(\chi=\pi/2)\right|^2 = 4\pi a^6k^4\left|\frac{\varepsilon-1}{\varepsilon+2}\right|^2 \tag{3.9}$$

This quantity is larger by a factor 3/2 than σ_s.

Amplitude scattering matrix

The scattering matrix consists of 2 non-zero elements: f_{11} and f_{22}; the cross-polarisation terms vanish.

$$f_{11} = a^3k^2\frac{\varepsilon-1}{\varepsilon+2};\quad f_{22} = a^3k^2\frac{\varepsilon-1}{\varepsilon+2}\cos\vartheta \tag{3.10}$$

Müller matrix

$$\mathbf{M} = a^6k^4\left|\frac{\varepsilon-1}{\varepsilon+2}\right|^2\begin{pmatrix}1 & 0 & 0 & 0\\ 0 & \cos^2\vartheta & 0 & 0\\ 0 & 0 & \cos\vartheta & 0\\ 0 & 0 & 0 & \cos\vartheta\end{pmatrix} \tag{3.11}$$

3.2 Rayleigh scattering and absorption by ellipsoids

Rayleigh scattering by ellipsoids follows the same rule as found for spheres (3.3), but with different polarisabilities. Equivalently, the ratio of the internal to the incident electric field is different, too, and may depend on the particle orientation. Therefore a tensor formulation is adequate. If the main axes of the ellipsoid are parallel to the Cartesian coordinate system used, the tensor **K** is diagonal:

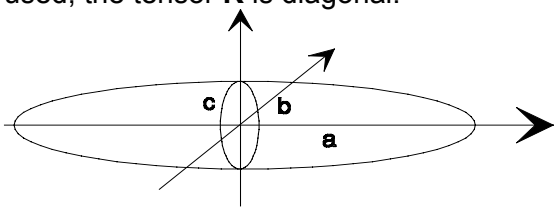

$$\mathbf{E}(\mathbf{r}') = \mathbf{K}\cdot\mathbf{E}_i;\quad \mathbf{K} = \begin{pmatrix} K_{11} & 0 & 0 \\ 0 & K_{22} & 0 \\ 0 & 0 & K_{33} \end{pmatrix} \qquad (3.12)$$

This field is homogeneous inside the particle, but may not be parallel to $\mathbf{E}_i$. For ellipsoids, the diagonal elements of **K** are given by

$$K_{jj} = \frac{1}{1+(\varepsilon-1)A_j};\quad j = 1,2,3\ ;\quad A_1 + A_2 + A_3 = 1 \qquad (3.13)$$

The parameters A_j are the so-called **depolarisation factors**; they are non-negative numbers, and their sum is unity. For **spheres** A_j=1/3 which leads to Equation (3.2). Another simplification is given by assuming **spheroidal** particles where two of the three main axes, and thus two of the three depolarisation factors, are equal. By choosing the equal parameters to be $A=A_1=A_2$, A_3 is found from (3.13):

$$A_3 = 1-2A \qquad (3.14)$$

Small values, A <1/3, represent **oblate** spheroids while higher values, A>1/3, the maximum being 0.5, represent **prolate** spheroids. It is possible to express A by the **axial ratio** X of the spheroids, defined by X= (minor axis)/(major axis) ≤1. For oblate and prolate spheroids A can be computed from the upper and lower Equation (3.15), respectively, as (e.g. von Hippel, 1954, Appendix):

$$A = \begin{cases} \dfrac{X}{2(1-X^2)}\left[\dfrac{\arccos(X)}{\sqrt{1-X^2}} - X\right]; & \textit{oblate} \\ \dfrac{1}{2(1-X^2)}\left[1 - \dfrac{X^2}{2\sqrt{1-X^2}}\ln\dfrac{1+\sqrt{1-X^2}}{1-\sqrt{1-X^2}}\right]; & \textit{prolate} \end{cases} \qquad (3.15)$$

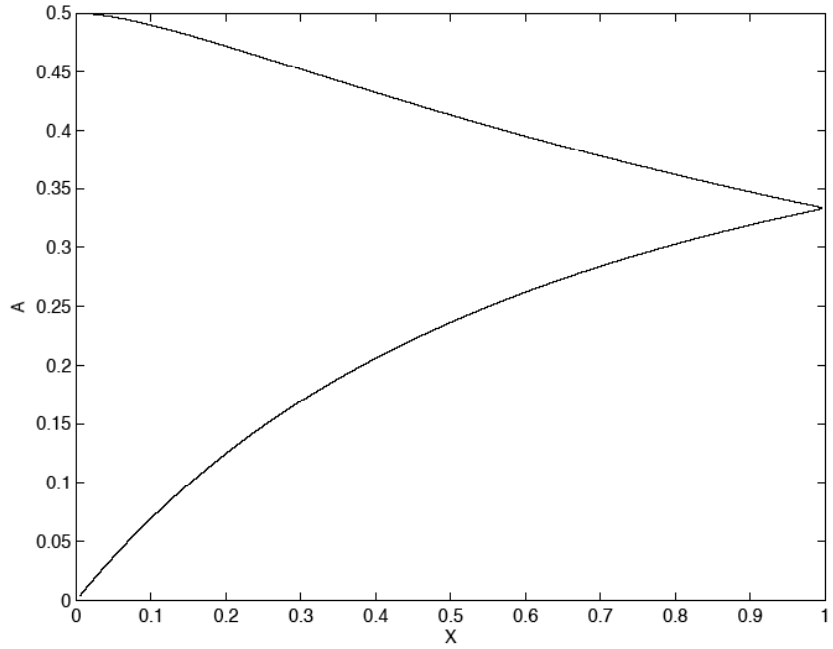

Figure 3.2:
Depolarisation factor A versus axial ratio X of prolate (upper) and oblate (lower curve) spheroids. The two curves join at the value 1/3 valid for spheres.

Inserting (3.12) in Equation (2.2), and noting that the scatterer volume is given by $V_s = 4\pi a_1 a_2 a_3 / 3$ where a_j (j=1,2,3,) are the semi axes of the ellipsoid, the scattering amplitude becomes

$$\mathbf{f}(\mathbf{s},\mathbf{i}) = \frac{a_1 a_2 a_3 k^2 (\varepsilon - 1)}{3} \left\{ -\mathbf{s} \times \left[\mathbf{s} \times (\mathbf{K} \cdot \mathbf{e}_i) \right] \right\} \tag{3.16}$$

If $\mathbf{e}_i$ is parallel to main axis j, the bistatic scattering coefficient is given by

$$\sigma_{bi}(\mathbf{s},\mathbf{i})_j = 4\pi \frac{(a_1 a_2 a_3)^2 k^4}{9} \left| \frac{\varepsilon - 1}{1 + (\varepsilon - 1) A_j} \right|^2 \sin^2 \chi \tag{3.17}$$

Since the different A_j may change between 0 and 1, the scattering may strongly depend on the particle orientation. The same is true for the absorption cross section

$$\sigma_{aj} = \frac{4\pi a_1 a_2 a_3 k \varepsilon''}{3} \left| \frac{1}{1 + (\varepsilon - 1) A_j} \right|^2 \tag{3.18}$$

Highest scattering and absorption are found for $A_j \rightarrow 0$, i.e. if $\mathbf{e}_i$ is parallel to needles or plates.

3.3 Born Approximation

For scattering by a medium whose dielectric constant is close to 1 (or more general close to the value of the surroundings) the internal field is close to the incident field. In the Born approximation (also called Rayleigh-Gans Approximation) these fields are assumed to be the same:

$$\mathbf{E}(\mathbf{r}') = \mathbf{E}_i = \mathbf{E}_{i0} \exp(\mathrm{i}\mathbf{k}\cdot\mathbf{r} - \mathrm{i}\omega t) = \mathrm{E}_{i0}\mathbf{e}_i \exp(\mathrm{i}\mathbf{k}\cdot\mathbf{r} - \mathrm{i}\omega t) \tag{3.19}$$

Examples include air volumes at different density, moisture and temperature in the atmosphere. Phase and amplitude errors of waves travelling through the particle can be neglected as long as kD(n'-1)<<1, kDε"<<1 where D is the particle diameter, and $n = n' + in'' = \sqrt{\varepsilon}$ is the complex refractive index. Substituting (3.19) in (2.2) and omitting the time factor gives

$$\mathbf{f}(\mathbf{s},\mathbf{i}) = \frac{k^2 \left\{ -\mathbf{s} \times \left[\mathbf{s} \times \mathbf{e}_i \right] \right\}}{4\pi} \int_{V_s} \left\{ \varepsilon(\mathbf{r}') - 1 \right\} \exp\left[ik\mathbf{r}' \cdot (\mathbf{i} - \mathbf{s}) \right] dV' \tag{3.20}$$

As an example let us assume that the scatterer is a sphere of radius a. Then

$$\mathbf{f}(\mathbf{s},\mathbf{i}) = \frac{k^2 \left\{ -\mathbf{s} \times \left[\mathbf{s} \times \mathbf{e}_i \right] \right\} (\varepsilon - 1)}{4\pi} F(\vartheta) \tag{3.21}$$

where F (with $\Delta\mathbf{k} = k(\mathbf{i} - \mathbf{s})$) is given by

$$F(\vartheta) = \int_V \exp(-i\Delta\mathbf{k} \cdot \mathbf{r}') dV' = \int_0^a \int_0^{\pi} \int_0^{2\pi} \exp(ik_d r \cos\theta) r^2 dr \sin\theta d\theta d\phi \tag{3.22}$$

where $\Delta\mathbf{k} = k(\mathbf{s} - \mathbf{i})$, $|\Delta\mathbf{k}| = k_d = 2k \sin\frac{\vartheta}{2}$, and θ is the angle between the -$\Delta\mathbf{k}$ and $\mathbf{r}$. The integral in (3.22) is to be taken over the sphere volume. Inserting the result

$$F(\vartheta) = \frac{4\pi a}{k_d^2} \left(\frac{\sin k_d a}{k_d a} - \cos k_d a \right) \tag{3.23}$$

in (3.21) gives

$$\mathbf{f}(\vartheta) = \left\{ -\mathbf{s} \times \left[\mathbf{s} \times \mathbf{e}_i \right] \right\} \frac{a^3 k^2 (\varepsilon - 1)}{(k_d a)^2} \left(\frac{\sin k_d a}{k_d a} - \cos k_d a \right) \tag{3.24}$$

The bistatic scattering cross section becomes

$$\sigma_{bi} = 4\pi\left|\mathbf{f}(\vartheta)\right|^2 = \sin^2\chi\,\frac{4\pi a^6 k^4\left|\varepsilon-1\right|^2}{(k_d a)^4}\left(\frac{\sin k_d a}{k_d a}-\cos k_d a\right)^2 \tag{3.25}$$

and the absorption cross section is simply given by

$$\sigma_a = \frac{\omega}{c}\int_V \varepsilon''(\mathbf{r}')dV' = \frac{4\pi a^3 k}{3}\varepsilon'' \tag{3.26}$$

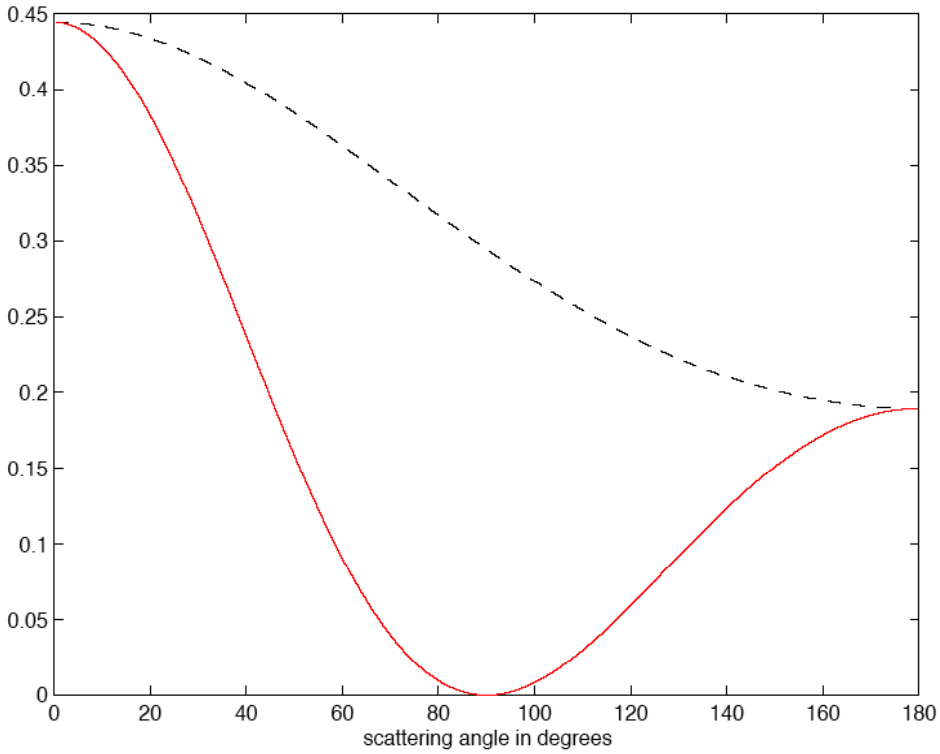

Figure 3.3: Bistatic scattering efficiencies $Q_{bi} = \sigma_{bi}/(\pi a^2)$ for $x = ka = 1$, ε=2, for perpendicular (dashed) and for parallel polarisation (solid line).

Bragg scattering

Another application of the Born approximation is for scattering by **periodic** or **random media** whose dielectric constant changes locally from point to point around a mean value. This is called **Bragg** scattering. Let us assume that the mean value of ε is 1. Then δ(**r**)=ε(**r**)-1 is a real random function with **zero mean**. Then

$$\mathbf{f}(\mathbf{s},\mathbf{i}) = \frac{k^2\left\{-\mathbf{s}\times\left[\mathbf{s}\times\mathbf{e}_i\right]\right\}}{4\pi}D(\Delta\mathbf{k});\; D(\Delta\mathbf{k}) = \int_{V_s}\delta(\mathbf{r}')\exp\left[-i\Delta\mathbf{k}\cdot\mathbf{r}'\right]dV' \tag{3.27}$$

Note that the integral is proportional to the **three-dimensional Fourier Transform** of δ(**r**) where δ(**r**)=0 at positions outside V_s. If we know the actual function δ(**r**) at all points, the integral can be computed directly. Often, only statistical properties of the medium may be known. This can be sufficient to compute the bidirectional scattering cross section, using the autocorrelation theorem (Bracewell, 1965). Let us first introduce the autocorrelation function

$$A(\mathbf{r}) = \frac{1}{V_s\sigma_\delta^2}\int_{V_s}\delta(\mathbf{r}')\delta(\mathbf{r}'+\mathbf{r})dV';\ \text{with the variance}\ \sigma_\delta^2 = \frac{1}{V_s}\int_{V_s}\delta^2(\mathbf{r}')dV' \tag{3.28}$$

This function tells how much spatial correlation exists in the dielectric function ε(**r**). Note that A is normalised to A(0)=1. Now, the autocorrelation theorem states that $\left|D(\Delta\mathbf{k})\right|^2$ is the three-dimensional Fourier Transform of A(**r**):

$$\left|D(\Delta\mathbf{k})\right|^2 = V_s\sigma_\delta^2\int_{V_s}A(\mathbf{r}')\exp\left[-i\Delta\mathbf{k}\cdot\mathbf{r}'\right]dV' \tag{3.29}$$

Thus we get

$$\sigma_{bi} = 4\pi\left|\mathbf{f}(\vartheta)\right|^2 = \frac{k^4 \sin^2 \chi}{4\pi}\left|D(\Delta\mathbf{k})\right|^2 \tag{3.30}$$

Random granular media, like sand or snow (see Figure 3.4), often have an exponential autocorrelation function

$$A(\mathbf{r}) = \exp(-r/p_c);\ \text{where}\ r = |\mathbf{r}|\ \text{and}\ p_c\ \text{is called}\ \textbf{correlation length} \tag{3.31}$$

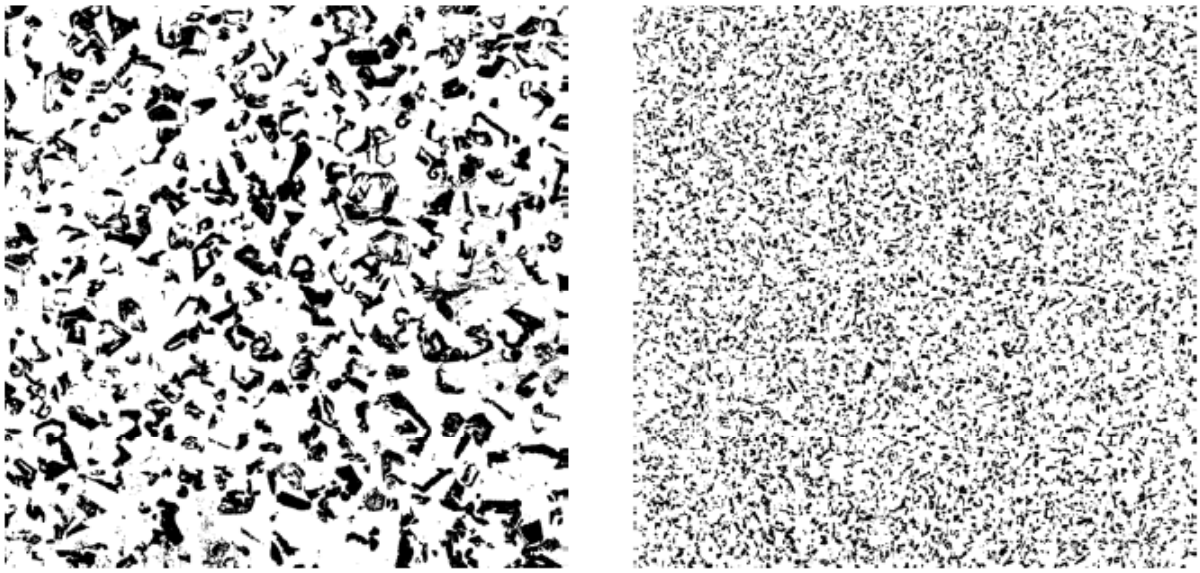

Figure 3.4a: Thin sections (3cmx3cm) of depth hoar (Schwimmschnee) left, and fine-grained snow (right).

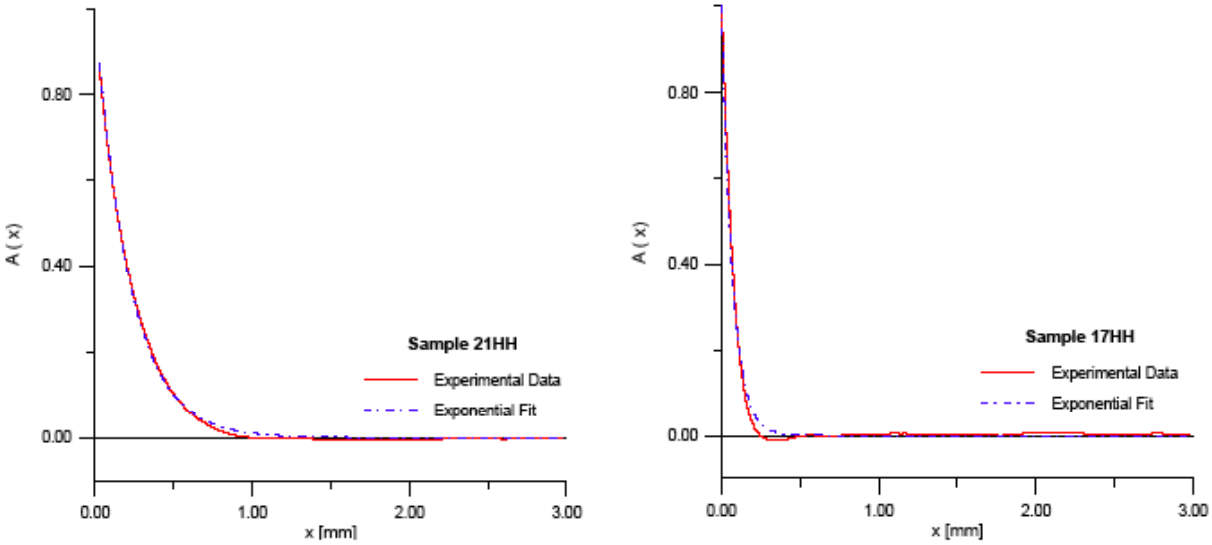

Figure 3.4b: Autocorrelation functions computed of thin sections of Figure 3.4a (from Wiesmann et al. 1998).

Inserting (3.31) into (3.29) leads to

$$\left|D(\Delta\mathbf{k})\right|^2 = 4\pi V_s \sigma_\delta^2 I;\ \ I = \frac{1}{k_d}\int_0^\infty A(r) r \sin(k_d r)\,dr = \frac{2p_c^3}{(1+k_d^2 p_c^2)^2} \tag{3.32}$$

$$\sigma_{bi} = \frac{2k^4 V_s \sigma_\delta^2 p_c^3 \sin^2 \chi}{(1+k_d^2 p_c^2)^2} \tag{3.33}$$

There is a certain similarity with Rayleigh scattering, compare with (3.4). The correlation length p_c functions as a grain "size". Assuming the grains to be N spheres of radius a in a diluted cloud volume $V_s >> 4\pi a^3/3$ we get from (3.28) for

$$V_s \sigma_\delta^2 = N \frac{4\pi a^3}{3} |\varepsilon - 1|^2 \tag{3.34}$$

For $k_d p_c << 1$ this corresponds to Rayleigh scattering by *N* independent spheres where $a \cong p_c$. For snow, see an improved Born Approximation by Mätzler (1998) and its application to microwave radiometry by Mätzler and Wiesmann (1999).
Whereas Rayleigh scattering diverges for large size parameters, this is not the case for the Born Approximation (3.33). If $k_d p_c$>>1 the bistatic scattering coefficient becomes frequency independent and converges to (for ϑ not too close to 0)

$$\sigma_{bi} = \frac{V_s \sigma_\delta^2 \sin^2 \chi}{8 p_c \sin^4 \frac{\vartheta}{2}} \tag{3.35}$$

Indeed this formula is not far from reality for scattering by snow crystals in the visible and near infrared range. Scattering decreases with increasing p_c. in contrast to the microwave range.

Remarks on the correlation length

To get a better idea about the **correlation length** we present 3 different, but equivalent definitions, assuming an isotropic 2-component granular medium in 3 dimensions.
1) The first definition is based on the derivative of the 3-dimensional, spatial **autocorrelation function** *A*(*r*), with *A*(0)=1, and with *r* being the scalar displacement (Debye et al. 1957):

$$p_c = -\left(\frac{dA(r)}{dr} \right)^{-1} \Bigg|_{r=0} \tag{3.36}$$

2) Secondly, according to Debye et al. (1957), p_c is related to the **specific surface** *s* =*S/V* (*S* is the total surface area in a volume *V, and f* is the **volume fraction** of the grains)

$$p_c = \frac{4 f (1-f)}{s} \tag{3.37}$$

3) From the mean **intercept lengths** (Durchstichslängen) in ice L_i and in air L_a (stereological parameters derived from thin sections), we get a third relationship:

$$p_c = \frac{L_a L_i}{L_a + L_i} \tag{3.38}$$

Particle Type	D_{max}	p_c
Sphere, diameter *D*	D	$\frac{2D}{3}$
Oblate spheroid (plate): thickness D_{min} << diameter D_p	D_p	$\frac{4D_{min}}{3}$
Prolate spheroid (needle): diameter D_{min} << length L_n	L_n	$\frac{8D_{min}}{3\pi}$
Cup (spherical shell): shell thickness *d* << diameter D_2	D_2	2*d*

Table 3.1: Relations between particle size D_{max} and correlation length p_c of isotropically distributed particles, according to Mätzler C. "Autocorrelation functions of granular media with free arrangement of spheres, spherical shells or ellipsoids", J. Applied Physics, **81**(3), 1509-1517, (1997).

Thus p_c is the **smallest** characteristic dimension of the particle.

3.4 Geometrical Optics

3.4.1 Reflecting sphere

A simple type of geometrical optics is obtained if we assume that matter consists of homogeneous objects with step-like transitions in between. The boundaries consist of smooth interfaces. In such a model **light rays are straight lines** within the object, and scattering results by **reflection** and **refraction** at the boundaries as described by the **Fresnel Equations** and **Snell's Law**, respectively. Diffraction is ignored.

As a simple example let us consider scattering by a homogeneously illuminated (from the left, s. Figure below) and perfectly reflecting sphere (surface reflectivity *r* =1). Due to the symmetry around the axis of illumination, the scattering (reflection) only depends on the **incidence angle** θ which is related to the **scattering angle** ϑ.

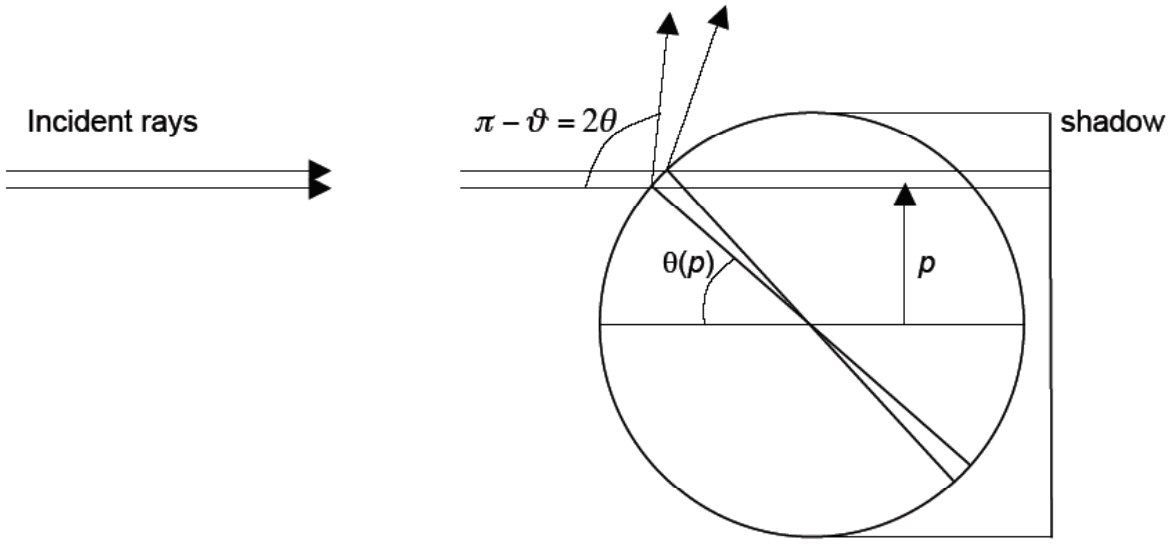

Figure 3.5: Reflection of rays on a sphere according to geometrical optics.

Since all incident radiation is completely reflected the refracted ray is missing. Thus we only consider reflected rays. Let us consider all radiation scattered within an angular interval $(\vartheta, \vartheta + d\vartheta)$. As shown in Figure 3.5, the **impact parameter** *p* and **sphere radius** a are related to the incidence angle θ (and thus to scattering angle ϑ) by

$$p = a\sin\theta; dp = a\cos\theta d\theta \tag{3.39}$$

The scattered power dPs with scattering angles in the range $(\vartheta, \vartheta + d\vartheta)$ and thus in the solid angle $d\Omega = 2\pi\sin\vartheta d\vartheta$ is $dP_s = I_i 2\pi p dp$, and thus with $2\sin\theta\cos\theta = \sin\vartheta$ we get

$$\frac{\sigma_{bi}}{4\pi} = \frac{1}{I_i}\frac{dP_s}{d\Omega} = \frac{pdp}{\sin\vartheta d\vartheta} = \frac{a^2\sin\theta\cos\theta}{\sin\vartheta}\frac{d\theta}{d\vartheta} = \frac{a^2}{4} \tag{3.40}$$

This result means that scattering is isotropic, and with Equation (2.6) and (2.7) we get

$$\sigma_{bi} = \sigma_s = \sigma_b = \sigma_g = \pi a^2 \tag{3.41}$$

Since no radiation enters the sphere, there is no absorption, and thus σ_a=0. Therefore $\sigma_e = \sigma_g$, and the efficiencies are

$$Q_{bi} = Q_s = Q_e = Q_b = 1, \text{ and } Q_a = 0. \tag{3.42}$$

In the following section we consider the situation of partly transparent spheres.

3.4.2 Partly transparent spheres, rainbows

Scattering by dielectric or magnetic spheres can also be treated in geometrical optics. This will reveal effects such as rainbows. In addition to the reflected ray there are transmitted rays and rays with internal reflections as shown in the following figure.

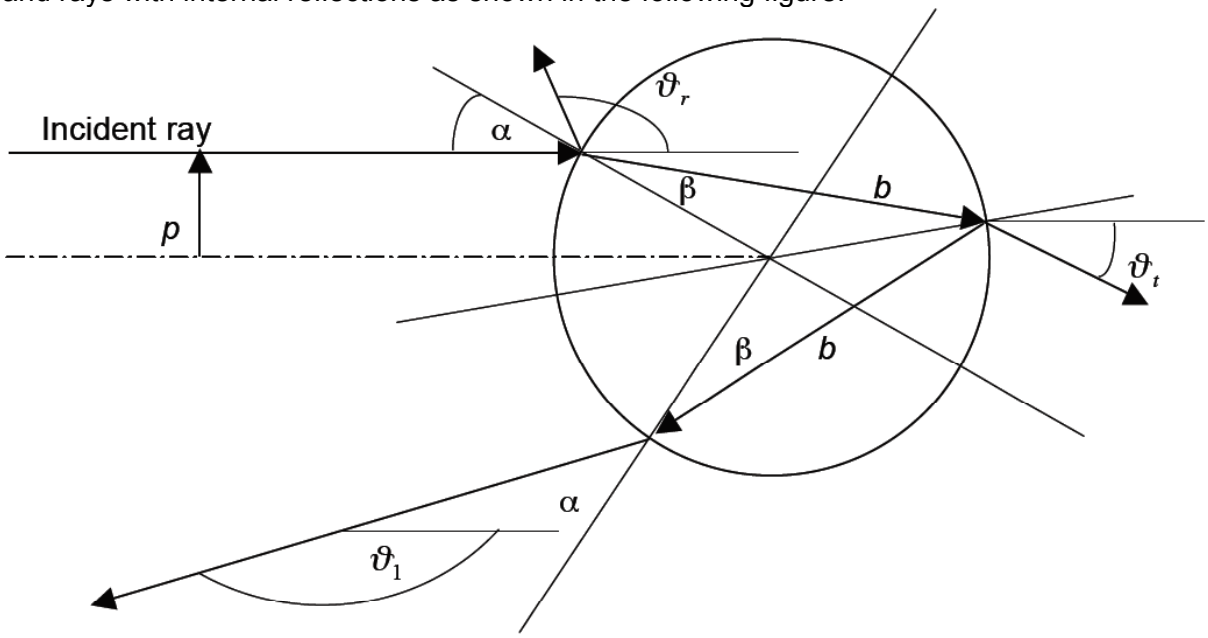

Figure 3.6: Refraction and reflection of light in a sphere, showing reflected and transmitted rays and ray of the first rainbow with scattering angles $\vartheta_r = \pi - 2\alpha$, $\vartheta_t = 2(\alpha - \beta)$, $\vartheta_1 = \pi + 2\alpha - 4\beta$, respectively. The sphere centre is in the scattering plane. Incidence angle is α, impact parameter *p*.

The scattered intensities of the reflected and transmitted rays and of the rainbow rays can be computed with geometrical optics. First, for a given **impact parameter** p and **radius** a, the **incidence angle** α is given by

$$\sin\alpha = p/a \tag{3.43}$$

The **transmitted angle** β after refraction is according to **Snell's Law**

$$\sin\beta = \sin\alpha/m \tag{3.44}$$

where *m* is the refractive index of the sphere. Note that, for a given *p*, all α and β are the same wherever the ray crosses the sphere surface. The scattering angles of the reflected and of the transmitted rays are given by

$$\vartheta_r = \pi - 2\alpha \;;\; \vartheta_t = 2(\alpha - \beta) \tag{3.45}$$

The scattering angle of rays with *j* internal reflections is according to van de Hulst (1957), Bohren and Huffman (1983)

$$\vartheta_j = \pi + 2\left[\alpha - (j+1)\beta\right];\; j \text{ odd, else: } \vartheta_j = 2\left[(j+1)\beta - \alpha\right] \tag{3.46}$$

After leaving the sphere, each ray contributes to the scattered power by $dP_{s,j} = I_j L_j dA$ where the projected impact area, seen by the ray, is $dA = pdpd\varphi = a^2\cos\alpha\sin\alpha d\alpha d\varphi$, I_i is the incident intensity, and L_j is the loss factor due to reflection and/or transmission. The contribution to the bistatic scattering coefficient by a given ray is determined by

$$\frac{\sigma_{bi,j}}{4\pi} = \frac{1}{I_i}\frac{dP_{s,j}}{d\Omega}; \qquad j = r,\ t,\ 1,\ 2,... \tag{3.47}$$

and since $d\Omega = -\sin\vartheta_j d\vartheta_j d\varphi$, we get

$$\sigma_{bi,j} = 4\pi a^2 L_j \left|\frac{\cos\alpha\sin\alpha}{\sin\vartheta_j}\frac{d\alpha}{d\vartheta_j}\right| = 2\pi a^2 L_j \left|\frac{\sin 2\alpha}{\sin\vartheta_j}\frac{d\alpha}{d\vartheta_j}\right| \tag{3.48}$$

The azimuth terms $d\varphi$ cancel, and the total bistatic scattering coefficient/efficiency is the sum

$$\sigma_{bi} = \sum_{j=r,t,1,2,\ldots} \sigma_{bi,j}\,;\quad Q_{bi} = \frac{1}{\pi a^2} \sum_{j=r,t,1,2,\ldots} \sigma_{bi,j} \tag{3.49}$$

Rainbows appear where rays are concentrated. Peaks occur at positions where $\frac{d\vartheta_j}{d\alpha} = 0$, there $\sigma_{bi,j} \to \infty$. This happens at angles α_j and β_j given by

$$\cos\alpha_j = \sqrt{\frac{m'^2 - 1}{(j+1)^2 - 1}}\,;\quad \sin\beta_j = \frac{1}{m'}\sqrt{\frac{(j+1)^2 - m'^2}{(j+1)^2 - 1}} \tag{3.50}$$

Values of ϑ_1 and ϑ_2 in the interval 1< *m*'=Re(*m)* <2 are shown in below.

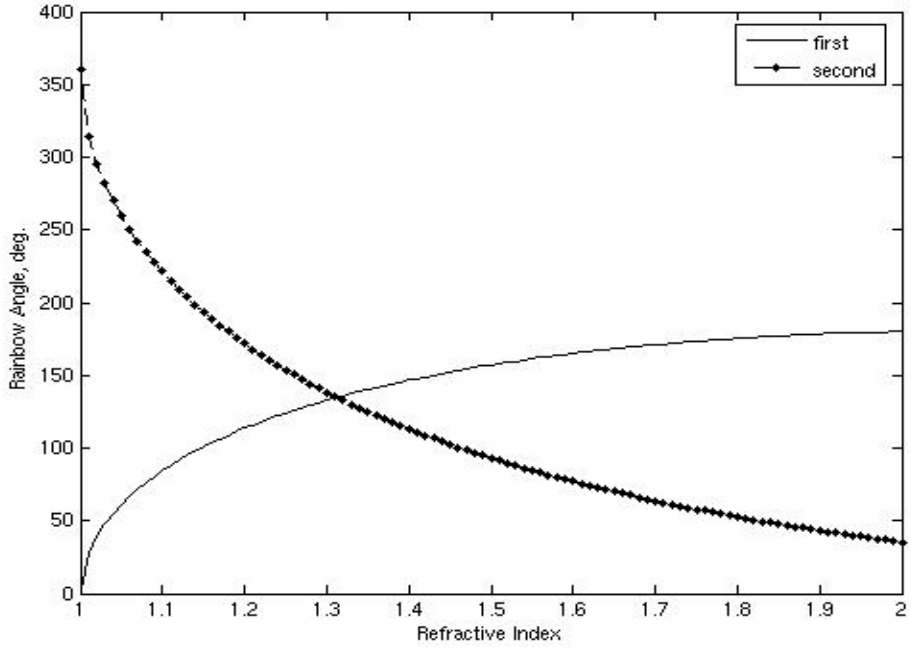

Figure 3.7: Scattering angles of first and second rainbow peaks versus refractive index *m*'.

Computation of $\sigma_{bi,j}$

Reflected ray, *j=r*:

L_r is the reflectivity at the sphere surface which can be computed with the **Fresnel Formulas**, using the (complex) relative impedance *Z* and refractive index *m* of the sphere

$$Z = \sqrt{\frac{\mu}{\varepsilon}}\,;\ m = \sqrt{\mu\varepsilon}; \tag{3.51}$$

For μ=1 we have *m*=1/*Z*. The reflection coefficients of the electric field at perpendicular and parallel polarisation with respect to the scattering plane can be expressed as

$$R_\perp = \frac{Z\cos\alpha - \cos\beta}{Z\cos\alpha + \cos\beta};\ R_{||} = \frac{Z\cos\beta - \cos\alpha}{Z\cos\beta + \cos\alpha} \quad \text{Fresnel Formulas for amplitude} \tag{3.52}$$

and the respective power reflectivities are

$$r_\perp = |R_\perp|^2;\ r_{||} = |R_{||}|^2 \quad \text{Fresnel Formulas for power} \tag{3.53}$$

Then

$$L_r = r = r_\perp(\alpha = \pi/2 - \vartheta_r/2)\cdot\sin^2\varphi + r_{||}(\alpha = \pi/2 - \vartheta_r/2)\cdot\cos^2\varphi \tag{3.54}$$

and from $\frac{d\alpha}{d\vartheta_r} = -\frac{1}{2}$ and $\sin 2\alpha = \sin\vartheta_r$ we get

$$\sigma_{bi,r} = 4\pi|\mathbf{f}_r|^2 = \pi a^2 r;\ Q_{bi,r} = r, \text{ and } r = r_\perp\sin^2\varphi + r_{||}\cos^2\varphi \tag{3.55}$$

Note that $Q_{bi} \to 1$ for $\vartheta = 0$ ($\theta = \pi/2$). For the scattering amplitudes we get

$$f_{11,r} = \frac{aR_{\perp}(\alpha = \pi/2 - \vartheta/2)}{2};\ f_{22,r} = \frac{aR_{||}(\alpha = \pi/2 - \vartheta/2)}{2} \tag{3.56}$$

Transmitted ray, *j*=*t*:

L_t is the loss due to 2 transmissions $(1-r)^2$ through the sphere surface and due to the absorption loss $\exp(-\gamma_a b)$ over the propagation path $b = 2a\cos\beta$ within the sphere; therefore

$$L_t = (1-r)^2 \exp(-2\gamma_a a\cos\beta) \tag{3.57}$$

The derivative $\frac{d\alpha}{d\vartheta_t}$ follows from $\vartheta_t = 2(\alpha - \beta)$ with $\sin\beta = \sin\alpha/m$:

Note: In case of an imaginary refractive index, *m* has to be replaced by its real part.

$$\frac{d\vartheta_t}{d\alpha} = 2\left(1 - \frac{d\beta}{d\alpha}\right) = 2\left(1 - \frac{\cos\alpha}{\sqrt{m^2 - \sin^2\alpha}}\right) \tag{3.58}$$

$$\sigma_{bi,t} = 4\pi a^2 L_t \left|\frac{\sin\alpha\cos\alpha}{\sin\vartheta_t}\frac{d\alpha}{d\vartheta_t}\right| \tag{3.59}$$

Ray of first rainbow, *j*=1:

L_1 is the loss due to 2 transmissions and one reflection $(1-r)^2 r$ through/at the sphere surface and due to the absorption loss $\exp(-2\gamma_a b)$ over the propagation path $2b = 4a\cos\beta$ within the sphere; therefore

$$L_1 = (1-r)^2 r \exp(-4\gamma_a a\cos\beta) \tag{3.60}$$

The derivative $\frac{d\alpha}{d\vartheta_1}$ follows from $\vartheta_1 = \pi + 2\alpha - 4\beta$:

$$\frac{d\vartheta_1}{d\alpha} = 2\left(1 - 2\frac{d\beta}{d\alpha}\right) = 2\left(1 - \frac{2\cos\alpha}{\sqrt{m^2 - \sin^2\alpha}}\right) \tag{3.61}$$

Ray of second rainbow, *j*=2:

L_2 is the loss due to 2 transmissions and 2 reflections $(1-r)^2 r^2$ through/at the sphere surface and due to the absorption loss $\exp(-3\gamma_a b)$ over the propagation path $3b = 6a\cos\beta$ within the sphere; therefore

$$L_2 = (1-r)^2 r^2 \exp(-6\gamma_a a\cos\beta) \tag{3.62}$$

The derivative $\frac{d\alpha}{d\vartheta_2}$ follows from $\vartheta_2 = 6\beta - 2\alpha$:

$$\frac{d\vartheta_2}{d\alpha} = 2\left(3\frac{d\beta}{d\alpha} - 1\right) = 2\left(\frac{3\cos\alpha}{\sqrt{m^2 - \sin^2\alpha}} - 1\right) \tag{3.63}$$

Absorption cross section

Absorption occurs for rays propagating through the sphere. The absorbed fractions on transects (secants of length $b = 2a\cos\beta$) No. 1, 2, 3, 4, etc. are

$$\begin{aligned}
&1: && (1-r)\left[1 - \exp(-2\gamma_a a\cos\beta)\right] \\
&2: && (1-r)\left[1 - \exp(-2\gamma_a a\cos\beta)\right] r \exp(-2\gamma_a a\cos\beta) \\
&3: && (1-r)\left[1 - \exp(-2\gamma_a a\cos\beta)\right] r^2 \exp(-4\gamma_a a\cos\beta) \\
&4: && (1-r)\left[1 - \exp(-2\gamma_a a\cos\beta)\right] r^3 \exp(-6\gamma_a a\cos\beta)
\end{aligned} \tag{3.64}$$

etc.

The sum of all terms is a geometrical series, giving

$$L_a = \frac{(1-r)\left[1-\exp(-2\gamma_a a\cos\beta)\right]}{1-r\exp(-2\gamma_a a\cos\beta)} \tag{3.65}$$

The power absorbed by these rays is

$$dP_a = pd\varphi dpI_i L_a \tag{3.66}$$

and the absorption cross section becomes

$$\sigma_a = \frac{P_a}{I_i} = \int_0^{2\pi} d\varphi \int_0^a L_a p dp \tag{3.67}$$

The integration over φ is approximated by replacing *r* by the mean value $0.5\left(r_\perp + r_{||}\right)$ in L_a. Then we are left with the numerical integration over *p*

$$\sigma_a = \frac{P_a}{I_i} = 2\pi \int_0^a L_a p dp \tag{3.68}$$

Scattering cross section

The scattering cross section is the mean value of σ_{bi}. It is easier, however, to use the fact that in geometrical optics we have $\sigma_e = \pi a^2$; then

$$\sigma_s = \pi a^2 - \sigma_a \tag{3.69}$$

Numerical example

Dielectric sphere with m=1.44+10^{-5}i, x=4000, MATLAB: `fresnelsphere1(ε, μ, x)`

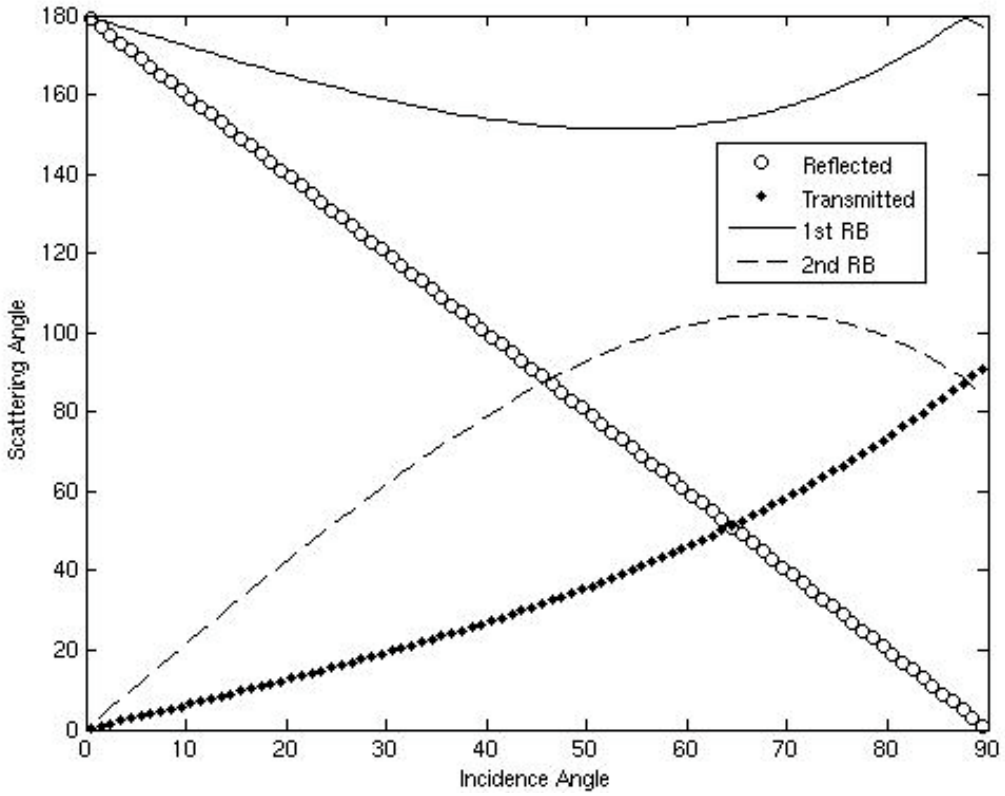

Figure 3.8: Scattering angles of the different rays versus incidence angle for *m*' =1.44.

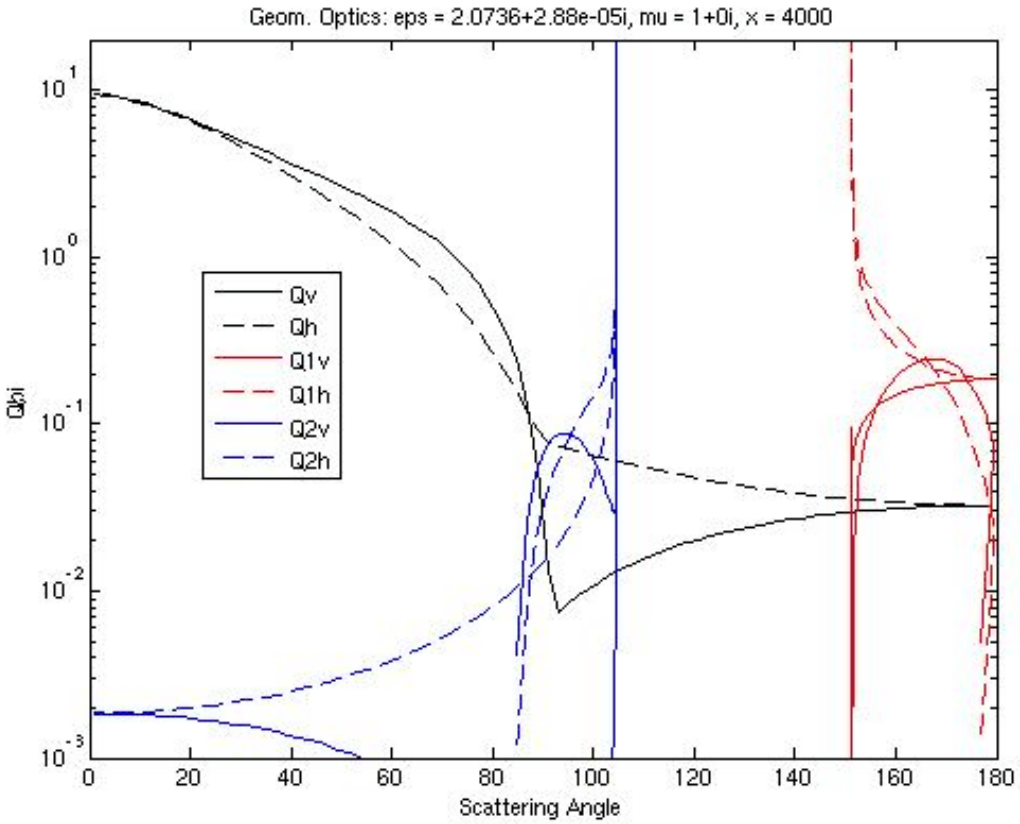

Figure 3.9: Bistatic scattering efficiencies at perpendicular (h) and parallel (v) polarisation in geometrical optics, showing results for the sums of the reflected and transmitted rays and for the 1st and 2nd rainbows for a dielectric sphere with m=1.44+10^{-5}i.

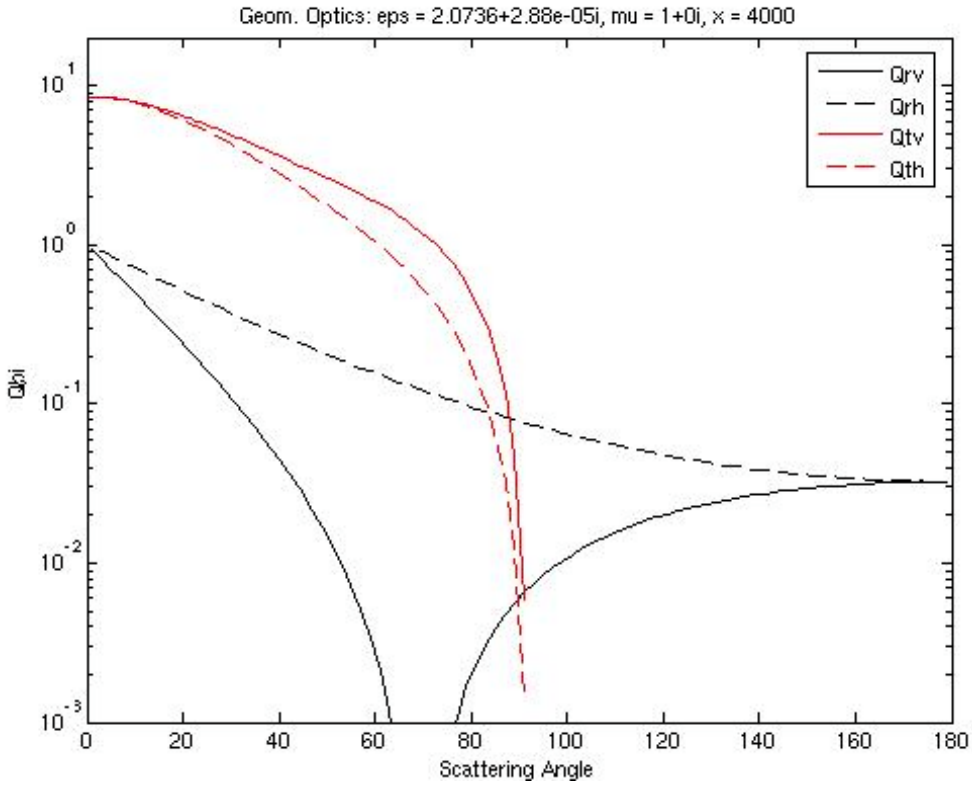

Figure 3.10: Bistatic scattering efficiencies at perpendicular (h) and parallel (v) polarisation in geometrical optics of the reflected and transmitted rays for the situation of Figure 3.9

4 Lorenz-Mie Scattering and Absorption by Spheres

There exists an exact theory for scattering and absorption by a homogeneous, dielectric and/or magnetic **sphere of any size**. It was developed by **Ludvig V. Lorenz** in 1890 and by **Gustav Mie** (1867-1957) in 1908. Here we will make use of the treatment by BH (1983), and of respective reports describing **MATLAB functions** for numerical computations by Mätzler (2002/04). The theory can be extended to coated spheres (spherical shells) or concentrically layered spheres. We will discuss situations of **coated spheres** consisting of a homogeneous core surrounded by a coating. For derivations and further discussions, see BH (1983), van de Hulst (1957), and Deirmendjian (1969).

4.1 The scattered field

The scattered far field in spherical coordinates for a unit-amplitude incident field (where the time variation exp(-iωt) has been omitted) is given by

$$E_{s\vartheta} = \frac{e^{ikr}}{-ikr}\cos\varphi \cdot S_2(\cos\vartheta)$$
$$E_{s\varphi} = \frac{e^{ikr}}{ikr}\sin\varphi \cdot S_1(\cos\vartheta) \tag{4.1}$$

with the scattering amplitudes S_1 and S_2 ($S_3 = S_4 = 0$)

$$S_1(\cos\vartheta) = \sum_{n=1}^{\infty}\frac{2n+1}{n(n+1)}(a_n\pi_n + b_n\tau_n);$$
$$S_2(\cos\vartheta) = \sum_{n=1}^{\infty}\frac{2n+1}{n(n+1)}(a_n\tau_n + b_n\pi_n) \tag{4.2}$$

As described in Chapter 2, $E_{s\vartheta}$ is the scattered far-field component in the scattering plane, defined by the incident and scattered directions, and $E_{s\varphi}$ is the orthogonal component. The angle φ is the angle between the incident electric field and the scattering plane. The functions π_n and τ_n describe the angular scattering patterns of the spherical harmonics used to describe S_1 and S_2 and follow from the recurrence relations

$$\pi_n = \frac{2n-1}{n-1}\cos\vartheta \cdot \pi_{n-1} - \frac{n}{n-1}\pi_{n-2};\quad \tau_n = n\cos\vartheta \cdot \pi_n - (n+1)\pi_{n-1} \tag{4.3}$$

starting with

$$\pi_0 = 0;\ \pi_1 = 1;\ \pi_2 = 3\cos\vartheta;\ \tau_0 = 0;\ \tau_1 = \cos\vartheta;\ \tau_2 = 3\cos(2\vartheta) \tag{4.4}$$

4.2 Mie Coefficients

The key parameters for Mie calculations are the **Mie Coefficients** a_n and b_n to compute the amplitudes of the scattered field, and c_n and d_n for the internal field, respectively. The coefficients are determined by the boundary conditions of the fields at the sphere surface, and they are given in BH (1983) on p.100. The coefficients of the scattered electrical field are:

$$a_n = \frac{\mu m^2 j_n(mx)[xj_n(x)]' - \mu_1 j_n(x)[mxj_n(mx)]'}{\mu m^2 j_n(mx)[xh_n^{(1)}(x)]' - \mu_1 h_n^{(1)}(x)[mxj_n(mx)]'}$$
$$b_n = \frac{\mu_1 j_n(mx)[xj_n(x)]' - \mu j_n(x)[mxj_n(mx)]'}{\mu_1 j_n(mx)[xh_n^{(1)}(x)]' - \mu h_n^{(1)}(x)[mxj_n(mx)]'} \tag{4.5}$$

where prime means derivative with respect to the argument; similar expressions exist for the coefficients c_n and d_n of the internal field (see below). The Index n runs from 1 to ∞, but the infinite series occurring in Mie formulas can be truncated at a maximum, n_{max}; for this number BH (1983) proposed

$$n_{\max} = x + 4x^{1/3} + 2 \tag{4.6}$$

and this value is used here as well. The size parameter is given by $x=ka$, a is the radius of the sphere, and $k=2\pi/\lambda$ is the wave number, λ the wavelength in the ambient medium, $m=(\varepsilon_1\mu_1)^{1/2}/(\varepsilon\mu)^{1/2}$ is the refractive index with respect to the ambient medium, ε_1 and μ_1 are the permittivity and permeability of the sphere and ε and μ are the permittivity and permeability of the ambient medium. The functions $j_n(z)$ and $y_n(z)$, and $h_n^{(1)}(z)=j_n(z)+iy_n(z)$, are **spherical Bessel** functions of order n of the arguments, $z= x$ or mx, respectively. The derivatives follow from the spherical Bessel functions themselves, namely

$$[zj_n(z)]' = zj_{n-1}(z) - nj_n(z);\ [zh_n^{(1)}(z)]' = zh_{n-1}^{(1)}(z) - nh_n^{(1)}(z) \tag{4.7}$$

Relationships exist between Bessel and spherical Bessel functions:

$$j_n(z) = \sqrt{\frac{\pi}{2z}} J_{n+0.5}(z) \tag{4.8}$$

$$y_n(z) = \sqrt{\frac{\pi}{2z}} Y_{n+0.5}(z) \tag{4.9}$$

Here, J_ν and Y_ν are **Bessel** functions of the **first and second kind**; for n=0 and 1 the spherical Bessel functions are given (BH, p. 87) by

$$\begin{aligned} j_0(z) &= \sin z / z; \quad j_1(z) = \sin z / z^2 - \cos z / z \\ y_0(z) &= -\cos z / z; \quad y_1(z) = -\cos z / z^2 - \sin z / z \end{aligned} \tag{4.10}$$

and the recurrence formula can be used to obtain higher orders

$$f_{n-1}(z) + f_{n+1}(z) = \frac{2n+1}{z} f_n(z) \tag{4.11}$$

where f_n is any of the functions j_n and y_n. Power-series expansions for small arguments of j_n and y_n are given on p. 130 of BH. The **spherical Hankel** Functions are linear combinations of j_n and y_n. Here, the first type is required

$$h_n^{(1)}(z) = j_n(z) + iy_n(z) \tag{4.12}$$

The related **Riccati-Bessel** Functions will also be used:

$$\psi_n(z) = zj_n(z);\ \chi_n(z) = -zy_n(z);\ \xi_n(z) = zh_n^{(1)}(z) \tag{4.13}$$

By proper transformation of (4.5) we get expressions that are more suitable for numerical computations; at the same time, the most delicate functions, $\psi_n(mx)=mx\cdot j_n(mx)$, and their derivatives are eliminated in the equations for the scattered field (Mie_ab and Mie2_ab). The function $\psi_n(mx)$ and its derivative diverge for lossy media, and the effect is especially strong for metals. On the other hand, the **logarithmic derivative** D_n of ψ_n

$$D_n = \frac{\psi_n'(mx)}{\psi_n(mx)} = \frac{[mx \cdot j_n(mx)]'}{mx \cdot j_n(mx)} \tag{4.14}$$

remains finite except for $x\to 0$. The function $D_n(z)$ with the complex argument $z=mx$ is computed as described in BH in Section 4.8, by downward recurrence

$$D_{n-1}(z) = \frac{n}{z} - \frac{1}{D_n(z) + n/z} \tag{4.15}$$

starting at n=nstart=round(max(n_{max},abs(z))+16), by using D_{nstart}=0, and ending at n=2. The values of D_1 to D_{nmax} are used by the (user-defined) **MATLAB Functions** `Mie(m, x)` for $\mu_1=\mu$ and `Mie2(eps1,mu1,x)` for $\mu_1\neq\mu$, i.e. magnetic spheres. Dividing nominator and denominator of the expression for a_n in (4.5) by $\psi_n(mx)=mx\cdot j_n(mx)$ we get

$$a_n = \frac{\mu m[xj_n(x)]' - \mu_1 xj_n(x)D_n(mx)}{\mu m[xh_n^{(1)}(x)]' - \mu_1 xh_n^{(1)}(x)D_n(mx)} = \frac{\psi_n'(x) - \psi_n(x)D_n(mx)\mu_1/(\mu m)}{\xi_n'(x) - \xi_n(x)D_n(mx)\mu_1/(\mu m)}$$
$$= \frac{[D_n(mx)\mu_1/(\mu m) + n/x]\psi_n(x) - \psi_{n-1}(x)}{[D_n(mx)\mu_1/(\mu m) + n/x]\xi_n(x) - \xi_{n-1}(x)} = \frac{[D_n(mx)z_1 + n/x]\psi_n(x) - \psi_{n-1}(x)}{[D_n(mx)z_1 + n/x]\xi_n(x) - \xi_{n-1}(x)} \quad (4.16)$$

Correspondingly, using the same transformation, we get for b_n

$$b_n = \frac{[D_n(mx)/z_1 + n/x]\psi_n(x) - \psi_{n-1}(x)}{[D_n(mx)/z_1 + n/x]\xi_n(x) - \xi_{n-1}(x)} \quad (4.17)$$

The impedance and refractive-index ratios z_1 and m, respectively, between inside and outside of the sphere are given by

$$z_1 = \frac{\mu_1}{\mu m} = \frac{\sqrt{\mu_1/\varepsilon_1}}{\sqrt{\mu/\varepsilon}}; \quad m = \frac{\sqrt{\mu_1\varepsilon_1}}{\sqrt{\mu\varepsilon}} \quad (4.18)$$

The coefficients of the internal field, including magnetic effects, are given by

$$c_n = \frac{\mu_1 j_n(x)[xh_n^{(1)}(x)]' - \mu_1 h_n^{(1)}(x)[xj_n(x)]'}{\mu_1 j_n(mx)[xh_n^{(1)}(x)]' - \mu h_n^{(1)}(x)[mxj_n(mx)]'}$$
$$d_n = \frac{\mu_1 m j_n(x)[xh_n^{(1)}(x)]' - \mu_1 m h_n^{(1)}(x)[xj_n(x)]'}{\mu m^2 j_n(mx)[xh_n^{(1)}(x)]' - \mu_1 h_n^{(1)}(x)[mxj_n(mx)]'} \quad (4.19)$$

Note that the function $j_n(mx)$ and its derivative cannot be eliminated in (4.19). However, as they appear in the denominator only, their divergence just leads to diminishing values of c_n and d_n. The computation of the functions with the real argument x is done by directly calling the **MATLAB built-in Bessel Functions**.

Mie Coefficients for coated spheres

MATLAB Functions: Miecoated_ab*opt*(m1, m2, x, y) produce a_n and b_n, for n=1 to n_{max} for Option *opt*=1, 2, 3.

Mie Coefficients a_n and b_n of coated spheres can be used in the same way as those for homogeneous spheres (BH, Section 8.1) to compute cross sections and scattering diagrams. Their model assumes non-magnetic materials. The sphere has an **inner (core) radius** a with size parameter $x = ka$ (k is the wave number in the ambient medium) and m_1 is the inner-medium refractive index relative to the ambient medium, an **outer (coating) radius** b with relative refractive index m_2, and size parameter $y = kb$.

One form (**Option 1**) used to compute the Mie Coefficients of coated spheres is the following (as presented in Appendix B of BH, p. 483):

$$a_n = \frac{(\widetilde{D}_n/m_2 + n/y)\psi_n(y) - \psi_{n-1}(y)}{(\widetilde{D}_n/m_2 + n/y)\xi_n(y) - \xi_{n-1}(y)}; \quad b_n = \frac{(m_2\widetilde{G}_n + n/y)\psi_n(y) - \psi_{n-1}(y)}{(m_2\widetilde{G}_n + n/y)\xi_n(y) - \xi_{n-1}(y)} \quad (4.20)$$

$$\widetilde{D}_n = \frac{D_n(m_2y) - A_n\chi_n'(m_2y)/\psi_n(m_2y)}{1 - A_n\chi_n(m_2y)/\psi_n(m_2y)}; \quad \widetilde{G}_n = \frac{D_n(m_2y) - B_n\chi_n'(m_2y)/\psi_n(m_2y)}{1 - B_n\chi_n(m_2y)/\psi_n(m_2y)}$$

$$A_n = \psi_n(m_2x)\frac{mD_n(m_1x) - D_n(m_2x)}{mD_n(m_1x)\chi_n(m_2x) - \chi_n'(m_2x)};$$

$$B_n = \psi_n(m_2x)\frac{D_n(m_1x)/m - D_n(m_2x)}{D_n(m_1x)\chi_n(m_2x)/m - \chi_n'(m_2x)}; \quad m = \frac{m_2}{m_1}$$

The computation of these coefficients can cause problems for certain combinations of the parameters (m1, m2, x, y) because of the diverging nature of some of the functions used (see e.g. Figures in the Appendix of the report Mätzler 2002b and the discussion in Appendix B of BH). Therefore three different options are available for tests and comparisons. Under good conditions, the results of all options are the same. Problems are indicated if the results

differ noticeably or if *NaN* values are returned. Option 1 uses the computation as formulated above, and the recurrence relation (4.15) for D_n. Careful treatment of diverging functions (e.g. avoiding direct products of them) is applied. **Option 2** uses the formulation on p. 183 of BH. The option is selected by the Option Parameter, *opt*, in MATLAB Function Miecoated (see below). Standard is *opt*=1.

4.3 Mie Efficiencies

MATLAB functions:
Mie(m, x) computes *Qext, Qsca, Qabs, Qb, g*=<*costeta*>, for non-magnetic spheres
Mie2(eps1, mu1, x) computes *Qext, Qsca, Qabs, Qb,* <*costeta*>, for magnetic spheres
Miecoated(m1,m2,x,y,opt) computes *Qext, Qsca, Qabs, Qb,* <*costeta*>, for non-magnetic, coated spheres for size parameters x and y, of core and coating, respectively, Option (*opt*=1,2,3).
Mie_xscan(m, nsteps, dx) and Mie2_xscan(eps1, mu1, nsteps, dx) are used to plot the efficiencies versus size parameter x in a number (nsteps) of steps with increment dx from x=0 to x=nsteps·dx.
Miecoated_*i*scan(m1,m2,y,nsteps), where *i*=w, wr, pr are used to plot the efficiencies (for given y) versus volumetric fraction w of the coating, fractional thickness wr and pr of core and coating, respectively, and Option for Miecoated is *opt*=1.

The efficiencies Q_i for the interaction of radiation with a sphere are cross sections σ_i normalised to the geometrical particle cross section, $\sigma_g=\pi a^2$, ($\sigma_g=\pi b^2$, in case of coated spheres), where *i* stands for extinction (*i*=*e*), absorption (*i*=*a*), scattering (*i*=*s*), backscattering (*i*=*b*), and radiation pressure (*i*=*pr*), thus

$$Q_i = \frac{\sigma_i}{\sigma_g} \tag{4.21}$$

$$Q_s = \frac{2}{x^2}\sum_{n=1}^{\infty}(2n+1)(|a_n|^2 + |b_n|^2) \tag{4.22}$$

$$Q_e = \frac{2}{x^2}\sum_{n=1}^{\infty}(2n+1)\,\mathrm{Re}(a_n + b_n) \tag{4.23}$$

and Q_a follows from the difference of (4.23) and (4.22). All infinite series can be truncated after n_{max} terms. Furthermore, the asymmetry parameter $g=\langle\cos\vartheta\rangle$ indicates the average cosine of the **scattering angle** ϑ with respect to power; it is used e.g. in Two-Stream Models (Meador and Weaver, 1980), and it is related to the efficiency Q_{pr} of radiation pressure:

$$Q_{pr} = Q_e - Q_s\langle\cos\vartheta\rangle \tag{4.24}$$

$$Q_s\langle\cos\vartheta\rangle = \frac{4}{x^2}\left\{\sum_{n=1}^{\infty}\frac{n(n+2)}{n+1}\mathrm{Re}(a_n a_{n+1}^* + b_n b_{n+1}^*) + \sum_{n=1}^{\infty}\frac{2n+1}{n(n+1)}\mathrm{Re}(a_n b_n^*)\right\}$$

Finally, the backscattering efficiency Q_b, applicable to monostatic radar, is given by

$$Q_b = \frac{1}{x^2}\left|\sum_{n=1}^{\infty}(2n+1)(-1)^n(a_n - b_n)\right|^2 \tag{4.25}$$

4.4 The internal field

The internal field $\mathbf{E}_1$ for an incident field with unit amplitude is given by

$$\mathbf{E}_1 = \sum_{n=1}^{\infty}\frac{2n+1}{n(n+1)}\left(c_n\mathbf{M}_{o1n}^{(1)} - d_n\mathbf{N}_{e1n}^{(1)}\right) \tag{4.26}$$

where the vector-wave harmonic fields are given in spherical (r,θ= ϑ,ϕ) coordinates by

$$\mathbf{M}_{o1n}^{(1)} = \begin{pmatrix} 0 \\ \cos\phi \cdot \pi_n(\cos\theta)\, j_n(rmx) \\ -\sin\phi \cdot \tau_n(\cos\theta)\, j_n(rmx) \end{pmatrix}$$

$$\mathbf{N}_{e1n}^{(1)} = \begin{pmatrix} n(n+1)\cos\phi \cdot \sin\theta \cdot \pi_n(\cos\theta) \dfrac{j_n(rmx)}{rmx} \\ \cos\phi \cdot \tau_n(\cos\theta) \dfrac{[rmx j_n(rmx)]'}{rmx} \\ -\sin\phi \cdot \pi_n(\cos\theta) \dfrac{[rmx j_n(rmx)]'}{rmx} \end{pmatrix} \tag{4.27}$$

and the coordinate system is defined as for the scattered field. The vector-wave functions **N** and **M** are orthogonal with respect to integration over directions. Furthermore for different values of n, the **N** functions are orthogonal, too, and the same is true for the **M** functions.

4.5 Computation of Q_a, based on the internal fields

MATLAB functions:

Mie_Esquare(m, x, nj), Mie2_Esquare(eps1, mu1, x, nj) to compute the absolute-squared electrical field inside the sphere (for nj values of kr from 0 to x)

Mie_abs(m, x), Mie2_abs(eps1, mu1, x) to compute the absorption coefficient, based on Ohmic losses (and including magnetic losses in case of Mie2_abs)

Dielectric losses only

The absorption cross section of a particle with dielectric (i.e. Ohmic) losses is given by $\sigma_a = k\varepsilon'' \int_V |\mathbf{E}_1|^2 dV$ where ε" is the imaginary part of the relative dielectric constant of the particle (here with respect to the ambient medium). Thanks to the orthogonality of spherical vector-wave functions, this integral becomes in spherical coordinates

$$\sigma_{abs} = k\varepsilon'' \pi \sum_{n=1}^{\infty} \int_{-1}^{+1} d(\cos\theta) \int_0^a r^2 dr \left(|c_n|^2 (m_\theta + m_\phi) + |d_n|^2 (n_r + n_\theta + n_\phi) \right) \tag{4.28}$$

The integration over azimuth ϕ has already been performed. The functions in the integrand are absolute-square values of the series terms of the components of the vector-waves

$$\begin{aligned} m_\theta &= g_n \pi_n^2(\cos\theta) \cdot |j_n(z)|^2 \\ m_\phi &= g_n \tau_n^2(\cos\theta) \cdot |j_n(z)|^2 \\ n_r &= g_n \sin^2\theta \cdot \pi_n^2(\cos\theta) \left| \frac{j_n(z)}{z} \right|^2 \\ n_\theta &= g_n \tau_n^2(\cos\theta) \left| \frac{(z j_n(z))'}{z} \right|^2 \\ n_\phi &= g_n \pi_n^2(\cos\theta) \left| \frac{(z j_n(z))'}{z} \right|^2 \end{aligned} \tag{4.29}$$

Here z=mrk, and g_n stands for

$$g_n = \left(\frac{2n+1}{n(n+1)} \right)^2 \tag{4.30}$$

For the integrals over cosθ, analytic solutions can be obtained. First, from BH we find

$$\int_{-1}^{1}\left(\pi_n^2(\cos\theta)+\tau_n^2(\cos\theta)\right)d(\cos\theta)=\frac{2n^2(n+1)^2}{2n+1} \tag{4.31}$$

and second, from (4.46) in BH and Equation 8.14.13 of Abramowitz and Stegun (1965), we get

$$\int_{-1}^{1}\left(\sin^2\theta\cdot\pi_n^2(\cos\theta)\right)d(\cos\theta)=\int_{-1}^{1}\left(P_n^1(\cos\theta)\right)^2 d(\cos\theta)=\frac{2(n+1)}{2n+1} \tag{4.32}$$

leading to the two parts of the angular integral in (4.28)

$$m_n=\int_{-1}^{1}\left(m_\theta+m_\phi\right)d(\cos\theta)=2(2n+1)\left|j_n(z)\right|^2 \tag{4.33}$$

$$n_n=\int_{-1}^{1}(n_r+n_\theta+n_\phi)d(\cos\theta)=2n(2n+1)\left\{(n+1)\left|\frac{j_n(z)}{z}\right|^2+\left|\frac{(zj_n(z))'}{z}\right|^2\right\} \tag{4.34}$$

Now, the absorption cross section follows from integration over the radial distance *r* inside the sphere up to the sphere radius *a*:

$$\sigma_a=k\varepsilon''\pi\sum_{n=1}^{\infty}\int_0^a\left(m_n\left|c_n\right|^2+n_n\left|d_n\right|^2\right)r^2dr \tag{4.35}$$

The integrand contains the radial dependence of the absolute-square electric field $\left\langle\left|\mathbf{E}\right|^2\right\rangle$ averaged over spherical shells (all θ and ϕ, constant *r*):

$$\left\langle\left|\mathbf{E}\right|^2\right\rangle=\frac{1}{4}\sum_{n=1}^{\infty}\left(m_n\left|c_n\right|^2+n_n\left|d_n\right|^2\right) \tag{4.36}$$

and in terms of this quantity, the absorption efficiency becomes

$$Q_a=\frac{4\varepsilon''}{x^2}\int_0^x\left\langle\left|\mathbf{E}\right|^2\right\rangle x'^2\,dx' \tag{4.37}$$

where *x'=rk=z/m*. Note that (4.36) is dimensionless because of the unit-amplitude incident field; In case of Rayleigh scattering (*x*<<1) the internal field is constant, and the corresponding squared-field ratio (4.34) is given by $\frac{9}{\left|m^2+2\right|^2}$. This quantity can be used to test the accuracy of the function, mie_Esquare, for small size parameters. In addition, Equation (4.37) or (4.38) can be used to test the accuracy of the computation of Q_a from the difference, $Q_e - Q_s$.

Dielectric and magnetic losses

For spheres including magnetic losses, the absorption efficiency also includes a magnetic current, the equivalent term due to the imaginary part μ"=imag(μ1/μ) of the magnetic permeability. By duality (Kong, 1986), the electrical field **E** has to be replaced by the magnetic field **H**, thus

$$Q_{abs}=\frac{4\varepsilon''}{x^2}\int_0^x\left\langle\left|\mathbf{E}\right|^2\right\rangle x'^2\,dx'+\frac{4\mu''}{x^2}\int_0^x\left\langle\left|\mathbf{H}\right|^2\right\rangle x'^2\,dx' \tag{4.38}$$

and $\left\langle\left|\mathbf{H}\right|^2\right\rangle$ is obtained by interchanging μ_1/μ=mu1 and $\varepsilon_1/\varepsilon$=eps1, i.e. calling Mie2_Esquare(mu1, eps1, x, nj).

4.6 Examples and tests

The situation of x=1, m=1000+1000i

Metals are characterised by large imaginary permittivity; the chosen value is an example of a metal-like sphere The execution of the command line
>> m =1000 + 1000i; x = 1; mie_ab(m,x)

returns the vectors [a_n; b_n] for n=1 to n_{max}=7:
0.2926 - 0.4544i 0.0009 - 0.0304i 0.0000 - 0.0008i 0.0000 - 0.0000i
0.0455 + 0.2077i 0.0003 + 0.0172i 0.0000 + 0.0005i 0.0000 + 0.0000i
0.0000 - 0.0000i 0.0000 - 0.0000i 0.0000 - 0.0000i
0.0000 + 0.0000i 0.0000 + 0.0000i 0.0000 + 0.0000i

whereas the function mie_cd(m,x) returns zeros.

Magnetic sphere with x=2, eps1=2+i, mu1=0.8+0.1i

The command line
>> eps1=2+1i; mu1=0.8+0.1i; x=2; mie2_ab(eps1,mu1,2)
leads to the Mie Coefficients [a_n; b_n] for n=1 to n_{max}=9:
0.3745 - 0.1871i 0.1761 - 0.1301i 0.0178 - 0.0237i 0.0010 - 0.0016i
0.3751 + 0.0646i 0.0748 + 0.0294i 0.0068 + 0.0044i 0.0004 + 0.0003i
0.0000 - 0.0001i 0.0000 - 0.0000i 0.0000 - 0.0000i 0.0000 - 0.0000i
0.0000 + 0.0000i 0.0000 + 0.0000i 0.0000 + 0.0000i 0.0000 + 0.0000i
0.0000 - 0.0000i
0.0000 + 0.0000i

whereas the command line
>>mie2(eps1,mu1,2)
returns the Mie Efficiencies Qe, Qs, Qa, Qb, *g*=<costeta> and Qb/Qs
= 1.8443, 0.6195, 1.2248, 0.0525, 0.6445, 0.0847

and the command line
>>mie2_abs(eps1,mu1,2)
gives the absorption efficiency by the alternative way

Qabse = 0.9630
Qabsm = 0.2618
sum = 1.2248

Here Qabse is the absorption efficiency due to the electrical field (Ohmic losses), Qabsm due to the magnetic field, and sum is the sum, i.e. the total absorption efficiency, in agreement with the third number of the result of Mie2(eps1, mu1, x), s. above.

Mie Efficiencies are plotted versus x ($0 \le x \le 5$) by Mie2_xscan(eps1, mu1, 501, 0.01) in Figure 4.1a. To plot the angular dependence of the scattered power in the two polarisations, the function Mie2_tetascan(eps1,mu1,x,201), for x=0.2, is used to provide Figure 4.1b.

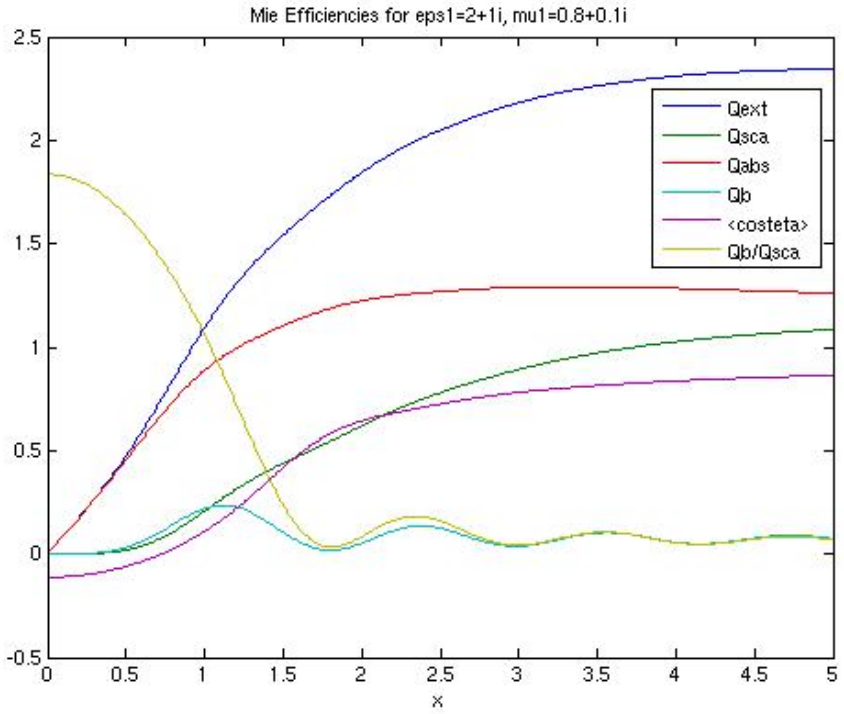

Figure 4.1a: Mie Efficiencies versus size parameter for a sphere with ε= 2+i, μ=0.8+0.1i.

mie2_xscan(eps1, mu1, 501, 0.01)

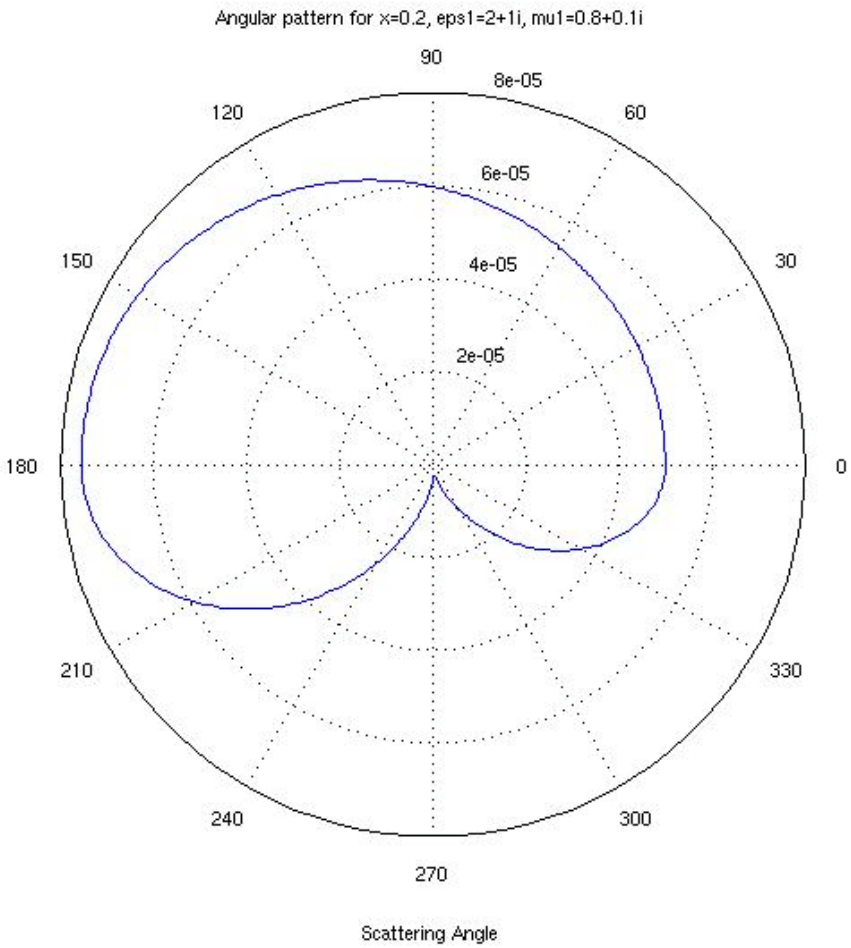

Figure 4.1b: Mie angular pattern for a sphere where S1 is shown in the upper and S2 in the lower half circle, with x=0.2, ε= 2+i, μ=0.8+0.1i. Note that here backscattering is stronger than forward scattering, in agreement with negative values of $< \cos \vartheta >$ at x=0.2 in upper figure.

mie2_tetascan(eps1,mu1,x,201), for *x*=0.2

Coated sphere

Typical examples are melting ice particles (hail). Also the opposite, freezing rain drops may occur. For water we assume a refractive index m_w=4+2i, and for ice we assume a real value m_i=1.8 (approximate values at 40 GHz, 0°C). Figure 4.2 shows the result of the Mie efficiencies. Note the difference in scale of the x axis, representing the relative thickness of the coating.

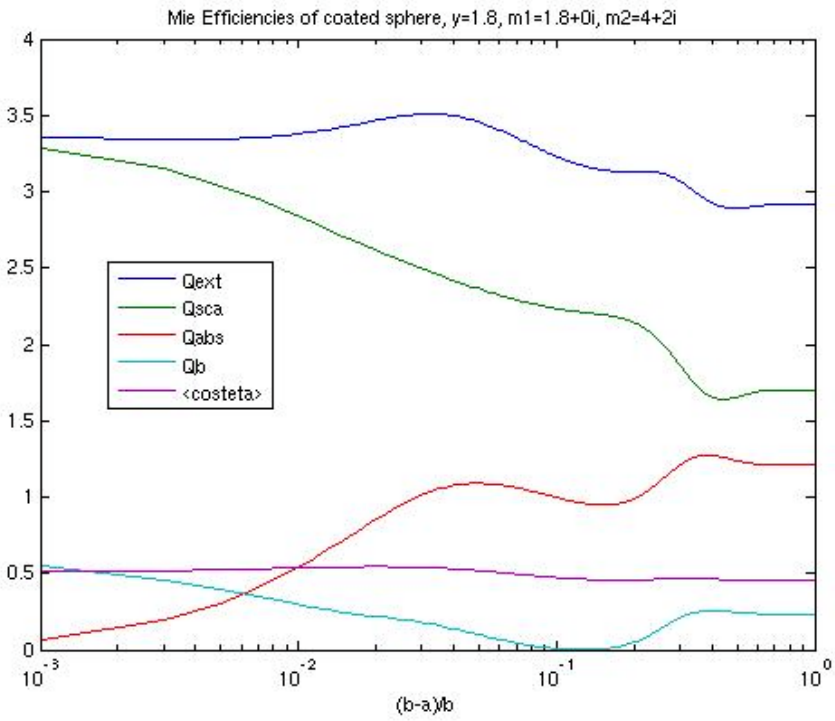

Figure 4.2a: Mie Efficiencies versus relative thickness (logarithmic scale) of coating for a sphere representative for a **melting graupel**, i.e. an ice core with a water coating, at a frequency near 40 GHz, size parameter $y = kb = 1.8$.

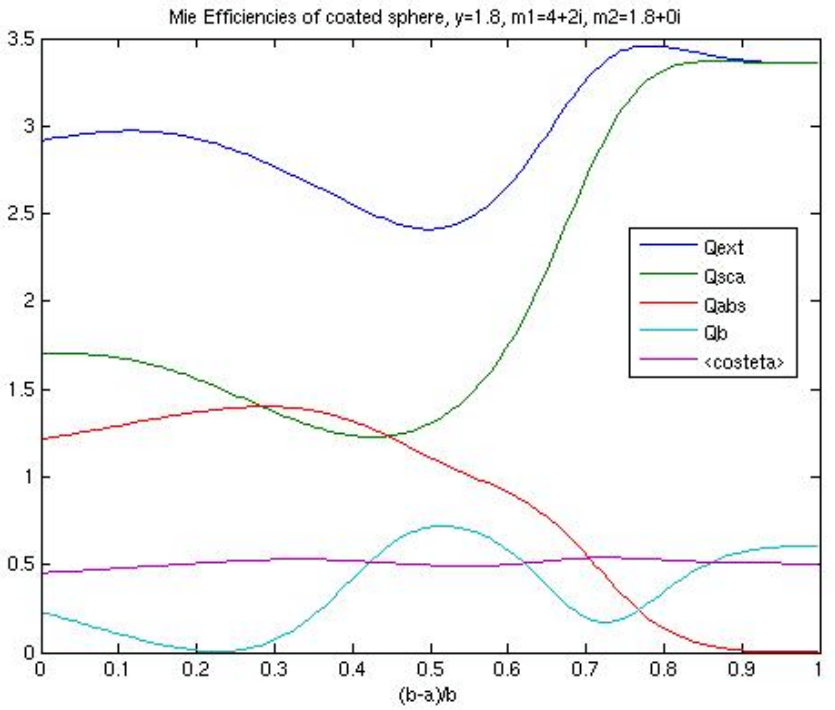

Figure 4.2b: Mie Efficiencies versus relative thickness of coating for a **freezing raindrop**, i.e. a water core with an ice coating, at a frequency near 40 GHz size parameter $y = kb = 1.8$.

Absorption is a result of the water losses only. Whereas a thin water coating already has a significant influence on absorption (Fig. 4.2a), a small water core (Fig. 4.2b) seems to be well shielded from electric fields, and thus $Q_a \to 0$. Scattering and backscattering behave quite differently. In addition the behaviour depends on all variables, and especially on y. Try other examples, using the **MATLAB function**: `miecoated_wrscan(m1,m2,y,nsteps)`.

The absolute-square internal **E** field is plotted versus the radial distance for *x*=5 by calling Mie2_Esquare(eps1,mu1,x,201). Examples for the electric field variation are shown in Figure 4.3 for two situations. In the first example the field is concentrated near the sphere surface due to the limited field penetration into the lossy material. The second example is typical for the strong field heterogeneity in large, low-loss spheres.

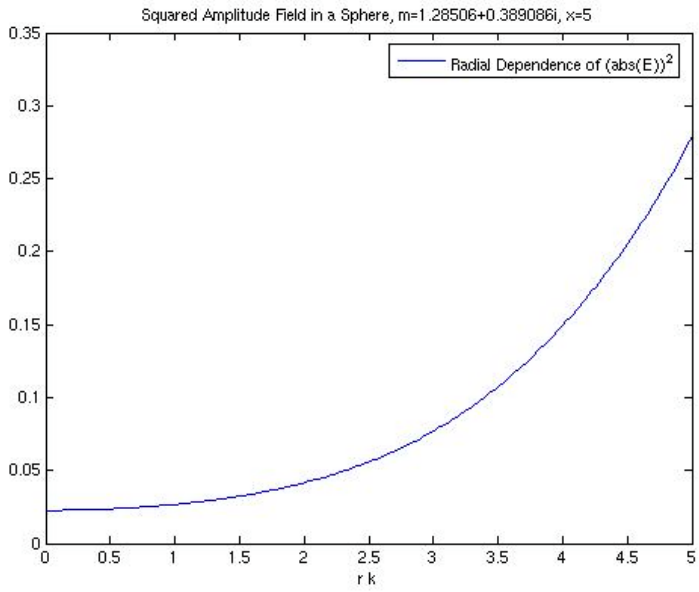

Figure 4.3a: Radial variation of the squared electric field for a dielectric sphere with ε= 2+i, μ=0.8+0.1i, x=5. The high losses lead to a decreasing field with increasing depth from the sphere surface.

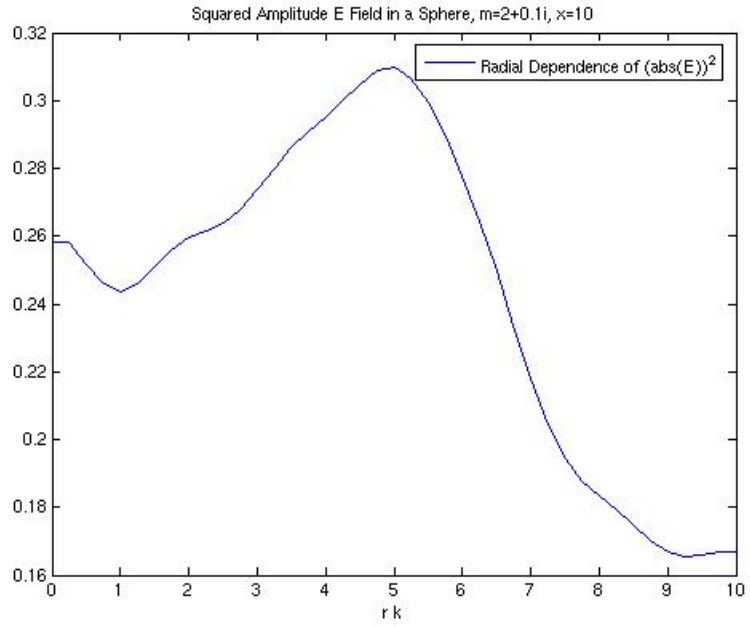

Figure 4.3b: Radial variation of the squared electric field for a dielectric sphere with $m=\sqrt{\varepsilon}=$2+0.1i, x=10. For x$\rightarrow$0, the values converge to the Rayleigh scattering result of Equation (3.2) giving a constant value of 0.250.

4.7 Extinction Paradox

See also van de Hulst (1957, p. 107). The **Extinction Paradox** follows from the fact that for large scatterers, here for spheres with x>>1, the extinction efficiency approaches $Q_e = 2$. As an example let us compute mie(m=3+0.001i,x=50'000) to find
(Qe, Qs, Qa, Qb, $g=\langle \cos\vartheta \rangle$, Qb/Qs)= (2.0015, 1.2775, 0.7240, 0.2500, 0.7998, 0.1957).
It means that the amount of radiative power lost from the incident radiation is twice as much as geometrically intercepted by the scatterer. The result is in contradiction to geometrical optics where we would expect $Q_e = 1$. Geometrical optics should be valid for sufficiently large spheres. How can this paradox be explained?

In short, both results can be true. The selection about which one is valid depends on the type of experiment. As an example, the shadow on the following image

corresponds to the size of the mountain, Niesen, with $Q_e = 1$, but a dust particle or a meteorite in space between a star and a telescope will screen twice this light ($Q_e = 2$). Let us recall that in the assumption made (by choosing the far field $R >> D^2/\lambda$ as the observation position) all affected radiation, including scattering at small ϑ, is counted as removed, and that the propagating wave is a plane wave without any shadow (smeared by diffraction). The assumption may be valid in the second example but not in the first one. Even in the second one we may have to choose an effective value $Q_e = 1$ (or $Q_e^* = 1$, see below), if the telescope cannot distinguish the direct star light from the halo of the diffracted radiation.
Now we are ready to understand the result of $Q_e = 2$: A first contribution of 1 to Q_e results from radiation intercepted by the large particle due to absorption and scattering. Besides that we have **diffraction**, forming an angular pattern that is identical with the diffraction through a hole of area σ_g by **Babinet's Principle** (Kong, 1985), giving the same contribution again. The total radiation removed from the wave corresponds to a total cross section $2\sigma_g$, i.e. $Q_e = 2$.

4.8 Lorenz-Mie scattering without diffraction

The diffraction peak can be a disturbing feature. Scattering in the forward direction does not appear as a loss if $\vartheta <$ than the resolution of the observing instrument. Also radiative transfer models may be unable to handle strongly peaked scattering functions. There is a need to separate the diffraction peak from the rest of the scattering function. We will discuss the situation for spheres (from Mätzler, 2004).
The scattered power is characterised by components S_R and S_L with polarisation perpendicula*R* and paralle*L* to the scattering plane.

$$S_R = \frac{|S_1|^2}{\pi x^2} = \frac{Q_{bi,R}}{4\pi} \quad \text{and} \quad S_L = \frac{|S_2|^2}{\pi x^2} = \frac{Q_{bi,L}}{4\pi} \tag{4.39}$$

With this normalisation, the integration of the sum $S=S_L+S_R$ over directions gives Q_s. For unpolarised illumination, such as sunlight, the scattered light becomes polarised with a **degree** ρ of **linear polarisation**:

$$\rho = \frac{S_R - S_L}{S_R + S_L} \tag{4.40}$$

Diffraction and its subtraction from the scattering signal

Parts of the scattering functions S_1 and S_2 are due to diffraction of the electromagnetic wave at the projected area of the sphere. The scalar **diffraction signal** representative for a planar, circular pattern of radius a, size parameter $x = ka$ is given by (BH, Section 4.4.3)

$$S_d = x^2 \frac{1+\cos\theta}{2} \cdot \frac{J_1(x\sin\theta)}{x\sin\theta} \tag{4.41}$$

where θ is the scattering angle. The scattered fields without diffraction become

$$E_{s\phi 0} = \frac{e^{ikr}}{ikr}\sin\phi\cdot(S_1 - S_d);\; E_{s\theta 0} = \frac{e^{ikr}}{-ikr}\cos\phi\cdot(S_2 - S_d) \tag{4.41}$$

Thus the S_i (i=1,2) are to be replaced by the differences $S_{i0} = S_i - S_d$ leading to the scattered power $S_0 = S_{L0} + S_{R0}$ of the **scattering patterns without diffraction**. The subtraction is performed at the field level (an alternative would be to subtract the signals at the power level, however, with a poorer quality of the peak removal due to the phase correlation near the forward direction).

The **MATLAB Function** `mie_tetascanall(m,x,nsteps,nsmooth,type)` computes the scattering amplitudes and plots their intensities. An example of a low-loss dielectric with m=1.44+10^{-5}i is shown below. Mie Efficiencies computed with `mie(m,x)`, the diffraction efficiency Q_d according to Equation (4.46), and the asymmetry parameter g are given.

x	Q_e	Q_s	Q_a	Q_b	Q_d	g
1	0.16711	0.16708	0.00003	0.14714	-	0.19335
2	1.36720	1.36711	0.00009	0.17569	-	0.64778
4	3.85533	3.85515	0.00019	0.42531	-	0.78837
10	2.25693	2.25635	0.00059	2.96921	0.52239	0.61738
20	2.62136	2.62050	0.00086	1.79805	1.13990	0.80666
40	2.32944	2.32771	0.00173	6.62629	1.05018	0.80999
100	2.10636	2.10239	0.00397	2.00493	1.01875	0.82599
200	2.00908	2.00193	0.00714	0.12152	0.98010	0.84008
400	2.03543	2.02080	0.01463	9.30592	1.00068	0.84094
1000	2.02624	1.99101	0.03523	21.9324	1.00279	0.84929
2000	2.00434	1.93629	0.06805	13.2710	0.99472	0.85376
4000	2.01376	1.88251	0.13124	5.05702	1.00470	0.86224
10000	2.00597	1.71366	0.29129	8.97102	1.00081	0.87975

Table 4.2: Mie Efficiencies Q_j for extinction (j=e), scattering (j=s), absorption (j=a), backscattering (j=b) and diffraction (j=d), and asymmetry parameter g for m=1.44+10^{-5}i, x=1 to 10^4.

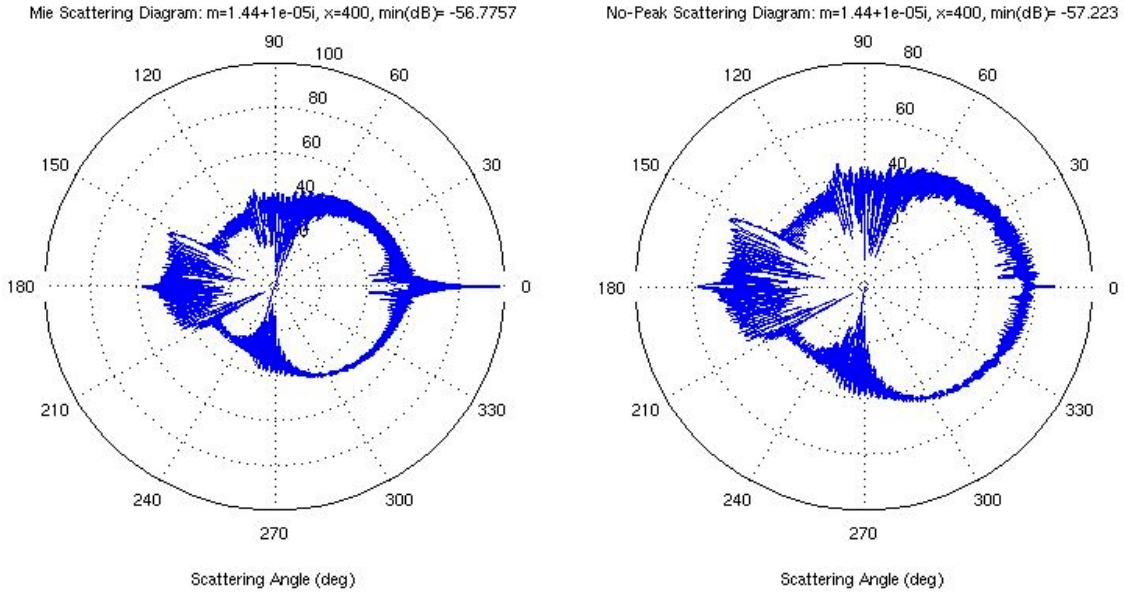

Figure 4.4: Angular scattering diagram in logarithmic (dB) scale with (left) and without (right) diffraction peak for m=1.44+10^{-5}i, x=400, S_1 upper, S_2 lower semicircle. Values normalised at the origin (0dB) to minimum.

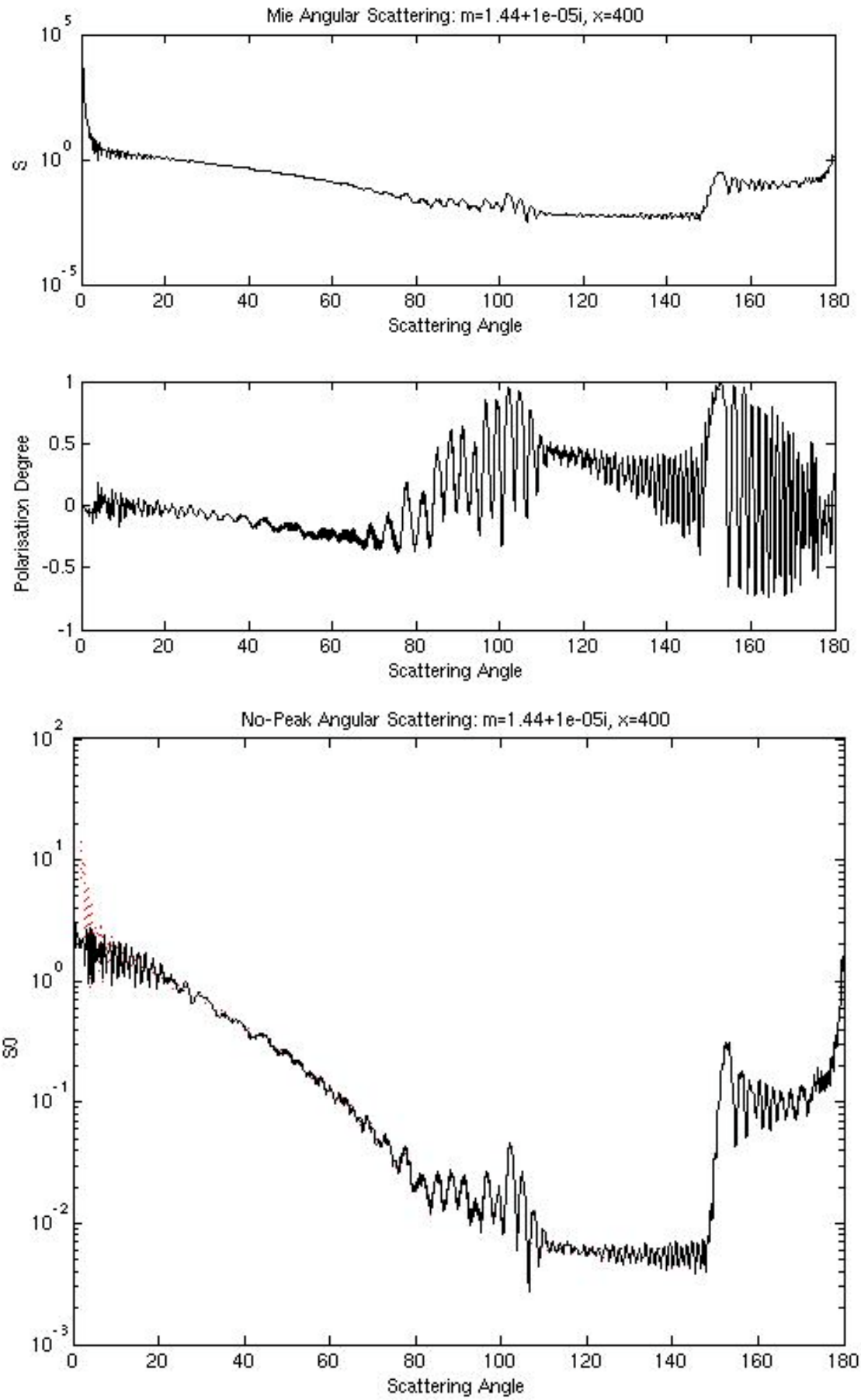

Figure 4.5: S (uppermost curve), S_0 (lowest curve), both in logarithmic scale, and degree of linear polarisation (middle curve) for m=1.44+10^{-5}i, x=400. Note glory (180°), first (151°) and second (105°) rainbow.

Figures 4.4 and 4.5 show angular plots obtained with mie_tetascanall for m=1.44+10^{-5}i, x=400, nsteps=10000, nsmooth=30, type='log'. Note the high linear polarisation near the first and second rainbow. The numerical results returned are (gi and g0i to be explained later):

S: [10000x9 double], Q: [2.0354 2.0208 0.0146 9.3059 1.0007 0.8409]
gi: [0.8410 0.7625 0.6214 0.5806 0.5261 0.5177 0.5102 0.4994 0.5010 0.4934]
g0i: [0.6858 0.5318 0.2544 0.1749 0.0675 0.0500 0.0338 0.0107 0.0130 -0.0019]

Beam efficiency and effective scattering efficiency

The **beam efficiency** η_b is a quantity known from antenna theory to describe the fraction of the radiation contained in the main lobe. In analogy, here η_b can be defined as the fraction of radiation scattered in a given angular range, such as the forward peak. This quantity depends on the scattering angle θ_{lim} at the upper limit of integration

$$\eta_b(\theta_{lim}) = \frac{1}{Q_{sca}} \int_0^{\theta_{lim}} S(\theta) \sin\theta \cdot d\theta \; ; \quad \eta_{b0}(\theta_{lim}) = \frac{1}{Q_{sca}} \int_0^{\theta_{lim}} S_0(\theta) \sin\theta \cdot d\theta \qquad (4.42)$$

The normalisation of S according to Equation (4.39) requires η_b =1 for θ_{lim} =π, which was used to test the numerical integration. An example with θ_{lim} ranging from very small values to π is shown in Figure 4.7 for x=400. The respective directional integration over S_0 gives η_{b0}; the result is also shown in Figure 4.7. These values are smaller because the diffraction peak is missing, and $\eta_{b0}(\theta_{lim})$ increases slowly with θ_{lim}, mostly in parallel to η_b beyond the diffraction angles. The difference

$$\eta_{bd} = \eta_b - \eta_{b0} \qquad (4.43)$$

shown as dotted line in Figure 4.6, corresponds to the beam efficiency of the diffraction signal. The dotted curve reaches constant values already for small angles, i.e. about 2°. The width of the diffraction peak is on the order of 180°/x. With increasing x, $\eta_{bd}(\theta_{lim})$ approaches a **step function** in the semi-logarithmic representation of the Figure 4.6, thus indicating a clear distinction between diffraction at small θ_{lim} and more or less diffuse scattering above. A small, but distinct backward peak is also visible for η_b and η_{b0} at the right-hand side of Figure 4.6 as a manifestation of the **glory effect** (van de Hulst, 1957).

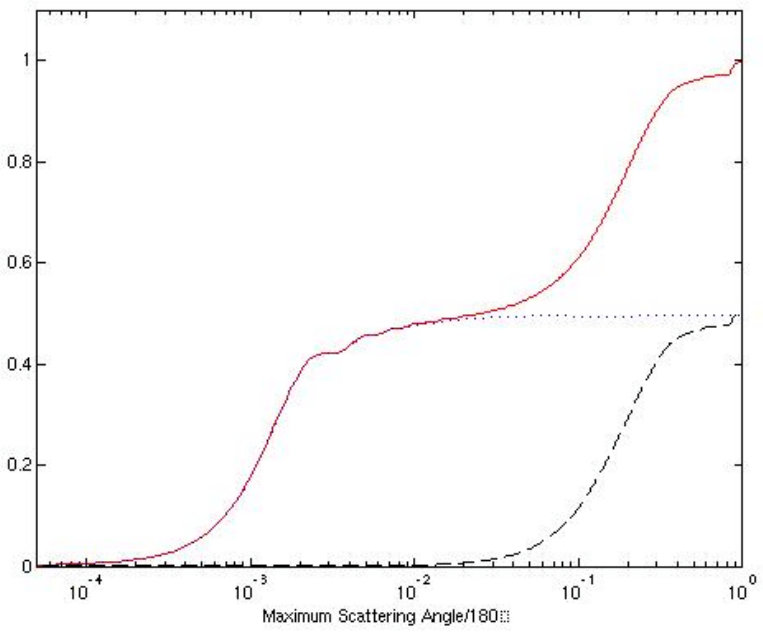

Figure 4.6: Beam efficiencies η_b (solid line) and η_{b0} (dashed) and their difference (dotted) of a dielectric sphere versus θ_{lim} for size parameter x=400, refractive index m=1.44+10^{-5}i. Absorption is almost negligible (Table 4.2) → maxima of the dashed and dotted lines are about equal and near 0.5.

The beam efficiencies can be used to estimate the effective scattering Q_s* and extinction Q_e* efficiencies (the absorption efficiency Q_a being unaffected) from the original values Q_s and Q_e = Q_a + Q_s where only the effect of scattering without diffraction is considered:

$$Q_s^* = Q_s - Q_s\eta_{bd};\ Q_e^* = Q_e - Q_s\eta_{bd} \tag{4.44}$$

Due to the step-like behaviour of η_{bd}, it is possible to avoid its dependence on θ_{lim}, at least for sufficiently large spheres, by choosing the value $\theta_{lim} = \pi$

$$\eta_{bd} = \eta_b(\pi) - \eta_{b0}(\pi) = 1 - \eta_{b0}(\pi) \tag{4.45}$$

The **diffraction efficiency** Q_d is related to η_{bd} by

$$Q_d = Q_s\eta_{bd} = Q_s - Q_s^* \ ; \quad x >> 1 \tag{4.46}$$

This quantity was computed from (4.45) by numerical integration according to (4.42). The results shown in Table 4.2 indicate that for sufficiently large x, Q_d is very close to 1. This means that $\eta_{bd} \cong 1/Q_s$ and

$$Q_s^* = Q_s - Q_d \cong Q_s - 1\ ;\ \ Q_e^* = Q_e - Q_d \cong Q_e - 1 \tag{4.47}$$

The result is not limited to the special value of m, but is generally valid for sufficiently large x, because the diffraction signal is independent of the physical properties of the sphere. If extinction is understood as the sum of losses by absorption, scattering and diffraction, the extinction paradox is resolved. After subtraction of the diffraction loss, the remaining extinction efficiency approaches $Q_e^* \to Q_e - 1 \to 1$ for $x \to \infty$.

Another example is presented in Table 4.3 for constant x=200 and variable m', covering the region around m' = 2 where the first rainbow merges with the backscatter peak, thus leading to enhanced backscatter; neither g nor Q_d seem to be strongly affected, all situations showing $Q_d \cong 1$.

m'	Q_e	Q_s	Q_a	Q_b	Q_d	g
1.2	2.099229	1.618585	0.480644	0.56835	1.05774	0.94924
1.3	2.041250	1.551503	0.489747	0.16558	0.97624	0.92507
1.4	2.049675	1.560148	0.489526	0.52057	0.99484	0.90501
1.5	2.075441	1.577244	0.498196	1.11266	1.03103	0.88640
1.6	2.041354	1.544187	0.497167	1.07622	0.97714	0.86441
1.7	2.062153	1.562900	0.499253	15.55968	1.00321	0.85068
1.8	2.067160	1.570164	0.496996	75.28368	1.01404	0.83251
1.9	2.053177	1.544784	0.508393	159.6981	0.99843	0.81382
2.0	2.070283	1.582501	0.487782	41.31594	1.01976	0.80902
2.1	2.062575	1.571687	0.490888	9.49542	1.00679	0.79171
2.2	2.053084	1.565909	0.487174	1.72237	1.00382	0.77902
2.3	2.080204	1.595842	0.484362	0.73189	1.02857	0.77294
2.4	2.032339	1.551666	0.480673	2.54836	0.97723	0.75444
2.5	2.057014	1.579909	0.477104	1.94581	0.99842	0.74733

Table 4.3: Mie Efficiencies Q_j for extinction (j=e), scattering (j=s), absorption (j=a), backscattering (j=b) and diffraction (j=d), and asymmetry parameters g for x=200, m=m'+0.001i, where m'=1.2 to 2.5.

4.9 Comparison of Mie results with approximations

Mie and Rayleigh

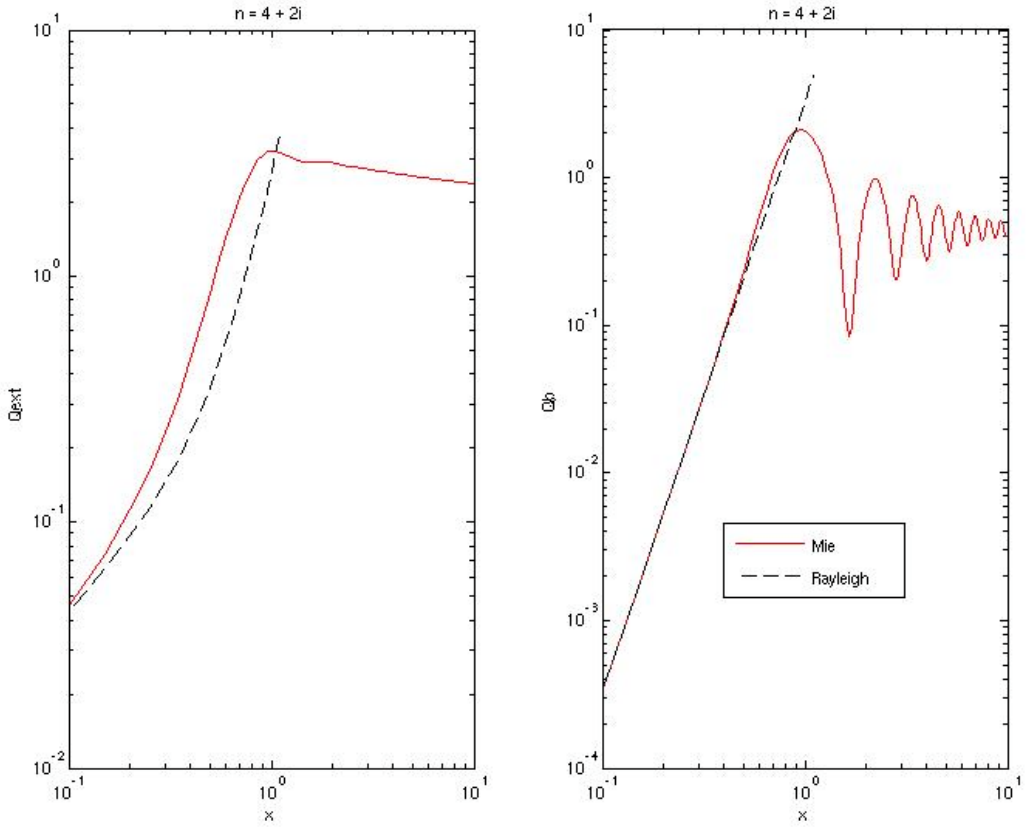

MATLAB: top: mierayleigxscan2(m=2+4i, nsteps=100, dx=0.1, xmax=1), bottom: mierayleigxscan1

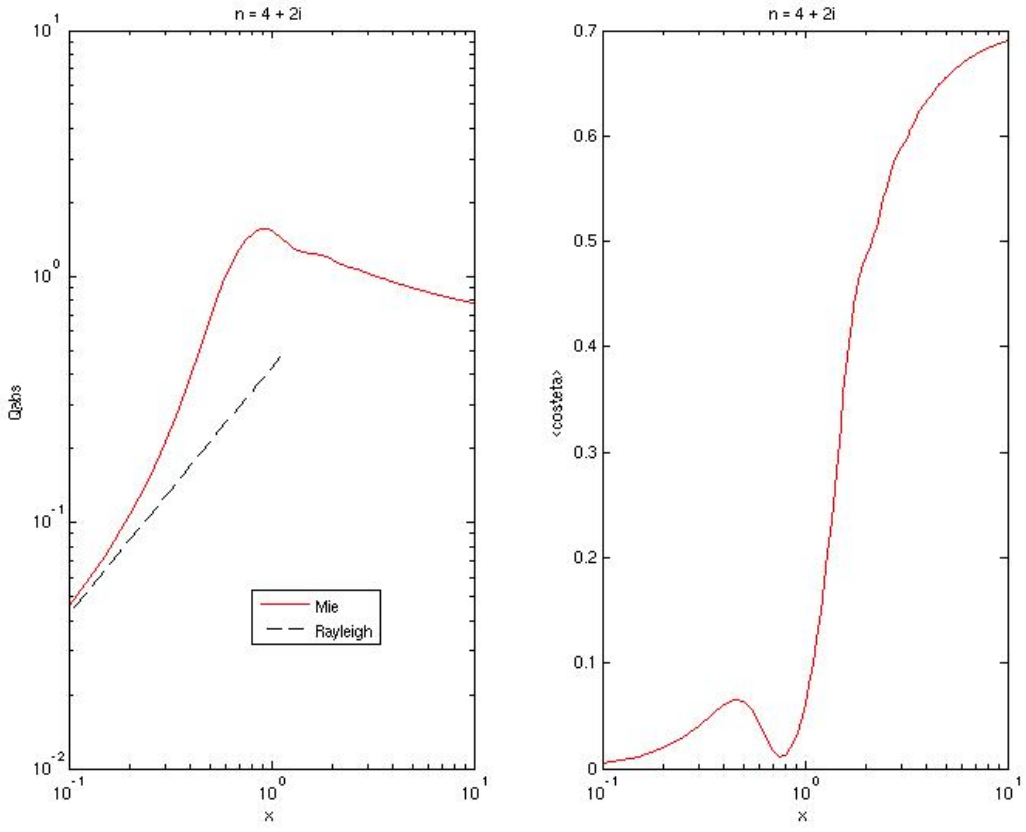

Figure 4.7: Extinction (upper left) and backscatter (upper right), absorption (lower left) efficiency and $\langle \cos \vartheta \rangle$ (lower right) versus x of a dielectric sphere with m=4+2i, comparison between Rayleigh and Mie scattering.

Whereas Rayleigh backscattering is quite accurate up to x=1, absorption often requires x<0.1.

Mie solution with limited number of spherical harmonics (nmax fixed)

MATLAB: miexscannmax(m, nsteps, dx, nmax)

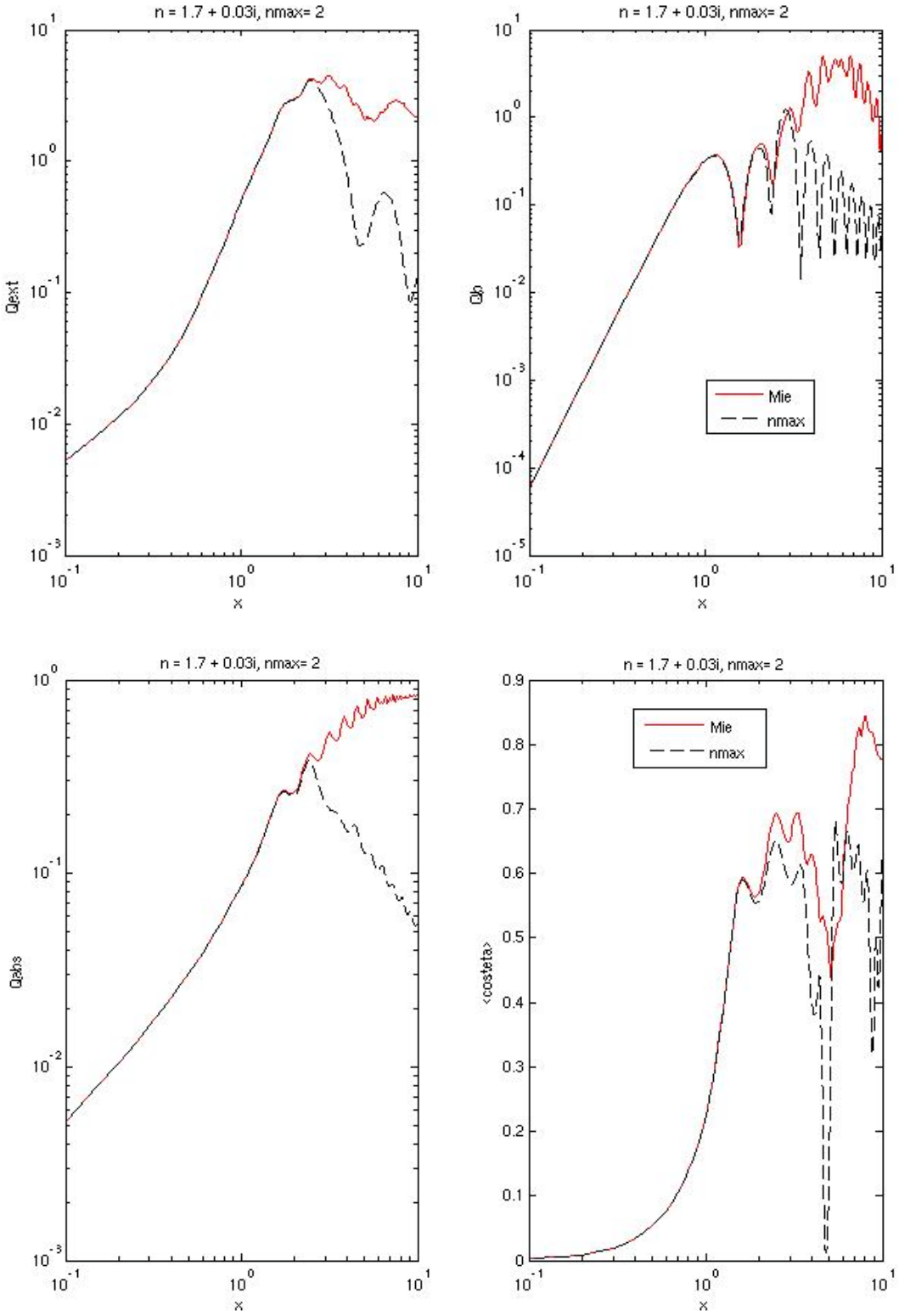

Figure 4.8: Extinction (upper left) and backscatter (upper right), absorption (lower left) efficiency and $\langle \cos\vartheta \rangle$ (lower right) versus x of a dielectric sphere with m=1.7+0.03i, comparison of full Mie scattering with the solution for nmax=2.

Mie Theory and Geometrical Optics

Angular behaviour of scattering, using the MATLAB function, tetascancompare1(m, x, nsteps, nsmooth, ymin, ymax):

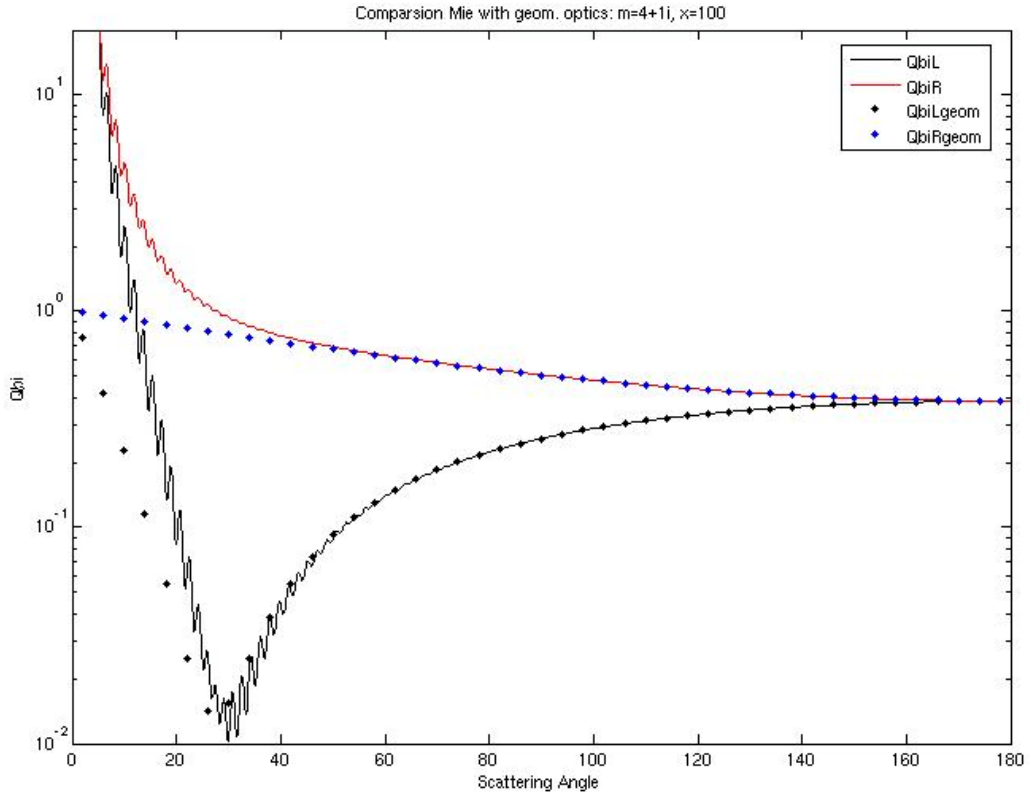

Figure 4.9: Lossy sphere: m=4+i, x=100 (above), transparent sphere m=1.44+10^{-5}i, x=1000 (below)

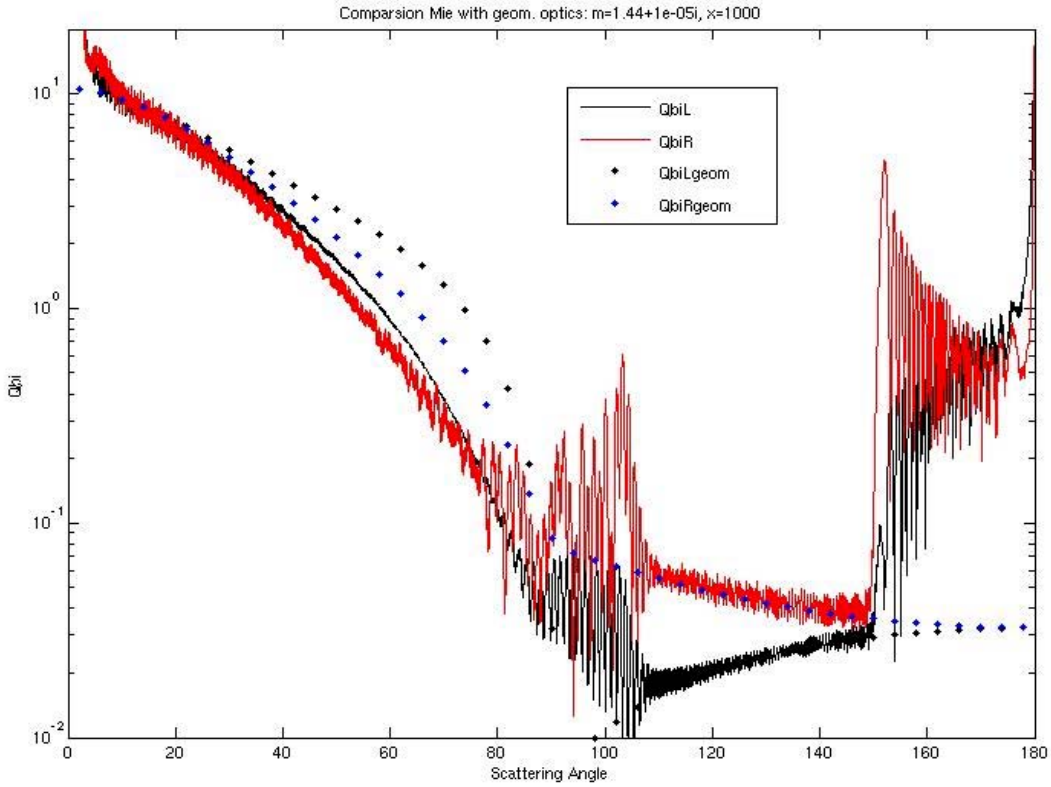

A comparison of the dependence on size parameter is shown in the following figures, computed with the MATLAB Function, mie2go2xscan(ε, μ, nsteps, xmin, xmax). Note that the x dependence in geometrical optics is only due to the penetration depth $1/\gamma_a$ of radiation in the sphere. For large spheres, limiting values are found for Q_a and Q_s.

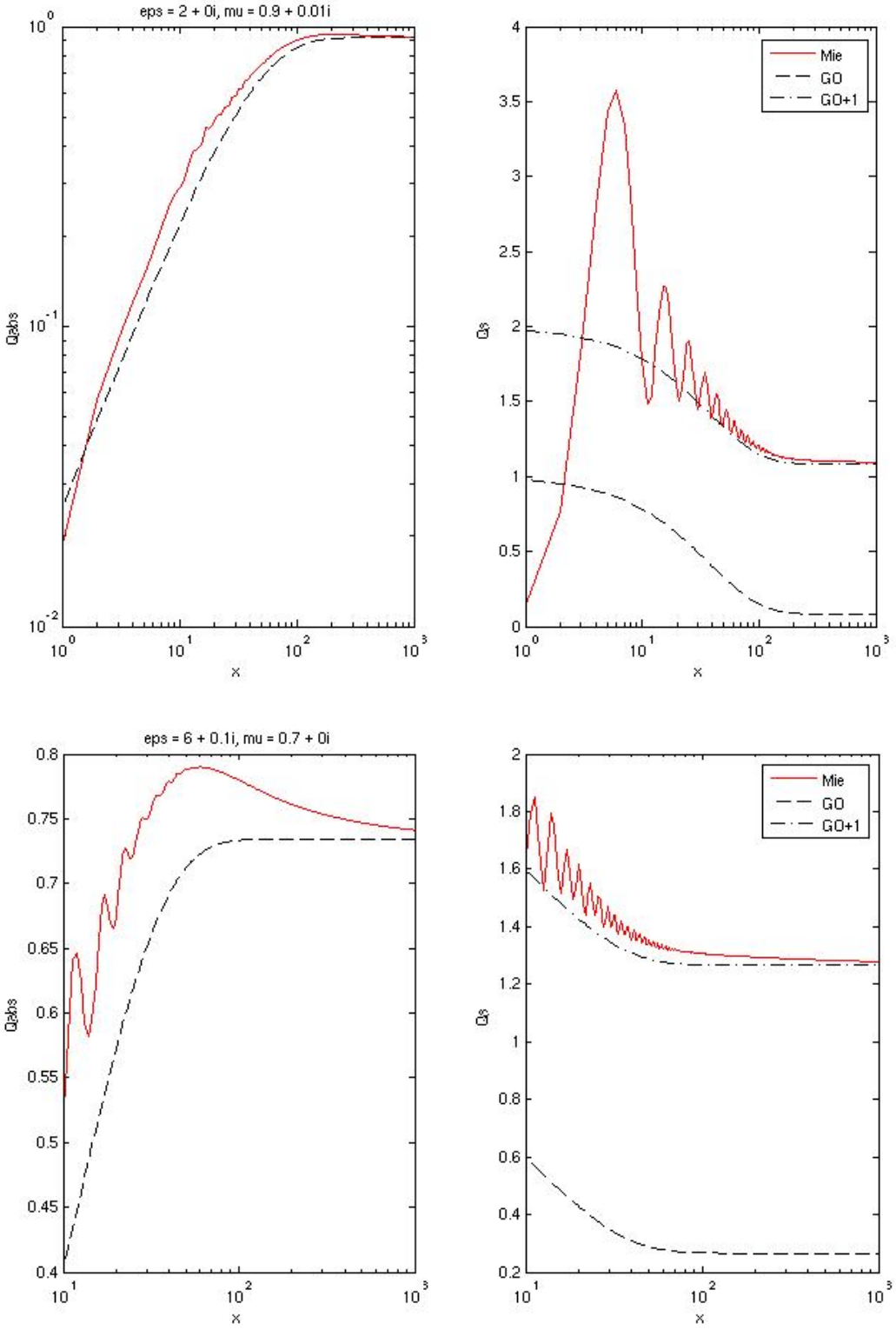

Figure 4.10: x variation of absorption (left) and scattering (right) efficiencies for dielectric-magnetic spheres according to Mie Theory (solid lines) and geometrical optics (dashed). GO+1 (dash-dotted line) means a correction (+1) of Q_s, taking into account the effect of diffraction.

Mie Theory and Born Approximation

MATLAB: tetascancompare2(m, x, nsteps, ymin, ymax)

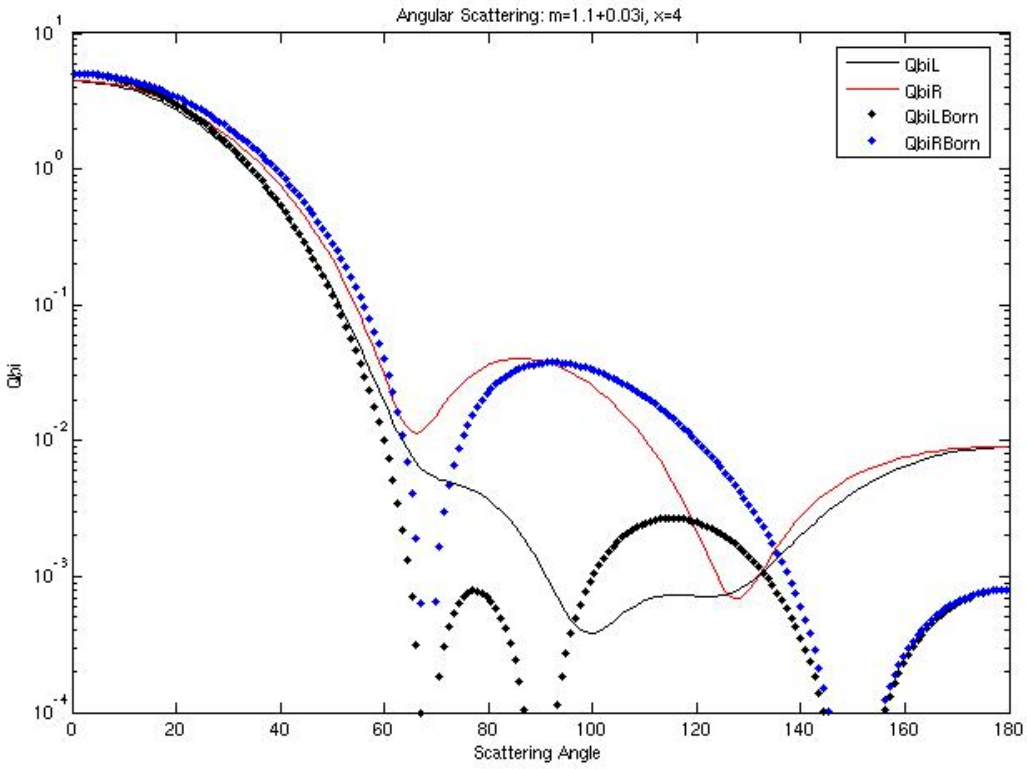

Figure 4.11: Comparison of Mie angular scattering with the Born Approximation for m=1.1+0.03i, x=4.

The results appear to agree better in the forward than in the backward hemisphere. The agreement improves as *m* gets closer to 1.

Exercise

Compare the Mie scattering and absorption efficiencies and $<\cos\vartheta>$ with results of the Born Approximation. Plot the results as in Figures 4.7, 4.8 and 4.10 versus size parameter (*x* from 0.01 to 100) for different *m* (e.g. 1.05, 1.05+0.05i, 1.5+0.01i, 2+i).

Realisation with MATLAB Function Mie_Born(m) by M. Schneebeli. Results in the following figure.

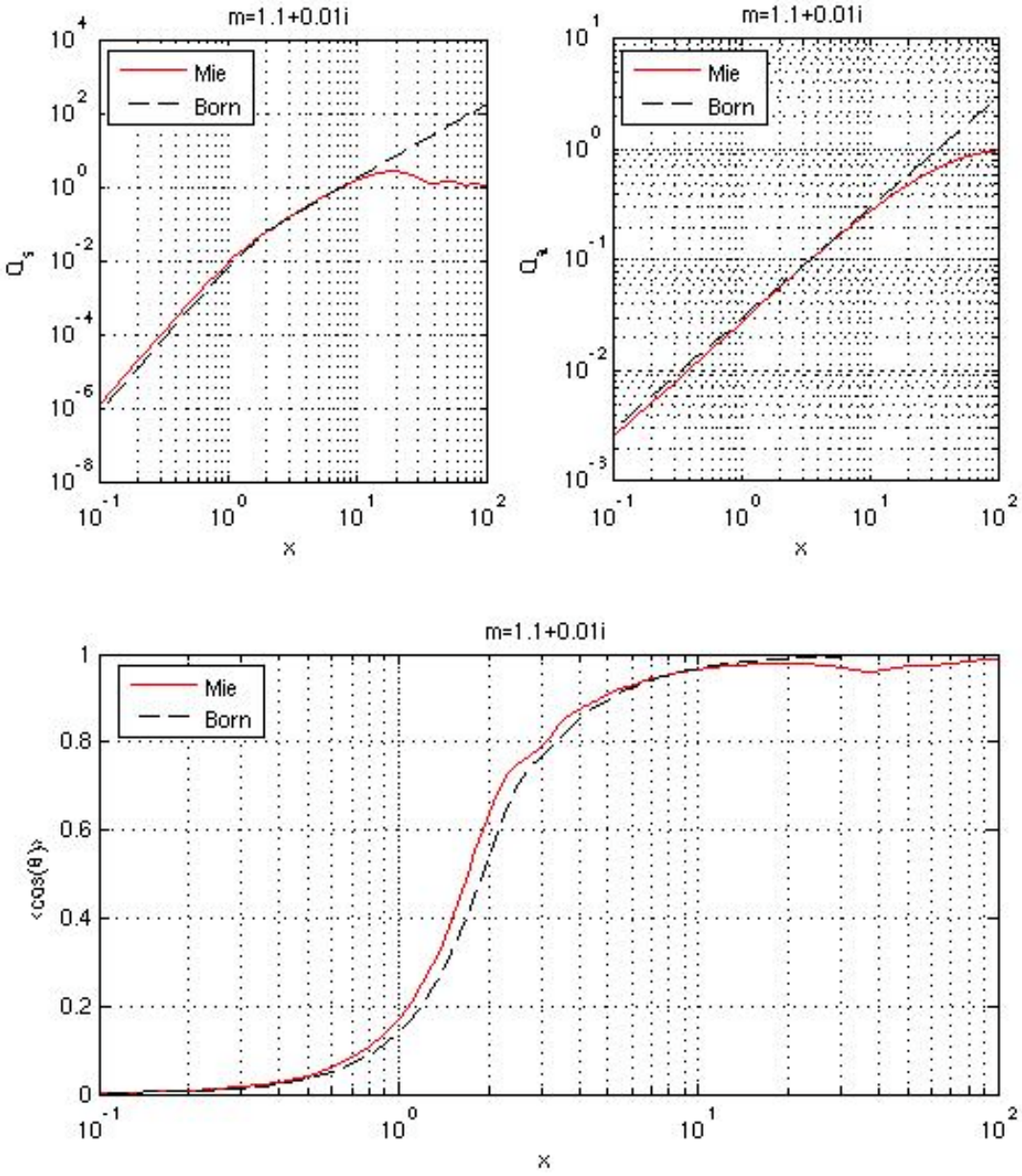

Figure 4.12: Comparison of Mie results with those of the Born Approximation for a refractive index of 1.1+0.01i.

5 On Scattering and Absorption by Non-Spherical Particles

Scattering problems of electromagnetic waves can be solved exactly if the boundary-value problem of the fields at the particle surface can be expressed in simple terms. This is possible if there exists a set of **orthogonal vector-wave functions** for the geometry in question. Apart from spherical particles this applies to plane interfaces, leading to the Fresnel Equations. Also for a few other particle shapes (e.g. ellipsoids) vector-wave functions have been constructed (Zhou, 1994).

However, most progress today is based on **numerical methods**. Unfortunately, these topics are beyond the coverage of this lecture. Interested readers may consult the literature, e.g. Mishchenko et al. (2000), Tsang et al. (2000), Warnick (2005).

Among the numerical methods are also relative simple, approximate ones, e.g. **ray tracing** methods using geometrical optics, or the WKB method (see Ishimaru, 1978).

6 Scattering and Absorption by a Cloud of Particles

6.1 The particle cloud

So far, scattering and absorption has been limited to the interaction with a **single particle** of volume V_s. Most often, radiation interacts with a large **number** N_v of particles in a given volume V. The set of particles describes a cloud with a particle **number density**

$$N = \frac{N_V}{V} \tag{6.1}$$

and the **volume fraction** f of particles in V is simply

$$f = NV_s \tag{6.2}$$

We will consider effects of radiative transfer in a small volume element ΔV, but still large enough to contain a representative number $\Delta N \cong N\Delta V$ >>1 of particles.

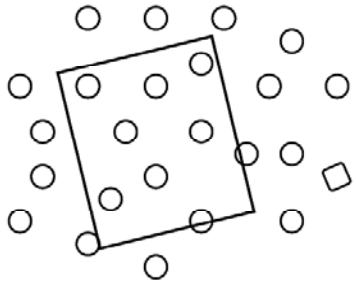

Figure 6.1: Particle cloud with volume element ΔV.

6.2 Size distributions

Clouds may consist of particles with different size, shape and orientation, and also their refractive properties may be different. A simplification is an isotropically oriented set of particles with the same refractive index, but allowing for different particle size. Since spheres are isotropic, their orientation is indifferent. We will characterise a given particle by a size or **diameter** D. The mean number of particles per unit volume in the diameter interval *(D, D+dD)* is given by *N(D)dD*. A number of mathematical functions is used to describe the **size distribution** *N(D)* to fit the functions found empirically from observations. The total number density then is

$$N = \int_0^\infty N(D)dD \tag{6.3}$$

The integral is the zero[th] moment of the distribution. More generally we define the m^{th} moment by

$$m_n = \int_0^\infty N(D)D^n dD \tag{6.4}$$

The mean diameter is the first moment

$$D_{mean} = \Delta V m_1 = \Delta V \int_0^\infty N(D)DdD \tag{6.5}$$

The mean geometrical cross section is proportional to m_2, and the mean volume is proportional to m_3. Further moments are used to describe other mean physical cloud properties.

Note than in the more general case of particles with anisotropic orientation, the probability distribution of the particle orientation has to be specified as well.

Modified Gamma Distribution

$$N(D) = N_0 D^\alpha \exp(-\Lambda D) \tag{6.6}$$

where N_0, α, Λ are free parameters. The moments are given by

$$m_n = N_0 \frac{\Gamma(n+a+1)}{\Lambda^{n+a+1}} \tag{6.7}$$

where $\Gamma()$ is the Gamma Function, and for an integer argument we have

$$\Gamma(n+\alpha+1) = (n+\alpha)! \tag{6.8}$$

A special case is the exponential distribution ($\alpha = 0$) often used to describe the raindrop size.

Lognormal Distribution

$$N(D) = \frac{N_T}{\sqrt{2\pi} D \ln\sigma} \exp\left(-\frac{\ln^2(D/D_g)}{2\ln^2\sigma} \right) \tag{6.9}$$

This is again a 3-parameter function with moments

$$m_n = N_T D_g^n \exp[0.5 n^2 \ln^2 \sigma] \tag{6.10}$$

where N_T is the total number density, D_g is a characteristic diameter, and σ describes the relative width of the distribution.

6.3 Scattering and absorption by clouds

The mean scattering and absorption properties of clouds will be described by the properties of single particles together with the distribution function. This is based on two assumptions:

1) the radiation homogeneously penetrates into the volume element ΔV, and
2) the superposition of radiation from different scattering centres is incoherent.

The behaviour was found to be true for scattering at a granular medium in the Born Approximation, see Equation (3.34).

Note, however, that scattering of monochromatic radiation in a medium with multiple scattering centres leads to speckle noise due to interference between different rays. The incoherent superposition only gives the mean value of actual situations. Therefore averaging procedures are needed in experiments to smear out the interference effects.

The absorption cross section of the volume element ΔV (Figure 6.1) is the sum of the absorption cross sections of the particles in this volume. The mean value can be described by the integral

$$\sigma_{a,mean} = \Delta V \int_0^\infty N(D)\sigma_a(D) dD \tag{6.11}$$

In the same way, the mean scattering cross section is given by the equivalent expression

$$\sigma_{s,mean} = \Delta V \int_0^\infty N(D)\sigma_s(D) dD \tag{6.12}$$

Also the extinction, mean bistatic scattering cross section and other additive quantities can be described in this way. Volume densities of the mean cross sections are called coefficients. Thus the **absorption coefficient**, **scattering coefficient** and **extinction coefficient** are

$$\gamma_a = \frac{\sigma_{a,mean}}{\Delta V}; \quad \gamma_s = \frac{\sigma_{s,mean}}{\Delta V}; \quad \gamma_e = \frac{\sigma_{e,mean}}{\Delta V} \tag{6.13}$$

or generally

$$\gamma_i = \int_0^\infty N(D)\sigma_i(D) dD; \text{ where } i\text{=a, b, bi, d, e, s, ...} \tag{6.14}$$

Their dimension is area/volume, thus the MKS unit is 1/m. These are quantities used in radiative transfer to be described in Part 2 of this lecture. Note also that they may depend on polarisation of the incident radiation.

Exercise: Show that the absorption coefficient (6.11) in the Rayleigh Approximation for a cloud of absorbing spheres in free space is identical to the result of the Maxwell-Garnett formula (1.15) with (1.10) at low volume fraction (linear in f).

Part 2: Radiative Transfer

7 Introduction to Radiative Transfer

Radiative transfer describes how the radiation field changes from point to point and for different directions under a given illumination or source distribution. The usual assumptions are that the scenario is stationary and that different rays interact incoherently. Also Local Thermodynamic Equilibrium (LTE) conditions are usually assumed. Deviations from these assumptions may need special treatments.
To find a selected ray path on a macroscopic scale, geometrical optics is generally used. Apart from Snell's Law, the Eikonal Equation is often used to find this path.
Radiative transfer concentrates on **standard geometries** such as plane-parallel media, semi-infinite half-spaces with flat surfaces, or spherically-symmetric media, and in **standard situations** a single source of illumination, such as a point source or a plane wave, are considered.
Applications beyond the topic of this lecture include 3-dimensional scenes. For this purpose it is necessary to use numerical methods, e.g. Monte Carlo simulations of the radiation field.

7.1 Radiance and related quantities

Radiance or specific intensity

The radiation field is described by a radiative intensity, called **radiance**, I_ν, at a given frequency ν (or I_λ at a given wavelength λ), polarisation, position and in a given direction (Figure 7.1). This quantity is defined in Equation (7.1) by the infinitesimal radiative power dP at the required polarisation within the frequency range $(\nu,\ \nu + d\nu)$ crossing a given test area dA in the given direction, defined by the unit vector $\hat{\mathbf{n}}(\theta,\phi)$, within an infinitesimal solid angle $d\Omega$ of spherical coordinates (θ,ϕ) centred at position $\mathbf{r}$. This power can be expressed as

$$dP = I_\nu(\mathbf{r},\hat{\mathbf{n}}(\theta,\phi)) \cdot d\nu \cdot dA \cdot \cos\theta \cdot d\Omega \tag{7.1}$$

Apart from the term, radiance, other terms are used as well: **specific intensity**, in German: **spektrale Strahlungsdichte**. The term **intensity** is normally used for power per unit area, which is not the same as I_ν. The factor, $\cos\theta$, is used to relate the power to the **projected area** as seen by the ray. With Equation (7.1) we are able to concentrate on the radiative power of a light ray of interest. The selected radiation is called a **pencil of radiation**. If we know I_ν at all positions and for all directions, the problem of radiative transfer is solved.

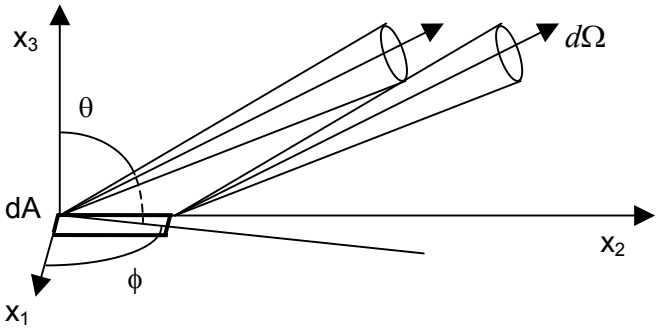

Figure 7.1: Geometrical situation used to define the radiance. Position **r** is at the origin of the coordinate system shown. Cones of solid angle $d\Omega$ of two limiting beams within area element dA are shown.

Spectral flux density

Integrating Equation (7.1) over all directions gives a new quantity, called spectral flux density *F*, here F_3, because the normal to dA is in direction of x_3. More generally, for a given unit vector $\hat{\mathbf{n}}_0$ at position **r,** the spectral flux density is defined by F_ν

$$F_\nu(\hat{\mathbf{n}}_0) = \int_{4\pi} I_\nu(\mathbf{r},\hat{\mathbf{n}})\hat{\mathbf{n}} \cdot \hat{\mathbf{n}}_0 d\Omega \tag{7.2}$$

If the integration is limited to the forward hemisphere ($\hat{\mathbf{n}}\cdot\hat{\mathbf{n}}_0>0$) we call the result $F_{\nu+}$, and for the backward hemisphere ($\hat{\mathbf{n}}\cdot\hat{\mathbf{n}}_0<0$), we call the integral $F_{\nu-}$:

$$F_{\nu\pm}(\hat{\mathbf{n}}_0)=\pm\int_{\pm 2\pi} I_\nu(\mathbf{r},\hat{\mathbf{n}})\hat{\mathbf{n}}\cdot\hat{\mathbf{n}}_0 d\Omega \tag{7.3}$$

The sign is such as to provide positive values, and we can write: $F_\nu = F_{\nu+} - F_{\nu-}$. **Isotropic radiation** fields have $F_\nu = 0$, and

$$F_{\nu+} = F_{\nu-} = \pi I_\nu \tag{7.4}$$

because $d\Omega = d\phi\sin\theta d\theta$, and the integral $\int_0^{2\pi} d\phi\int_0^{\pi/2}\cos\theta\sin\theta d\theta = 2\pi\int_0^1 x dx = \pi$. This result is the reason why some authors (e.g. Chandrasekhar) call the flux density πF instead of F. Then (7.4) changes to $\pi F_{\nu+} = \pi F_{\nu-} = \pi I_\nu$.

Since $\hat{\mathbf{n}}_0$ is arbitrary we can define the **spectral flux density** and the **radiative flux density** of the radiation field at position **r** as the vectors

$$\mathbf{F}_\nu = \int_{4\pi} I_\nu(\mathbf{r},\hat{\mathbf{n}})\hat{\mathbf{n}}\, d\Omega, \quad \text{and} \quad \mathbf{F} = \int_0^\infty \mathbf{F}_\nu d\nu \tag{7.5}$$

Mean intensity and spectral energy density

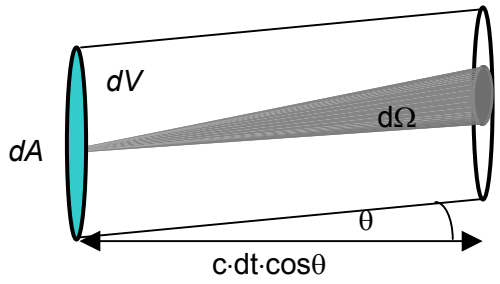

Figure 7.2: Volume *dV* of a ray passed in time *dt* where *c* is the speed of light

Let us compute the spectral energy density in *J/m³/Hz* of the radiation field. According to Figure 7.2 the energy of a given ray is dispersed in time dt over volume $dV = dA\cos\theta\cdot cdt$. Then the energy density of this ray is

$$du_\nu = \frac{dU}{dV} = \frac{dPdt}{dV} = \frac{I_\nu\cos\theta d\Omega dA d\nu dt}{cdtdA\cos\theta} = \frac{I_\nu}{c}d\Omega d\nu \tag{7.6}$$

The **spectral energy density** u_ν is the integral over all directions

$$u_\nu = \frac{w_\nu}{c};\ \text{where}\ \ w_\nu = \int_{4\pi} I_\nu d\Omega; \qquad \text{and} \qquad u = \int_0^\infty u_\nu d\nu \tag{7.7}$$

and *c* is the speed of light (more exactly, the group velocity) in the medium. The quantity w_ν is the mean (spectral) **intensity**, and *u* is the total **radiative energy density**. For an **isotropic** radiation field we have $w_\nu = 4\pi I_\nu$ and

$$u_\nu = \frac{4\pi I_\nu}{c} \tag{7.8}$$

Polarised quantities

The quantities defined in this section apply to any state of polarisation. Therefore the radiance can be generalised to a vector whose elements are Stokes Parameters

$$\mathbf{I}_\nu = (I_{\nu 1}, I_{\nu 2}, U_\nu, V_\nu)^{tr} \tag{7.9}$$

and the total radiance is the sum, $I_\nu = I_{\nu 1} + I_{\nu 2}$. For all quantities defined above there are respective quantities for polarised radiation. We will also use, in analogy to $I_{\nu 1}$ and $I_{\nu 2}$, the radiances $I_{\nu U+}$, $I_{\nu U-}$ of linear polarisation at +45° and -45°, and $I_{\nu V+}$, $I_{\nu V-}$ of left- and right-handed circular polarisation. The total radiance is equivalently given by the sums,

$I_\nu = I_{\nu U+} + I_{\nu U-} = I_{\nu V+} + I_{\nu V-}$, and the 3rd and 4th Stokes Parameters are given by $U_\nu = I_{\nu U+} - I_{\nu U-}$ and $V_\nu = I_{\nu V+} - I_{\nu V-}$.

7.2 Radiation in thermal equilibrium

Radiation in **thermal equilibrium** is characterised by a single **temperature** *T*. As we will see later, a medium that emits this type of radiation is a **black body**, i.e. a medium without reflection and without transmission. Since photons follow the Bose-Einstein statistics, the radiance is given by the Planck function B_ν

$$I_\nu(\theta,\phi) = B_\nu(T) = \frac{2h\nu^3}{c^2\left(\exp(h\nu/k_bT)-1\right)} \tag{7.10}$$

where h =6.6256·10^{-34}Js Planck constant, k_b = 1.3805·10^{-23}J/K Boltzmann constant. The radiance is isotropic and unpolarised: $\mathbf{I}_\nu = (I_{\nu 1} = B_\nu/2,\ I_{\nu 2} = B_\nu/2,\ U_\nu = 0,\ V_\nu = 0)^{tr}$; thus the spectral energy density (*J/m*^{3}*/Hz*) is

$$u_\nu = \frac{4\pi B_\nu}{c} = \frac{8\pi h\nu^3}{c^3\left(\exp(h\nu/k_bT)-1\right)} \tag{7.11}$$

Integration over frequency from 0 to ∞, for details see Ulaby et al. (1981), gives

$$u = \frac{8\pi^5(k_bT)^4}{15(hc)^3} \tag{7.12}$$

and the power radiated by an area *dA* is (since $F_{\nu+} = \pi I_\nu = u_\nu c/4$)

$$dP = dA\cdot u(T)\cdot c/4 = dA\cdot\sigma_{sb}\cdot T^4 \tag{7.13}$$

where the Stefan-Boltzmann constant σ_{sb} is given by

$$\sigma_{sb} = \frac{2\pi^5 k_b^{\,4}}{15h^3c^2} = 5.67\cdot10^{-8}\mathrm{Wm^{-2}K^{-4}} \tag{7.14}$$

For sufficiently low frequency ($h\nu << k_bT$) the Rayleigh-Jeans Approximation is applicable for $B_\nu(T)$, leading to a linear relationship with temperature:

$$B_\nu(T) \cong \frac{2k_bT\nu^2}{c^2} \tag{7.15}$$

The linearity enables us to express the radiance by the temperature; and this temperature is called brightness temperature T_b, even if the radiation is not from a region in full thermal equilibrium. From (7.10) and (7.15) we have for $T=T_b$, and for the Stokes Vector form (7.9)

$$T_b = \frac{c^2 I_\nu}{2k_b\nu^2};\qquad \mathbf{T}_b = (T_{b1}, T_{b2}, T_{bU}, T_{bV}) = \frac{c^2\mathbf{I}_\nu}{k_b\nu^2} \tag{7.16}$$

Exercises:

1. Test the relative error of the Rayleigh-Jeans formula for frequencies given by $\nu=0.01k_bT/h$ and $\nu=0.1k_bT/h$, $\nu=k_bT/h$. How large are these frequencies and corresponding vacuum wavelengths for T=3K, 300K, 6000K? Plot (log-log scale) the Planck spectra B_ν for these temperatures and determine the maxima of the curves. Find a formula to express the frequency of the maximum as a function of temperature (Wien displacement law).
2. Compare the radiative energy density u at 300K with the kinetic, internal energy density $u_T = \rho c_\nu T$ of dry air at the same temperature, where the specific heat is 718J/kg/K and $\rho = 1kg/m^3$. At which temperature would both be the same?

7.3 Radiation in Local Thermodynamic Equilibrium: Kirchhoff's Law

If the medium, accessible by radiation, is not at a single temperature, the Planck radiation law may still be valid in an adapted way found by Kirchhoff in 1860 before the Planck formula was known. **Kirchhoff's law** relates **emission and absorption** of radiation in **Local Thermodynamic Equilibrium** (LTE), meaning that the emission is governed by thermal conditions as defined by a unique temperature at any given location. The space is assumed to be divided into *N* volumes of temperatures T_i where *i*= 1 to *N*. The temperature inside each volume is homogeneous. A receiver with a **reciprocal, single-mode antenna** is used to measure this radiation. The received power must be a linear combination of the blackbody radiances corresponding to the different temperatures.

$$P_{A,p} = A\Omega\sum_{i=1}^{N} e_{i,p}\frac{B_\nu(T_i)}{2} \tag{7.17a}$$

where A and Ω are the receiving aperture and solid angle. The factor ½ takes care of the fact that a (single-mode) sensor is sensitive to one state of polarisation. If the power is expressed in terms of the **antenna temperature** $T_{A,p}$ (Ulaby et al. 1981), representing the spectrally and angularly averaged brightness temperature of the sensor antenna (at polarisation *p*) and filter, the linear combination in the Rayleigh-Jeans approximation is simply

$$T_{A,p} = \sum_{i=1}^{N} e_{i,p}T_i \tag{7.17b}$$

To determine the **emissivities** $e_{i,p}$ (non-dimensional constants with *i* =1 to *N*, polarisation *p*), the **reciprocal** condition is considered in which the radiometer is replaced by a stationary **transmitter** with the **same spectral and polarisation** properties.
Let us define $a_{i,p}$ as the fraction of the transmitted power absorbed in volume V_i. Then $a_{i,p}$ is the **absorptivity** of this volume for the given transmitter configuration. Energy conservation requires that all radiation is absorbed somewhere which means that

$$\sum_{i=1}^{N} a_{i,p} = 1 \tag{7.18}$$

Kirchhoff's law states that

$$e_{i,p} = a_{i,p} \tag{7.19}$$

for all *i*=1 to *N*, and for any polarisation. Then

$$T_{A,p} = \sum_{i=1}^{N} a_{i,p}T_i \;\; ; \qquad P_{A,p} = A\Omega\sum_{i=1}^{N} a_{i,p}\frac{B_\nu(T_i)}{2} \tag{7.20}$$

Since (7.19) and (7.20) apply to any sensor (with any spectral properties, polarisation and angular pattern), they also hold for an ideal **monochromatic**, **pencil-beam** radiometer, and thus for the brightness temperature (in the Rayleigh-Jeans Approximation), or more generally for the radiance:

$$T_{b,p}(\nu) = \sum_{i=1}^{N} a_{i,p}(\nu)T_i \;\; ; \;\; I_{\nu,p} = \sum_{i=1}^{N} a_{i,p}(\nu)\frac{B_{\nu,i}}{2} \tag{7.21}$$

where $a_{i,p}(\nu)$ is the monochromatic absorptivity at any of the standard-polarisation states ($p = 1,\ 2,\ U+,\ U-,\ V+,\ V-$) of volume V_i for radiation propagating in the reciprocal (opposite) direction of the radiation considered for emission. Thus the alternate Stokes Parameters of thermal radiation at a given position **r** and in a given direction $\hat{\mathbf{n}}$ are

$$\mathbf{I}_\nu(\mathbf{r},\hat{\mathbf{n}}) = \left(I_{\nu,1},\ I_{\nu,2},\ I_{\nu,U+} - I_{\nu,U-},\ I_{\nu,V+} - I_{\nu,V-}\right) \tag{7.22}$$

The complication with the differences is a consequence of the definition of Stokes Parameters. The absorptivity is defined for a given radiance or power, but not for differences. Also Kirchhoff's Law applies to radiating power, but not to differences. These have to be constructed in the way shown in (7.22). Furthermore absorptivities $a_i \geq 0$, obeying (7.18).

An Example

Let us consider the situation of Figure 7.3, showing a night scene with parts of a tree, of the moon, and of a cloud. A decomposition into *N*=8 objects at different temperatures is proposed. Let us assume that a radiative sensor sees this scene as a whole in a given wavelength range, and that, in the reciprocal situation, the sensor illuminates the scene in the same wavelength range. A fraction $a_{1,\mathrm{p}}$ of the power will be absorbed by the tree, a fraction $a_{2,\mathrm{p}}$ will be absorbed by the ambient air; the rest of the radiation will at least reach the atmospheric cloud level where another fraction $a_{3,\mathrm{p}}$ of the radiation will be absorbed. Again the remaining radiation will reach the upper troposphere where the fraction $a_{4,\mathrm{p}}$ will be absorbed. The remaining atmosphere is assumed to be completely transparent. A small fraction will reach the moon with $a_{5,\mathrm{p}}$ on the shadow side and $a_{6,\mathrm{p}}$ on the sun side. A tiny fraction $a_{7,\mathrm{p}}$ of the transmitted power will be scattered towards the sun where it will be completely absorbed. Finally, the fraction $a_{8,\mathrm{p}}$ will escape to space. Now, the received radiance is $I_{\nu,p} = \sum_{i=1}^{8} a_{i,p} \frac{B_{\nu,i}}{2}$.

The decomposition can be expanded (e.g. by a fraction of radiation reflected by the tree and absorbed by the ground surface, and by radiation scattered in the atmosphere). The more detailed it is, the more accurate will be the result.

Figure 7.3: Night scene with a tree and the moon with the following decomposition:

i	Object
1	Tree
2	Ambient air
3	Air at cloud level
4	Upper troposphere
5	Moon without sun light
6	Moon with sun light
7	Sun
8	Cosmic background

To prove his law, Kirchhoff used *thought experiments* to show that any deviation leads to violations of thermodynamic principles. By special insulation the object is allowed to interact with the environment only by radiation. First assume that the emissivity of an object is larger than its absorptivity. Under isothermal conditions, the object cools because it loses more energy than it gains. This is against the second law of thermodynamics. On the other hand if the emissivity is smaller than the absorptivity the object is heated in violation of the first law of thermodynamics. The solution is to accept Kirchhoff's law. To show that the principle holds independently at each frequency and polarisation was a main effort of Kirchhoff. For this purpose the path between the object and the environment is restricted to radiation with the selected properties, the rest being reflected by filters, polarisers and single-mode waveguides. The only way to exchange energy is at the selected frequency and polarisation. Since they are arbitrary, the law must hold at all frequencies and polarisations.

A statement of **Sören Kirkegaard** (1813 to 1855) with regard to life may be regarded as a **metaphor** to Kirchhoff's Law: *Although life happens toward the future, it can only be understood when looking backward in time*.

Kirchhoff's law applies to all types of radiometers, not only to radiation represented by plane waves or by infinitesimally diverging beams. Therefore it is very general as long as the **LTE** condition and **reciprocity** are valid. Boundary conditions, diffraction and coherent effects are

automatically included if correct absorptivities are taken into account. Their determination is the main task, requiring special tools. One of them is the **Radiative Transfer Equation**. Other tools may have to be used, e.g. to solve problems with coherent interactions.

8 The Radiative Transfer Equation

This chapter is used to introduce the radiative transfer equation with increasing complexity.

8.1 Radiative transfer without absorption and scattering

Free or homogeneous space

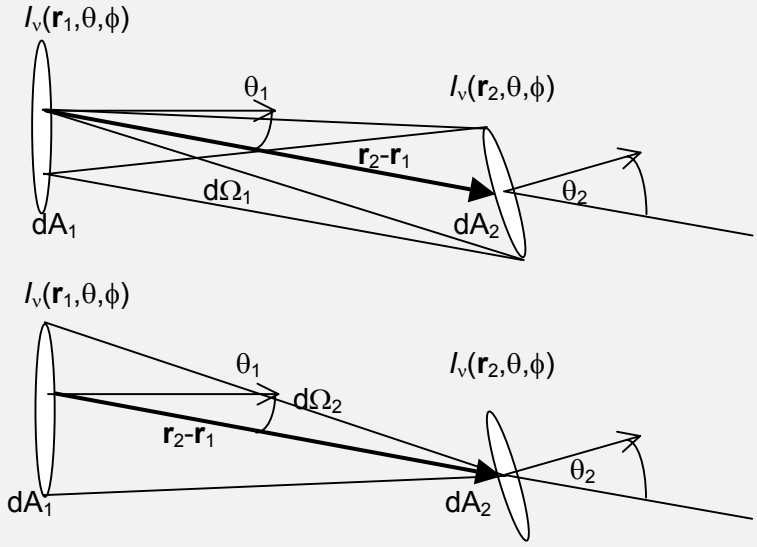

Figure 8.1: Following a pencil of radiation in free space from point $\mathbf{r}_1$ to $\mathbf{r}_2$ to show that the radiance is conserved.

Energy conservation of stationary radiation means power conservation. Furthermore, in free space (or in a homogeneous medium), rays propagate on straight lines. Therefore

$$dP_1 = I_\nu(\mathbf{r}_1,\hat{\mathbf{n}})\,d\nu dA_1\cos\theta_1 d\Omega_1 = dP_2 = I_\nu(\mathbf{r}_2,\hat{\mathbf{n}})\,d\nu dA_2\cos\theta_2 d\Omega_2 \tag{8.1}$$

Since $d\Omega_1 = \dfrac{dA_2\cos\theta_2}{|\mathbf{r}_2-\mathbf{r}_1|^2}$, and $d\Omega_2 = \dfrac{dA_1\cos\theta_1}{|\mathbf{r}_2-\mathbf{r}_1|^2}$, Equation (8.1) means that $I_\nu(\mathbf{r}_1,\hat{\mathbf{n}}) = I_\nu(\mathbf{r}_2,\hat{\mathbf{n}})$ or if ds is an infinitesimal path element along the ray, we can write

$$\frac{dI_\nu}{ds} = 0;\ \text{also valid for Stokes Vector: } \frac{d\mathbf{I}_\nu}{ds} = 0 \tag{8.2}$$

Equation (8.2) is the radiative-transfer equation of free space. It is independent of position, and it is valid for all ray directions.

Slightly inhomogeneous medium

Now we assume that the medium is slightly inhomogeneous, but scattering and absorption are still negligible. Reflection and scattering are negligible if the gradient of the real part of the refractive index is sufficiently small: $|\nabla n'| << k$, and absorption is negligible if the imaginary part is $n''=0$. Now the rays are no longer straight lines, but they follow the rules of geometric optics (Snell's Law, Fermat's Principle of the shortest path, Eikonal Equation). It can be shown (Mobley 1994) that the following quantity is conserved:

$$I_{1\nu} = \frac{I_\nu}{n'^2};\ \text{or in Stokes Vector form } \mathbf{I}_{1\nu} = \frac{\mathbf{I}_\nu}{n'^2} \tag{8.3}$$

Note that $n'=n$ because $n''=0$. In the more general situation of an anisotropic medium, n' has to be replaced by the *ray-refractive index* (Bekefi, 1966).
For illustration and verification of (8.3), we investigate the situation of a one-dimensionally inhomogeneous medium where the refractive index deceases in a transition region with increasing height (Figure 8.2).

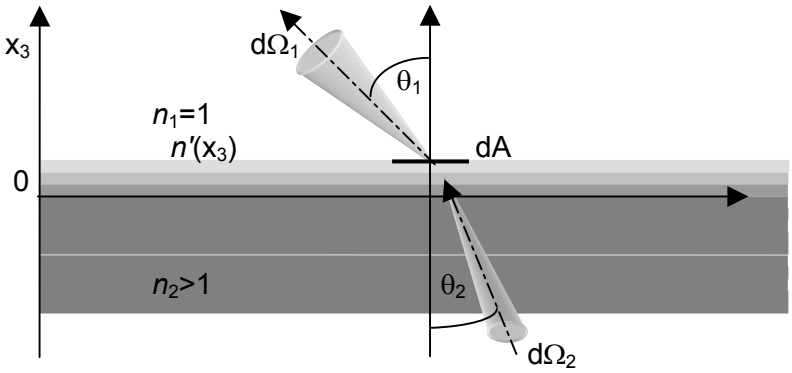

Figure 8.2: Power conservation for a refracted ray passing from one medium in another through dA. Reflection is avoided by a soft transition $\left|\frac{dn}{dx_3}\right| << \frac{1}{\lambda}$

Power conservation requires $dP_1=dP_2$, thus

$$I_\nu(1,\theta_1,\phi_1)\cdot\cos\theta_1\cdot d\Omega_1\cdot dA\cdot d\nu = I_\nu(n_2,\theta_2,\phi_2)\cdot\cos\theta_2\cdot d\Omega_2\cdot dA\cdot d\nu \qquad (8.4)$$

From Snell's law we have $\sin\theta_1 = n_2 \sin\theta_2$. Furthermore, since $d\Omega_1 = \sin\theta_1 d\theta_1 d\varphi$, $d\Omega_2 = \sin\theta_2 d\theta_2 d\varphi$, and $\cos\theta_1 d\theta_1 = d(\sin\theta_1) = n_2 d(\sin\theta_2) = n_2 \cos\theta_2 d\theta_2$, we get

$$\cos\theta_1 d\Omega_1 = n_2^2 \cos\theta_2 d\Omega_2 \qquad (8.5)$$

Equations (8.4) and (8.5) lead to (8.3). Equation (8.3) also means that the Planck function is not conserved, but the following quantity is:

$$B_{1\nu} := \frac{B_\nu(\mathbf{r},T_b)}{n'(\mathbf{r})^2} = \frac{2h\nu^3}{c_0^2\left(\exp(h\nu/k_bT_b)-1\right)} = \text{constant} \qquad (8.6)$$

Since the quantities on the right side are either fundamental constants (h, k_b, c_0), an independent but fixed variable (ν), or the brightness temperature T_b, it means that T_b does not change along the path of propagation. Thus $I_{1\nu} = B_{1\nu}$ and T_b are conserved quantities. This is a first important result, the **fundamental theorem of radiometry** (Mobley, 1994). If the brightness temperature T_b did change, it would violate principles of thermodynamics.

8.2 Absorbing medium

Consider a volume element $dV = ds \cdot dA$, as shown in Figure 8.3, illuminated by an incident light beam of (normalised) radiance $I_{1\nu}$ over an infinitesimal solid angle $d\Omega$. Here ds is a path element of the beam, and dA is the projected area of the volume element. The incident intensity is $I_i = I_{1\nu}\, d\Omega$. The power lost from the beam by absorption follows from Equations (6.11-14) as $dP_a = \gamma_a I_i dV$. According to Kirchhoff's Law, in LTE there is an equivalent emission term: $dP_e = \gamma_a B_{1\nu} d\Omega dV$.

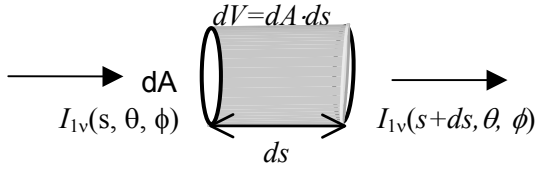

Figure 8.3: An interacting volume element where absorption and emission take place.

Remark: Apart from (6.14) the absorption coefficient may also be expressed by the imaginary part n'' of the complex refractive index

$$\gamma_a(\mathbf{r}) = 2k\cdot n''(\mathbf{r}); \qquad (1/\mathrm{m}) \qquad (8.7)$$

The **radiative transfer equation** considers the changes that occur to $I_{1\nu}$ or $\boldsymbol{I}_{1\nu}$ along the propagation path *s*. Budgeting the source and loss terms over the infinitesimal step *ds* the resulting differential equation is

$$\frac{dI_{1\nu}(s)}{ds} = \gamma_a(s)\big(B_{1\nu}(s) - I_{1\nu}(s)\big) \tag{8.8}$$

The path dependence of $B_{1\nu}$ arises from the dependence on the local temperature $T(s)$. By the use of the normalised quantities, ($I_{1\nu}$ and $B_{1\nu}$), the refractive index does not appear explicitly. In the Rayleigh-Jeans Approximation, the radiative transfer equation simplifies to:

$$\frac{dT_b}{ds} = \gamma_a(s)\big(T(s) - T_b(s)\big) \tag{8.9}$$

8.3 Including absorption, emission and scattering

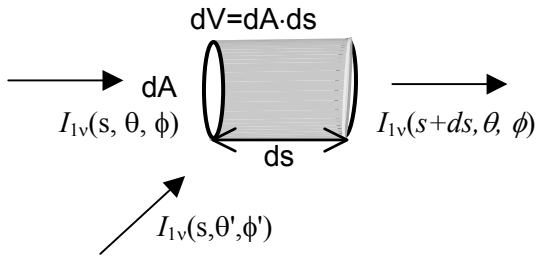

Figure 8.4: An interacting volume element where absorption, emission and scattering take place.

In the final step towards the complete **Radiative Transfer Equation (RTE)**, **volume scattering** in the volume element d*V* is included. The losses contain contributions from absorption and scattering, the sum $\gamma_e = \gamma_a + \gamma_s$ being the extinction coefficient, and the ratio

$$\varpi_0 = \frac{\gamma_s}{\gamma_e} \tag{8.10}$$

is called the **single-scattering albedo**. The radiative transfer equation now reads

$$\frac{dI_{1\nu}(s)}{ds} = -\gamma_e(s) \cdot I_{1\nu}(s) + \varepsilon_{1\nu}(s) \tag{8.11}$$

The source term

$$\varepsilon_{1\nu}(s) = \gamma_a(s) \cdot B_{1\nu}(s) + \frac{\gamma_e(s)}{4\pi} \int_{4\pi} p(\theta,\phi,\theta',\phi') \cdot I_{1\nu}(s,\theta',\phi') \cdot d\Omega' \tag{8.12}$$

consists of thermal emission (first term) and of radiation scattered from other directions into the considered ray path (second term). The integral in the second term contains the normalised radiance $I_{1\nu}$ at path position *s* propagating in all directions. The so-called **phase function** or **indicatrix** $p(\theta, \phi, \theta', \phi')$ describes the transfer of radiance from direction (θ', ϕ') to direction (θ, ϕ) of the considered propagation path. The phase function is **reciprocal** (in reciprocal media): $p(\theta',\phi',\theta,\phi) = p(\theta,\phi,\theta',\phi')$. Energy conservation requires that

$$\frac{1}{4\pi} \int_{4\pi} p(\theta,\phi,\theta',\phi') \cdot d\Omega = \frac{\gamma_s}{\gamma_e} = \varpi_0 \tag{8.13}$$

If the scattering in the volume element dV can be treated by a spherical wave, it can also be expressed by the formalism of Part 1. This should be possible if *dV* is sufficiently small. Then the phase function is related to the mean bistatic scattering cross section $\sigma_{bi,mean}$ of the volume element (see also Equations (6.11) to (6.14)):

$$p(\theta,\phi,\theta',\phi') = \frac{\sigma_{bi,mean}(\vartheta)}{\sigma_{e,mean}} = \frac{\gamma_{bi}(\vartheta)}{\gamma_e} \tag{8.14}$$

where the coordinate system has changed from the scattering plane to a laboratory perspective, defined by the spherical (θ,ϕ) coordinates with one preferred direction $(\theta=0)$. For $\mu=\cos\theta$ and $\mu'=\cos\theta'$, the scattering angles follows from

$$\cos\vartheta=\mu\mu'+\sqrt{\left(1-\mu^2\right)\left(1-\mu'^2\right)}\cos\left(\phi-\phi'\right) \tag{8.15}$$

In the Rayleigh-Jeans Approximation, the RTE is obtained by replacing $I_{1\nu}$ by T_b, and $B_{1\nu}$ by T:

$$\frac{dT_b(s)}{ds}=-\gamma_e(s)\cdot T_b(s)+\gamma_a T(s)+\frac{\gamma_e(s)}{4\pi}\int_{4\pi}p(\theta,\phi,\theta',\phi')\cdot T_b(s,\theta',\phi')\cdot d\Omega' \tag{8.16}$$

This is an integro-differential equation for T_b in the propagation direction, including T_b in all other directions. The coupling of radiation propagating in different directions causes inherent difficulties in practical solutions. However, a formal solution is obtained as shown below.

8.4 Formal solution: integral form of the RTE

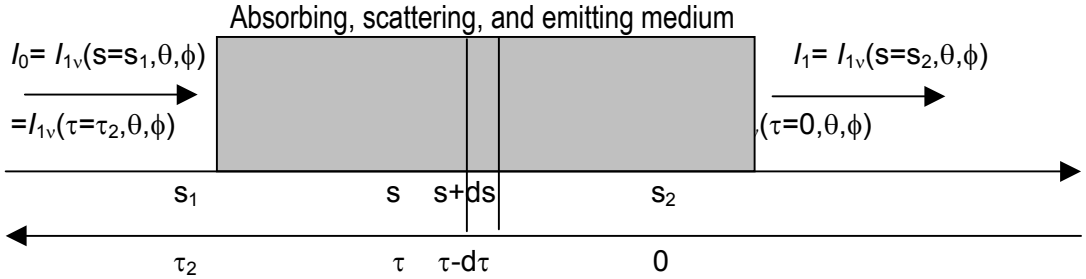

Figure 8.5: Integration paths in s and τ through the medium of radiative interaction.

Let us recall that we are looking for an expression to describe how T_b or $I_{1\nu}$ changes along the path from a starting point at s_1 to an end point at s_2. First the radiative transfer equation is simplified by making the path variable **non dimensional** and calling it **optical depth**. This optical depth, also called **opacity** $\tau(s)$ at a variable path position s as seen from the end position s_2 is defined by

$$\tau(s):=\int_s^{s_2}\gamma_e(s')ds' \tag{8.17}$$

Note that $d\tau = -ds\,\gamma_e$ and ds are in opposite directions. The opacity replaces the geometrical path by an **interaction - weighted path**. Regions without interaction are not "counted". Furthermore the **source function** $J_{1\nu}$ is defined by

$$J_{1\nu}:=\frac{\varepsilon_{1\nu}}{\gamma_e}=(1-\varpi_0)B_{1\nu}(T)+\frac{1}{4\pi}\int_{4\pi}p(\theta,\phi,\theta',\phi')\cdot I_{1\nu}(s,\theta',\phi')\cdot d\Omega' \tag{8.18}$$

With these quantities the radiative transfer equation is simplified to

$$\frac{dI_{1\nu}}{d\tau}-I_{1\nu}=-J_{1\nu} \tag{8.19}$$

which can also be written as

$$\frac{d}{d\tau}\left(e^{-\tau}I_{1\nu}(\tau)\right)=-e^{-\tau}J_{1\nu} \tag{8.20}$$

Integration from $\tau=0$ to $\tau=\tau_2=\int_{s_1}^{s_2}\gamma_e ds$ gives the change of $\exp(-\tau)\cdot I_{1\nu}$ in the considered medium, leading to a formal solution or **integral form** of the RTE at the output position s_2:

$$I_{1\nu}(s=s_2)=I_{1\nu}(\tau=0)=I_{1\nu}(s_1)e^{-\tau_2}+\int_0^{\tau_2}e^{-\tau}J_{1\nu}(\tau)d\tau \tag{8.21}$$

where $I_{1\nu}(s_1)$ is the input, and τ is given by (8.17). In the Rayleigh-Jeans Approximation this is

$$T_b(s_2) = T_b(s_1)e^{-\tau_2} + \int_0^{\tau_2}\left[(1-\varpi_0)T(\tau) + \frac{1}{4\pi}\int_{4\pi} p(\theta,\phi,\theta',\phi')\cdot T_b(\tau,\theta',\phi')\cdot d\Omega'\right]e^{-\tau}d\tau \quad (8.22)$$

Again, this form is the same for refractive and non-refractive media. It reduces to the scatter-free situation for $\gamma_s = 0$ and thus $p=\varpi_0=0$, in which case $d\tau = -ds\,\gamma_a$ and

$$T_b(s_2) = T_b(s_1)e^{-\tau_2} + \int_0^{\tau_2} T(\tau)e^{-\tau}d\tau \quad (8.23)$$

where τ is given by (8.17), but with $\gamma_e = \gamma_a$.

8.5 The Flux Equation

First it is noted that the path derivative in the RTE can be written as

$$\frac{dI_{1\nu}(\mathbf{r},\hat{\mathbf{n}})}{ds} = \hat{\mathbf{n}}\cdot\nabla I_{1\nu}(\mathbf{r},\hat{\mathbf{n}}) = \nabla\cdot(\hat{\mathbf{n}}I_{1\nu}(\mathbf{r},\hat{\mathbf{n}})) \quad (8.24)$$

where $\hat{\mathbf{n}}$ is the unit vector in the direction of the path *s*. Integrating (8.24) over direction gives the flux divergence $\nabla\cdot\mathbf{F}_{1\nu}$ where $\mathbf{F}_{1\nu}$ corresponds to (7.5), but for the normalised radiance $I_{1\nu}$. Integrating the right-hand side of the RTE (8.11-8.12) gives

$$\nabla\cdot\mathbf{F}_{1\nu} = \left(-\gamma_e w_{1\nu} + \gamma_a 4\pi B_{1\nu} + \frac{\gamma_e}{4\pi}\int_{4\pi} I_{1\nu}(\theta',\phi')\int_{4\pi} p(\theta,\phi,\theta',\phi')d\Omega d\Omega'\right) \quad (8.25)$$

The integrals are eliminated with the normalisation (8.13): $\left(-\gamma_e w_{1\nu} + \gamma_a 4\pi B_{1\nu} + \gamma_s w_{1\nu}\right)$ and with the introduction of $w_{1\nu} = \int_{4\pi} I_{1\nu}d\Omega = cu_{1\nu}$. Then we get:

$$\nabla\cdot\mathbf{F}_{1\nu} = \gamma_a\left(-w_{1\nu} + 4\pi B_{1\nu}\right) \quad (8.26)$$

This is the net source (+), sink (-) of radiative power per unit volume element and per unit frequency interval at the given location. The equation states that $\mathbf{F}_{1\nu}$ changes by the **absorption coefficient only**. The role of scattering has disappeared. In a **conservative** medium, defined by $\gamma_a = 0$, the flux is free of divergence: $\nabla\cdot\mathbf{F}_{1\nu}$=0. This is also true for $\gamma_a > 0$ in thermodynamic equilibrium where the two terms in the bracket of (8.26) cancel.
Integration of (8.26) over frequency gives the rate of change of radiation energy density which is related to the local **cooling /heating rate by radiation**.

$$\nabla\cdot\mathbf{F}_1 = \int_0^{\infty}\gamma_a\left(-w_{1\nu} + 4\pi B_{1\nu}\right)d\nu = -\rho c_p\frac{\partial T}{\partial t} \quad (8.27)$$

where ρ is the mass density and c_p the specific heat at constant pressure in the given volume element. This is the **continuity equation** for the balance of radiation and heat energy (expansion and internal). In the special case where the absorption coefficient is constant over frequency, we can directly express the emission term by the temperature:

$$\nabla\cdot\mathbf{F}_1 = \gamma_a\left(-w_1 + \frac{8\pi^5(k_bT)^4}{15h^3c_0^2}\right) \quad (8.28)$$

Exercise:
Compute the radiative heat loss and cooling rate at night at the top of the atmosphere for $T = 220,\ 250,\ 270K$, if we assume Equation (8.28) to apply and if $\gamma_a = 0.1/km$. Use $c_p = 1005J/kg/K$ (dry air) and $\rho = 0.4kg/m^3$ (typical value at 10km altitude. Furthermore, assume that $w_1 = \frac{4\pi^5(k_bT)^4}{15h^3c_0^2}$ (radiation comes mainly from the lower hemisphere).

8.6 Plane-parallel medium

Radiation in a 3-dimensional medium is difficult to handle. Simpler are 1-dimensional media where the parameters depend on one spatial coordinate, only. We will concentrate on plane-parallel media to mimic situations close to the surface of a planet (Figure 8.6). The **medium parameters depend on *z*** (**or** τ_z) **only**.

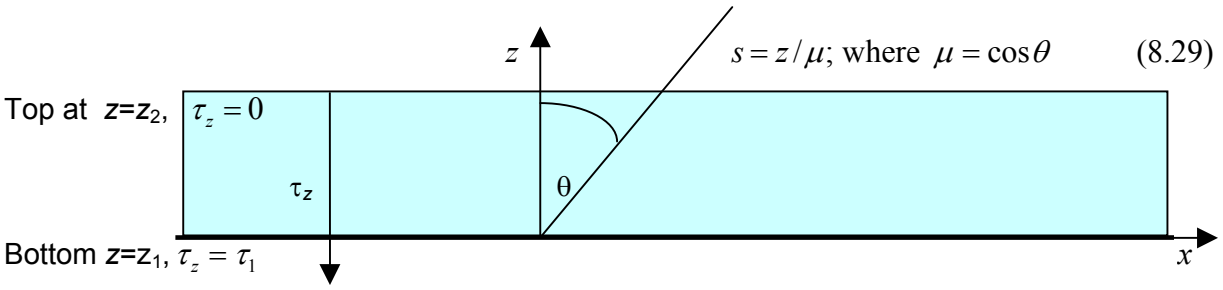

Figure 8.6: Geometry in a plane-parallel atmosphere with height variable z. The path is at an angle θ with respect to the z axis. An azimuth angle (ϕ) measured from the horizontal x axis is used to orient the path around the z axis.

A first ray path s in direction (θ,ϕ) is shown in Figure 8.6. Another ray path s' in a direction (θ',ϕ') may be defined similarly by $s'=z/\mu'$, where $\mu'=\cos\theta'$. By the **convention** of Chandrasekhar (1960), we understand μ>0, writing $-\mu$ to express downwelling rays.

Two rays may interact through scattering through the phase function, given by (8.14), depending also on z (or τ_z). The scattering angle ϑ is determined by (8.15).

Eliminating s by z and μ, the radiative transfer equation reads

$$\mu\frac{dI_{1\nu}(z,\mu,\phi)}{dz} = -\gamma_e(z)\cdot I_{1\nu}(z,\mu,\phi) + \varepsilon_{1\nu}(z,\mu,\phi) \tag{8.30}$$

and with the introduction of the **zenith optical depth** τ_z

$$\tau_z := \int_z^{z_2} \gamma_e(z')dz' \tag{8.31}$$

thus $\tau = \tau_z/\mu$, giving (see also Chandrasekhar, 1960, p. 12)

$$\mu\frac{dI_{1\nu}}{d\tau_z} = I_{1\nu} - J_{1\nu} \tag{8.32}$$

with the formal solutions for upwelling and for downwelling radiation at ***z*** (or τ_z):

$$I_{1\nu}(\tau_z,+\mu,\phi) = I_{1\nu}(\tau_1,\mu,\phi)\exp\left(-\frac{\tau_1-\tau_z}{\mu}\right) + \int_{\tau}^{\tau_1}\exp\left(-\frac{\tau_z'-\tau_z}{\mu}\right)J_{1\nu}(\tau_z',+\mu)\frac{d\tau_z'}{\mu} \tag{8.33}$$

$$I_{1\nu}(\tau_z,-\mu,\phi) = I_{1\nu}(0,-\mu,\phi)\exp\left(-\frac{\tau_z}{\mu}\right) + \int_{0}^{\tau}\exp\left(-\frac{\tau_z-\tau_z'}{\mu}\right)J_{1\nu}(\tau_z',-\mu)\frac{d\tau_z'}{\mu} \tag{8.34}$$

where $\tau_1 = \tau_z(z=z_1)$ is the zenith opacity of the total layer, and the source function $J_{1\nu}$ is, according to (8.18), given by

$$J_{1\nu} := \frac{\varepsilon_{1\nu}}{\gamma_e} = (1-\varpi_0)B_{1\nu}(T) + \frac{1}{4\pi}\int_{4\pi} p(\tau_z,\mu,\phi,\theta',\phi')\cdot I_{1\nu}(\tau_z,\mu',\phi')\cdot d\Omega' \tag{8.35}$$

The escaping radiances are solutions at the boundaries ($\tau_z = 0,\ \tau_1$) of the layer:

$$I_{1\nu}(0,+\mu,\phi) = I_{1\nu}(\tau_1,\mu,\phi)\exp\left(-\frac{\tau_1}{\mu}\right) + \int_{0}^{\tau_1}\exp\left(-\frac{\tau_z'}{\mu}\right)J_{1\nu}(\tau_z',+\mu)\frac{d\tau_z'}{\mu} \tag{8.36}$$

$$I_{1\nu}(\tau_1,-\mu,\phi)=I_{1\nu}(0,-\mu,\phi)\exp\left(-\frac{\tau_1}{\mu}\right)+\int_0^{\tau_1}\exp\left(-\frac{\tau_1-\tau_z'}{\mu}\right)J_{1\nu}(\tau_z',-\mu)\frac{d\tau_z'}{\mu} \qquad (8.37)$$

and respective expressions apply to the Rayleigh-Jeans Approximations.

9 Solutions Without Scattering

Here we consider examples of the scatter-free solution (8.23) in the Rayleigh-Jeans Approximation:

$$T_b(s_2)=T_b(s_1)e^{-\tau_2}+\int_0^{\tau_2}T(\tau)e^{-\tau}d\tau \qquad (8.23)$$

The same types of solutions apply to the radiance (instead of T_b), with the blackbody radiance (instead of T) if the Rayleigh-Jeans Approximation is not valid. Required is, apart from boundary conditions, the spatial distribution of temperature T and of the absorption coefficient γ_a at the frequencies ν of interest.

9.1 Note on spectroscopy

For given physical conditions (composition of the medium, temperature, pressure), γ_a is determined by a suitable physical or empirical model. Spectral lines, bands, and continua occur in gases due to molecular **relaxation and rotation** (microwave), **vibration** (infrared), and due to **electronic excitation** (visible and UV range). With increasing density, and especially in liquids and solids, the lines broaden, getting increasingly distorted, especially at lower frequencies. **Spectroscopy** describes these effects and deals with the physics behind, a topic beyond this lecture. Spectroscopy in the microwave range is part of the lecture on **Microwave Physics**.

Ready-to-use models are available today for different media over specified frequency ranges. For the terrestrial atmosphere, a number of models are available, e.g. **MODTRAN** (Abreu and Andersen, 1996), covering a very wide spectral range, and for microwaves, a standard is the **Microwave Propagation Model** (MPM93) by Liebe et al. (1993), here available as the MATLAB function, `mpm93.m`. See also Rosenkranz (1998) for further improvements (`ros98.m`)

9.2 Layers at constant temperature

Single layer

If the ray passes through a medium at constant temperature T_2, the integration of (8.23) is straightforward, yielding

$$T_b(s_2)=T_b(s_1)e^{-\tau_2}+T_2(1-e^{-\tau_2}) \qquad (9.1)$$

and $\tau_2=\int_{s_1}^{s_2}\gamma_a ds$. There is no need for homogeneity of γ_a because the quantity is eliminated by the transformation to τ. Comparing (9.1) with Kirchhoff's law (7.21), it is obvious that N=2, with Volume 1 being the background, T_1=T_b(s_1), and a_1= exp(-τ_2), Volume 2 being the homogeneous layer at T_2, with a_2= 1- a_1, and thus Equation (7.18) is fulfilled.

1. In optically thin media (τ_2 <<1), we have $a_1 \cong 1$-τ_2, $a_2 \cong \tau_2$, and T_b(s_2) is **linear in** τ_2.
2. For optically thick media (τ_2 >>1), the background radiation is hidden, and T_b(s_2) =T_2. Thus the quantity is **independent of** τ_2.

Further layers at different temperatures

Assume in the example of a single layer that the ray path continues beyond s_2 crossing a third volume at temperature T_3 for s_2< s <s_3. The input brightness to this volume is T_b(s_2), and

the modification by Volume 3 is equivalent to the second term in (9.1), but with the index increased to 3:

$$T_b(s_3) = T_b(s_2)e^{-\tau_3} + T_3(1-e^{-\tau_3}) \tag{9.2}$$

and $\tau_3 = \int_{s_2}^{s_3} \gamma_a ds$. Kirchhoff's law is again confirmed, now with N=3, a_1=exp(-τ_2-τ_3), a_2= exp(-τ_3)·[1- exp(-τ_2)], and a_3= 1- exp(-τ_3). This type of solution can be iterated to any number of layers. The concept is useful in numerical solutions.

9.3 Effective mean temperature

The solution (8.23) in the form of Equation (9.1) is very practical, even in situations where T is not constant. There exists an effective mean temperature $T_m = T_2$ for which (9.1) is valid:

$$T_m = \frac{\int_0^{\tau_2} T(\tau)e^{-\tau} d\tau}{1-e^{-\tau_2}} \tag{9.3}$$

Linear temperature profile

As an example let us consider the situation of a **linear temperature profile**:

$$T = T_c + T_d \tau \tag{9.4}$$

Inserting (9.4) in (9.3) gives

$$T_m = T_c + T_d\left[1 - \frac{\tau_2 e^{-\tau_2}}{1-e^{-\tau_2}}\right]; \quad \text{thus } T_b(s_2) = T_b(s_1)e^{-\tau_2} + T_m(1-e^{-\tau_2}) \tag{9.5}$$

$$= T_b(s_1)e^{-\tau_2} + (T_c + T_d)(1-e^{-\tau_2}) - T_d\tau_2 e^{-\tau_2}$$

Again, two different cases are to be distinguished:

1. In an optically thin layer (τ_2 <<1), T_m converges to the average physical temperature of the volume $\langle T \rangle = T_c + 0.5T_d\tau_2$, and this value is again linear in τ_2.
2. For τ_2 >>1, T_m converges to the physical temperature at position τ=1, giving $T_m = T(\tau = 1) = T_c + T_d$. Geometrically, the position is situated at a distance, Δs = 1/γ_a, from s_2. This property is used for temperature profiling in spectral bands with high absorption (see Figure 9.5).

9.4 Linear temperature profile in an exponentially decreasing atmosphere

9.4.1 Planetary troposphere

In the **planetary troposphere** the density of an absorbing agent, and thus γ_a, often deceases exponentially with increasing height z (e.g. absorption by oxygen in the 50 to 70 GHz range, water vapour near 22 GHz, 183 GHz), whereas T decreases linearly with z (up to the tropopause at height z_p) due to adiabatic cooling:

$$T = T_c - \Gamma z \,; 0 \le z \le z_p; \text{ else } T = T_p = T_0 - \Gamma z_p \tag{9.6}$$

$$\gamma_a = \gamma_0 e^{-z/z_0} \tag{9.7}$$

Here we will assume a plane-parallel atmosphere (Figure 9.1), and we will first consider the situation for observations from the surface and then from space. The integration of the RTE requires some efforts, but the results will be instructive. They are useful for the **calibration** of instruments (**tipping curve**) and in the **retrieval of atmospheric properties**. Main MATLAB functions are `expat` (for x=1) and expatrec (for x<1) for downwelling radiation, `expatup` (x=1) and expatuprec (x<1) for upwelling radiation to compute the functions $L_{\downarrow,\uparrow}$ (see below). All related function names begin with "expat".

9.4.2 Downwelling radiation

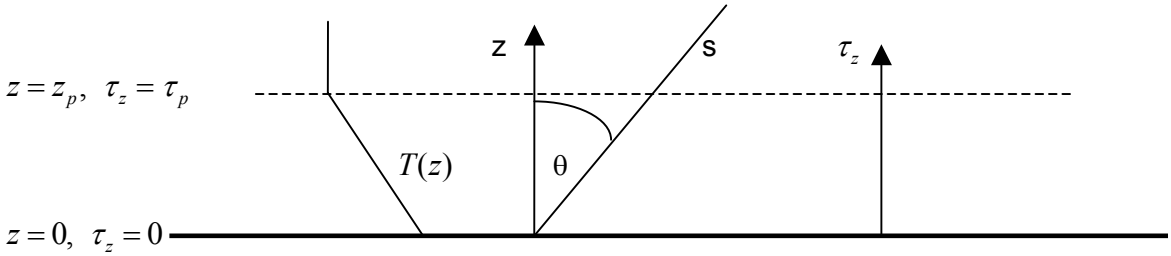

Figure 9.1: Plane-parallel atmosphere with a linear temperature profile up to height z_p.

First we assume observation of T_b from the surface at $z = 0,\ \tau_z = 0$ in a direction with a zenith angle θ, thus $s = z/\mu$ where $\mu = \cos\theta$. Equation (8.23) is adapted to the plane-parallel medium:

$$T_b(\tau = 0,\ \mu) = T_{b1}\exp\left(-\frac{\tau_p}{\mu}\right) + \frac{1}{\mu}\int_0^{\tau_p} T(\tau_z)\exp\left(-\frac{\tau_z}{\mu}\right)d\tau_z \tag{9.8}$$

where T_{b1} is the brightness temperature at the tropopause, and the directions of τ_z and of s (from $-\mu$ to $+\mu$) have been changed by defining

$$\tau_z = \int_0^z \gamma_a(z')dz';\ \tau_p = \int_0^{z_p} \gamma_a(z')dz' \text{ and } \tau_1 = \int_0^{\infty} \gamma_a(z')dz' \tag{9.9}$$

Inserting (9.7) into (9.9) gives $\tau_z = \tau_1\left(1 - e^{-z/z_0}\right)$ and $\tau_1 = \gamma_0 z_0$, therefore $z = -z_0\ln\left(1 - \frac{\tau_z}{\tau_1}\right)$ is used together with (9.6) to define the τ_z dependence of temperature:

$$T(\tau_z) = T_0 + \Gamma z_0\ln\left(1 - \frac{\tau_z}{\tau_1}\right);\ 0 \le \tau_z \le \tau_p \tag{9.10}$$

Equation (9.8) now reads $T_b = T_{b1}e^{-\beta} + \frac{1}{\mu}\int_0^{\tau_p}\left(T_0 + \Gamma z_0\ln\left(1 - \tau_z/\tau_1\right)\right)\exp\left(-\frac{\tau_z}{\mu}\right)d\tau_z$; where $\beta = \tau_p/\mu$, and with $x' = \tau_z/\tau_1$ and $\alpha = \tau_1/\mu$ the equation can be written as

$$T_{b\downarrow} = T_{b1}e^{-\beta} + T_0(1 - e^{-\beta}) - \Gamma z_0\alpha L_\downarrow;\ \text{where}\ L_\downarrow = -\int_0^x \ln(1 - x')e^{-\alpha x'}dx', \tag{9.11}$$

and $x = \tau_p/\tau_1 = \beta/\alpha = 1 - \exp(-z_p/z_0)$. The arrow ↓ indicates the downwelling direction. Unfortunately there is no direct analytical solution for $L_\downarrow$. Note that the integrand is negative because the argument of the logarithm is in the interval $[0,1]$. For the $[0 \le x' \le x \le 1]$ limited values we replace the logarithmic function by its Taylor Series: $\ln(1 - x') = -\sum_{n=1}^{\infty}\frac{x'^n}{n}$, leading to a convergent series of integrals

$$L_\downarrow = \sum_{n=1}^{\infty} L_{n\downarrow};\ \text{where}\ \ L_{n\downarrow} = \frac{1}{n}\int_0^x x'^n\exp(-\alpha x')dx';\ \ 0 < x \le 1 \tag{9.12}$$

The integral $L_{n\downarrow}$ of (9.12) cannot directly be solved, but for *n*=1 we find by partial integration

$$L_{1\downarrow} = \frac{1 - t(1+\beta)}{\alpha^2};\ \text{where}\ \beta = \alpha x;\ \ t = e^{-\beta} \tag{9.13}$$

and for $n > 1$, there exists a recurrence relation, also found by partial integration

$$L_{n\downarrow} = \frac{-tx^n}{\alpha n} + \frac{1}{\alpha}\int_0^x x'^{n-1}\exp(-\alpha x')dx' = \frac{-tx^n}{n\alpha} + \frac{n-1}{\alpha}L_{n-1,\downarrow} \tag{9.14}$$

Instead of directly computing $L_{n\downarrow}$, it is advantageous to introduce $J_n = L_{n\downarrow}/t$. For this quantity we find the downward recurrence formula

$$J_{n-1} = \frac{x^n}{n(n-1)} + \frac{\alpha J_n}{n-1}; \quad J_n = L_{n\downarrow}/t \tag{9.15}$$

Downward recurrence is used to get stable solutions from (9.15), starting at *m*=maximum(*n*), noting that $\sum_{j=1}^{\infty} J_{m+j} < 1/m \to 0$, for sufficiently large *m*. For the starting value we have

$$J_m = \frac{x^{m+1}}{m(m+1)} \tag{9.16}$$

The remaining terms then follow from (9.15). This recurrence is computed with the MATLAB function `expatrec(m, alfa, x)`. The convergence is fast for x<0. However, for x=1 (this value means that the stratosphere has no influence on $T_{b\downarrow}$), either a very large *m* has to be selected or a special treatment is needed: MATLAB: `expat(alfa), expatN(alfa)`. The function was approximated for α to at least 40 by the fit:

$$L_{\downarrow}(\alpha, x=1) \cong \begin{cases} \exp\left(-\dfrac{0.794\alpha}{1+0.0677\alpha}\right); & 0 \le \alpha \le 6; \quad \text{stdev} = 1.4\% \\ \exp\left(-0.692 - \dfrac{0.649\alpha}{1+0.0732\alpha}\right); & 6 < \alpha < 40; \quad \text{stdev} \cong 2\% \end{cases} \tag{9.17}$$

The following figure shows results of $L_{\downarrow}$ for a number of x values. It is found that for x >0.6 the functions rapidly converge to the top curve (x=1).

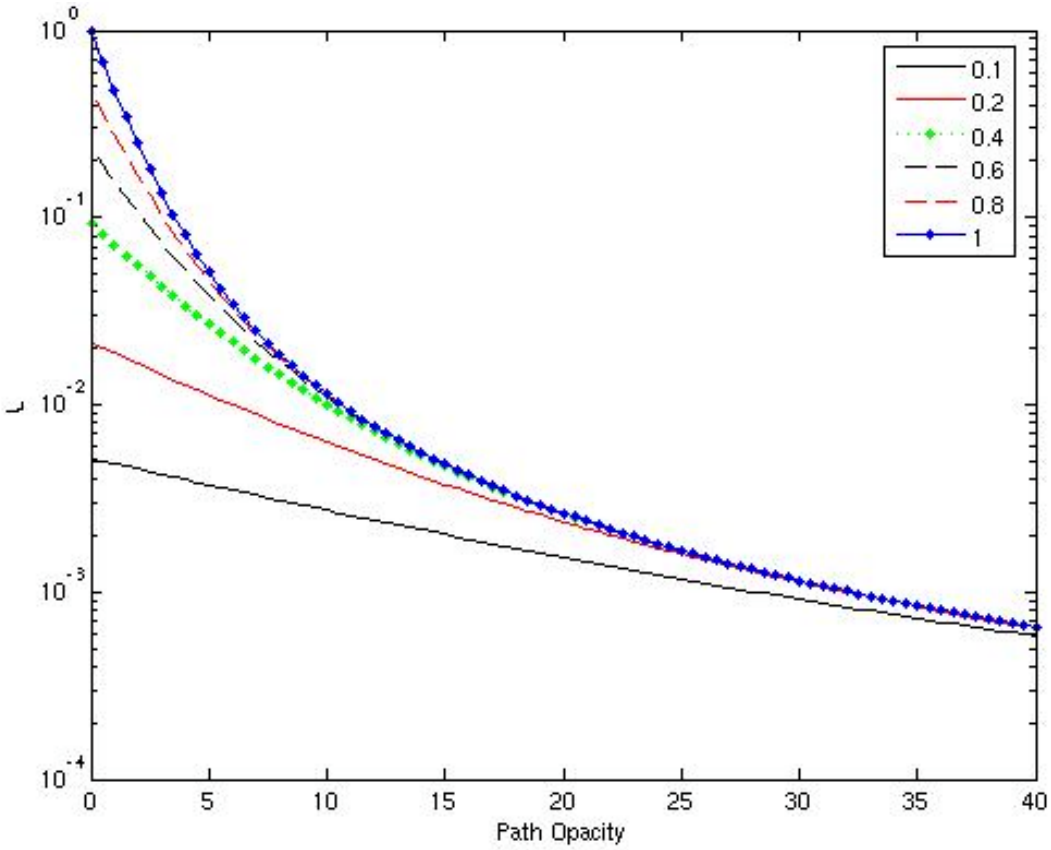

Figure 9.2: Semi-logarithmic plot of the function $L_{\downarrow}(\alpha)$ versus total path opacity α for x= 0.1, 0.2, 0.4, 0.6, 0.8, 1.

Now, with the neglect of the cosmic background, we can write for the downwelling brightness temperature at the tropopause

$$T_{b1} = T_p\left(1 - e^{\beta-\alpha}\right) = \left(T_0 - \Gamma z_p\right)\left(1 - e^{\beta-\alpha}\right) \tag{9.18}$$

The brightness temperature $T_{b\downarrow} = T_{b1}e^{-\beta} + T_0\left[1 - e^{-\alpha}\right] - \alpha\Gamma z_0 L_\downarrow(\beta)$ at the surface becomes

$$T_{b\downarrow} = T_0\left[1 - e^{-\alpha}\right] - \Gamma z_p\left(e^{-\beta} - e^{-\alpha}\right) - \alpha\Gamma z_0 L_\downarrow(\alpha, x) \tag{9.19}$$

Remember that $\alpha = \tau_1/\cos\theta$ is the total opacity of the atmosphere along the view direction, and $\beta = \alpha x$ is the corresponding value for the troposphere. The effective mean temperature (9.3) follows from (9.19)

$$T_m = T_0 - \Gamma z_0 F_\downarrow(\alpha, x);\ F_\downarrow = \frac{z_p\left(e^{-\alpha x} - e^{-\alpha}\right) + \alpha z_0 L_\downarrow(\alpha, x)}{z_0(1 - e^{-\alpha})} \tag{9.20}$$

The factor $F_\downarrow$ in (9.20) is shown in Figure 9.3 versus zenith angle for the zenith opacities of τ_1= 0.1, 0.4 and 2 and for two values of x: 0.7 and 1. For small τ_1 the curves are very flat over a large angular range, meaning that T_m is nearly constant. This fact is important for the tipping calibration which is an extrapolation to the cosmic brightness (≅ 3K).

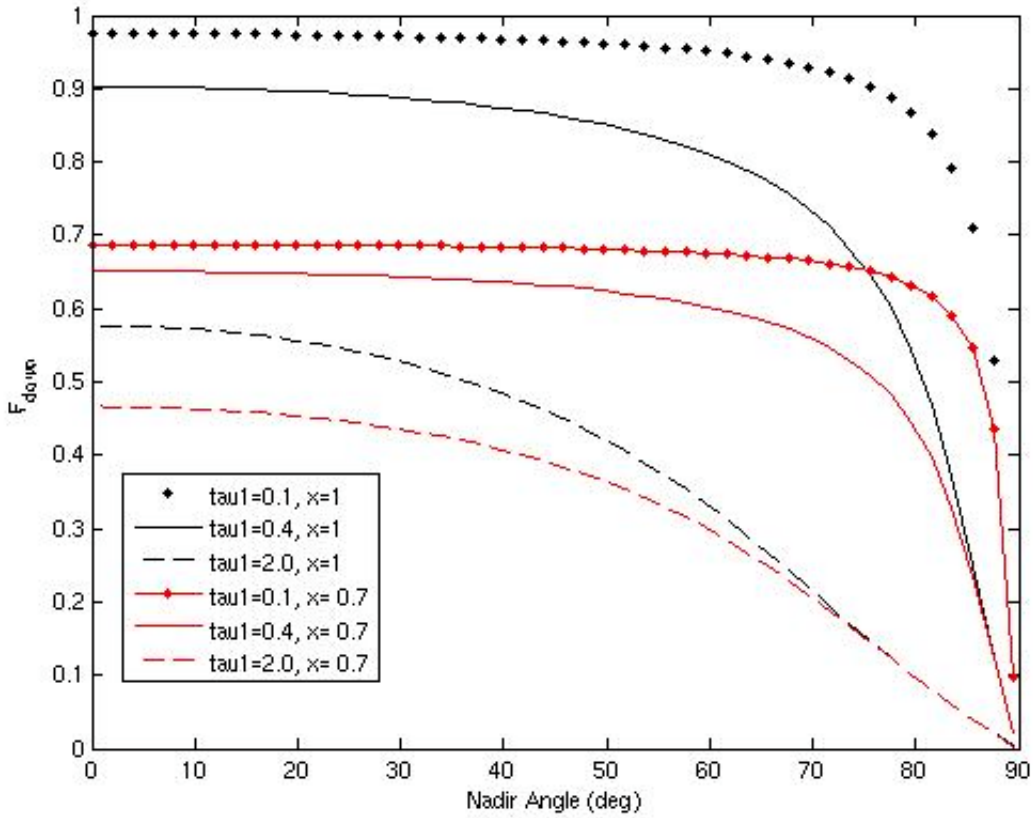

Figure 9.3: Angular variation of the factor $F_\downarrow$ in (9.20) affecting T_m for zenith opacities τ_1 of 0.1, 0.4 and 2.0 for x= 0.7 and x=1.

As an **example** we compute and present in Figure 9.4 the angular dependence of $T_{b\downarrow}$ for zero background for the situations of Figure 9.3, and for standard values of the **terrestrial troposphere** (Γ= 6.5K/km and z_0 =7.5 km). The difference between x=0.7 and x=1 is quite small in all cases.

Figure 9.5 shows a comparison of measured and computed brightness temperatures at 52.5 and 53.94 GHz versus zenith angle. The agreement is reasonable.

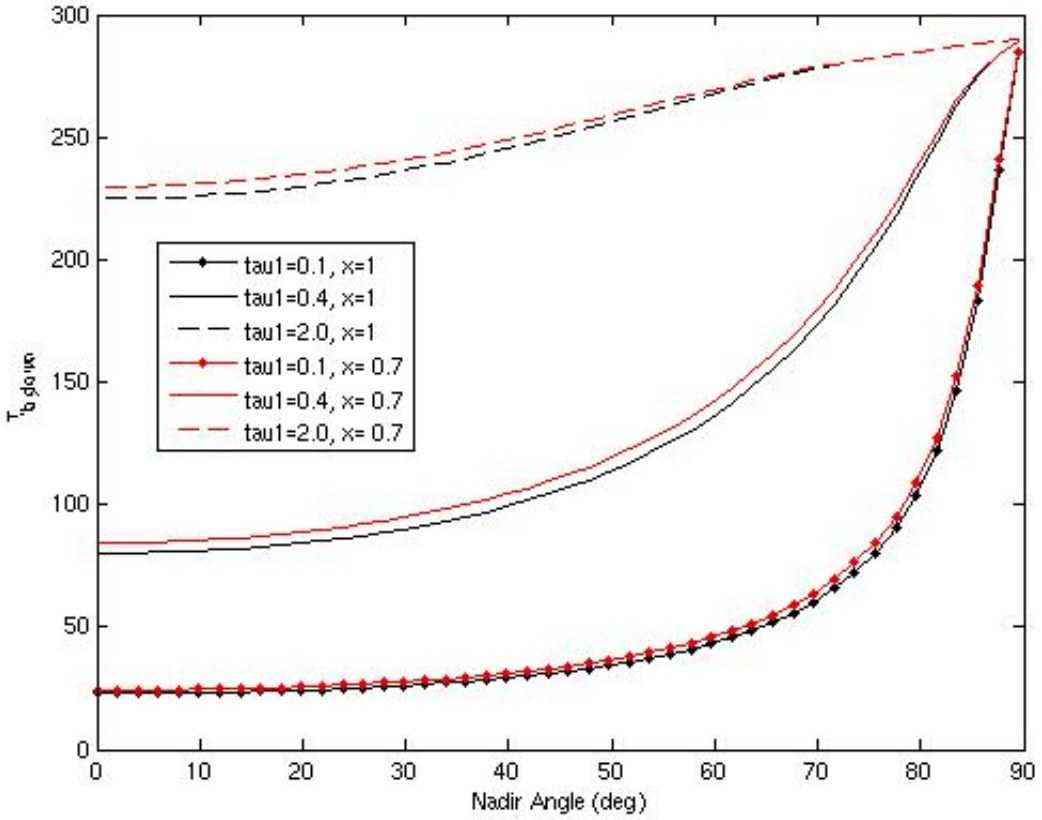

Figure 9.4: Angular dependence (tipping curves) of $T_{b\downarrow}$ in K for the situations of Figure 9.3, for $T_0 = 290K$, $\Gamma = 6.5K/km$, $z_0 = 7.8km$.

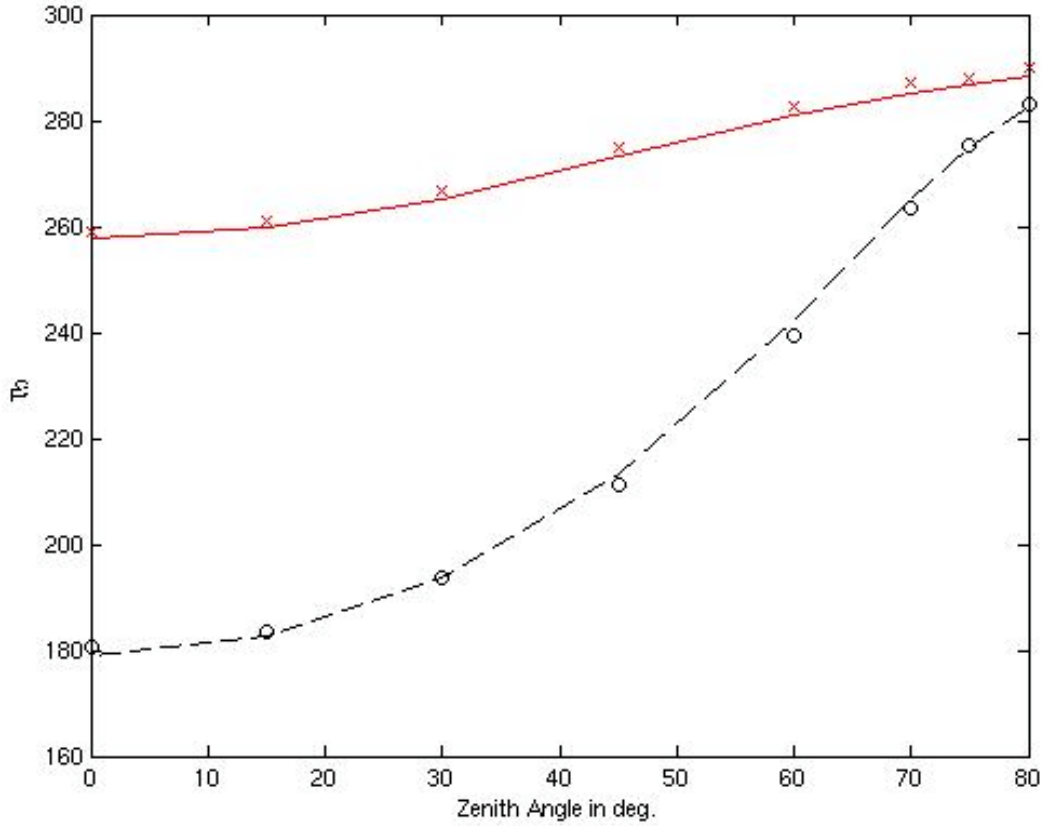

Figure 9.5: Measured angular dependence of $T_{b\downarrow}$ in K at 52.5 (o) and 53.94 (x) GHz and comparison with computations for $T_0 = 291K$, $\Gamma = 6.5K/km$, $z_p = 12km$, 52.5 GHz: $\gamma_0 = 0.18/km$ $z_0 = 6.4km$ and at 53.94 GHz: $\gamma_0 = 0.48/km$, $z_0 = 6.0km$. ASMUWARA measurements of 18. 09. 2002 (Martin, 2003).

9.4.3 Upwelling radiation

For upwelling radiation we are interested in the brightness temperature $T_{b\uparrow}$ above the atmosphere. First we have to consider the brightness temperature at the height z_p of the tropopause where $\tau_z = \tau_p = \tau_1\left(1 - e^{-z_p/z_0}\right)$. In analogy to (9.8), and using (9.9) for τ_z, the formal solution reads

$$T_{bp} = T_b(\tau_z = \tau_p,\ \mu) = T_{b0}e^{-\beta} + \frac{1}{\mu}\int_0^{\tau_p} T(\tau_z)\exp\left(-\frac{\tau_p - \tau_z}{\mu}\right)d\tau_z \tag{9.21}$$

where T_{b0} is the upwelling brightness temperature at the surface ($\tau_z = 0$). Expressing $T(\tau_z)$ by (9.10) as before gives again the form of (9.11), adapted to upwelling radiation

$$T_{bp} = T_{b0}e^{-\beta} + T_0(1 - e^{-\beta}) - \Gamma z_0 \alpha L_\uparrow(\beta) \tag{9.22}$$

where $L_\uparrow$ is given by

$$L_\uparrow = -e^{-\beta}\int_0^{\beta/\alpha} \ln(1-x)e^{\alpha x}dx = \sum_{n=1}^{\infty} L_{n\uparrow};\ \text{where}\ L_{n\uparrow} = \frac{e^{-\beta}}{n}\int_0^{\beta/\alpha} x^n \exp(+\alpha x)dx \tag{9.23}$$

Now we have (again with $t = e^{-\beta}$) the recurrence relation

$$L_{n\uparrow} = \frac{t}{\alpha}\left(\frac{x^n}{nt} - \int_0^x x'^{n-1}\exp(+\alpha x')dx'\right) = \frac{x^n}{n\alpha} - \frac{n-1}{\alpha}L_{n-1,\uparrow} \tag{9.24}$$

which is again more stable in the downward direction,

$$L_{n-1,\uparrow} = \frac{x^n}{n(n-1)} - \frac{\alpha L_{n,\uparrow}}{n-1} \tag{9.25}$$

An approximation to $L_\uparrow(\alpha, x=1)$ (for more accurate computations, use the MATLAB functions `expatup(alfa)`, `expatupN(alfa)`) is given by

$$L_\uparrow(\alpha, x=1) \cong 0.0257 + \frac{1 - 0.0257}{1 + 0.2709\alpha};\quad \text{stdev=0.0012} \tag{9.26}$$

For 0.5<x<1 the function can be roughly approximated by

$$L_\uparrow(\alpha, x) \cong \left(0.0257 + \frac{1 - 0.0257}{1 + 0.2709\alpha}\right)\exp\left(-3.7(1-x)\right) \tag{9.27}$$

The function $L_\uparrow(\alpha, x)$ (MATLAB: `expatuprec` computed with the recursive formula) is shown in Figure 9.6 versus α for various x values. For x=1 the function is also decreasing from 1, but in much weaker way than $L_\downarrow$. Furthermore for x<1 all function values are decreased, in contrast to the downwelling situation.

The effective mean temperature (9.3) at the tropopause level follows from (9.22)

$$T_m = T_0 - \Gamma z_0 F_\uparrow;\ \text{where}\quad F_\uparrow = \frac{\alpha L_\uparrow(\alpha, x)}{1 - t} \tag{9.28}$$

The upwelling brightness temperature $T_{b,\uparrow}$ above the atmosphere follows from T_{bp} after further transformation in the stratosphere. If it can be represented by a constant temperature, namely by the one at the tropopause $T_p = T_0 - \Gamma z_p$, we get

$$T_{b,\uparrow} = T_{bp}e^{-(\alpha-\beta)} + T_p(1 - e^{-(\alpha-\beta)}) \tag{9.29}$$

This function, for $T_{b0} = T_0$, is plotted versus incidence angle in Figure 9.7, where the data are also compared with **satellite** observations. The parameters listed in the figure caption are reasonable for the selected frequency of 53.4 GHz with a zenith opacity τ_1 of 2.25.

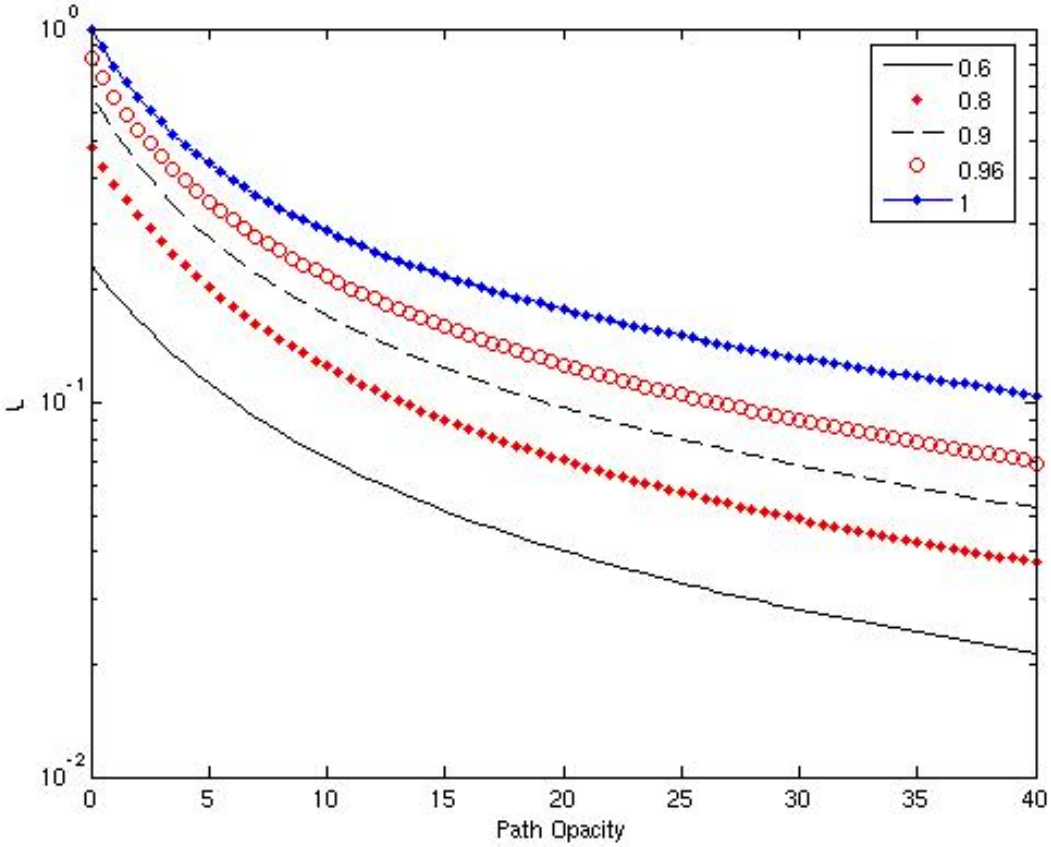

Figure 9.6: The function $L_{\uparrow}(\alpha, x)$ versus α for x values (from top to bottom) of 1, 0.96, 0.9, 0.8, and 0.6 (computed with the MATLAB function `expatuprec` and plotted with `expatuprecscan`).

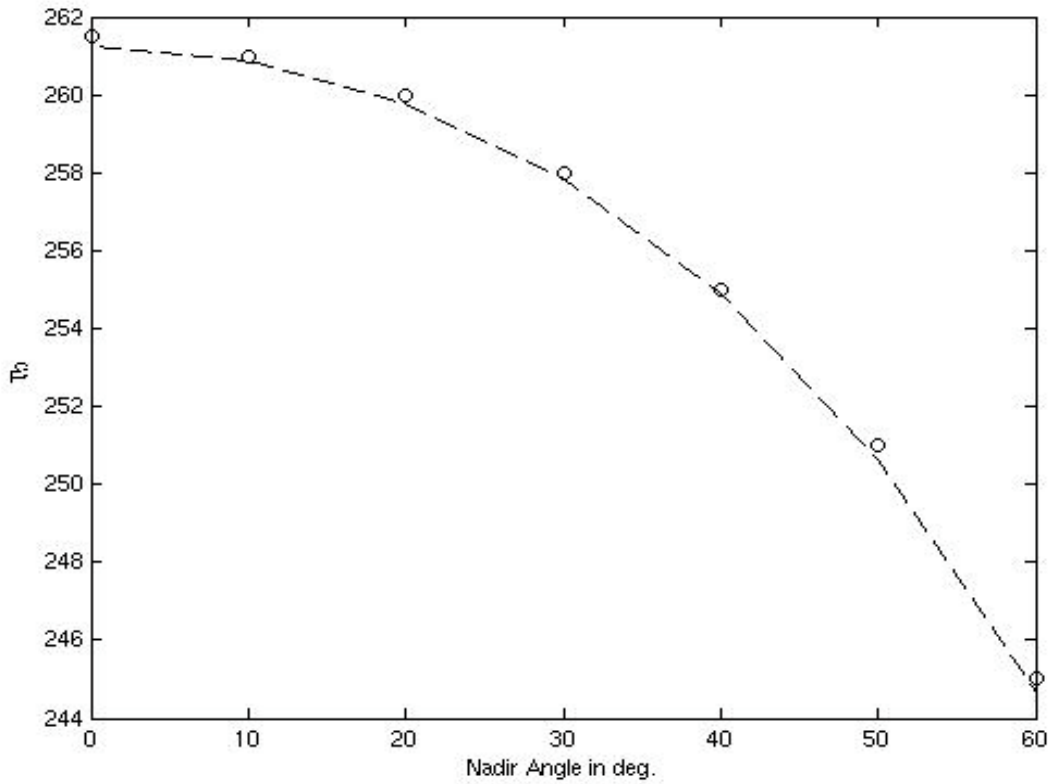

Figure 9.7: Angular variation of measured (o) and computed (dashed line) $T_{b,\uparrow}$ at 53.4 GHz over tropical rain forest. Measurements by AMSU-A (NOAA satellite), computations for $\gamma_0 = 0.5/km$, $\Gamma = 6.5K/km$, $z_0 = 4.5km$, $z_p = 14km$, $T_0 = 300K$, thus τ_1 and *x* turn out to be 2.25 and 0.955, respectively.

10 Standard Problems for Scattering

In this chapter **emission of thermal radiation is neglected**; it can be included afterwards by the application of Kirchhoff's law. Furthermore, from here on, the zenith opacity is simplified from τ_z to τ, and the Index 1 for $1/n^2$ normalised radiance is omitted as well.

10.1 Scattering at a half-space

Even to solve the scatter-free situations, we need to know the interaction of the downwelling radiation once it reaches the surface. Part of this radiation may be absorbed whereas another part may be returned to the atmosphere by reflection and scattering at or below the surface. In this way the downwelling and the upwelling solutions of the RTE get linked: $T_{b0} = (1 - r_1)T_0 + r_1 T_{b,\downarrow}(z = 0)$, see e.g. Mätzler (2005) and references therein.

Geometry

The standard geometry is a non-scattering upper half-space, a scattering half-space below, and the two are separated by the plane z=0 (Figure 10.1). Downwelling radiation from the upper half-space is from a single direction $(-\mu_0, \phi_0)$ where $-\mu_0 = \cos\theta_0,\ \pi \geq \theta_0 > \pi/2$. The task is to determine the radiance $I_\nu(0,\mu,\phi)$ that escapes from the lower to the upper half-space.

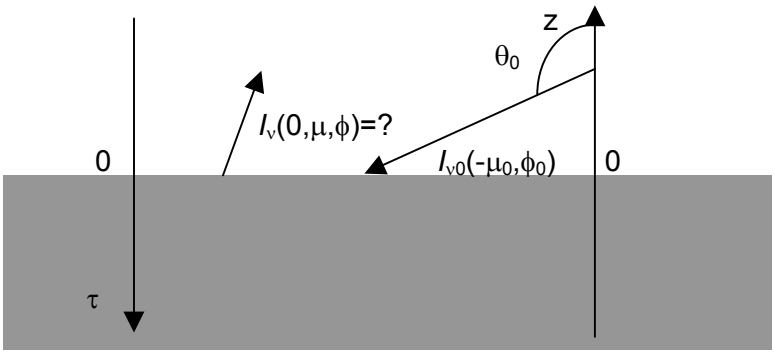

Figure 10.1: Geometry of illumination of a semi-infinite scattering medium, called half-space, at z<0.

The scattering function

The solution of the task is formally solved by the definition of the non-dimensional scattering function S, see Chandrasekhar (1960), p. 17:

$$I_\nu(0,\mu,\phi) = \frac{1}{4\pi\mu} \int_{2\pi} d\Omega' S(\mu,\phi,\mu',\phi') \cdot I_\nu(0,-\mu',\phi') \qquad (10.1)$$

where the integration (at z=0) is over all downwelling directions (μ': 0 to 1, ϕ': 0 to 2π), and $d\Omega' = d\mu d\phi$. If the downwelling radiation is limited to a single direction, as for the **standard situation**

$$I_\nu(0,-\mu',\phi') = F_\nu \delta(\mu' - \mu_0)\delta(\phi' - \phi_0) = I_{\nu 0}(-\mu_0,\phi_0) \qquad (10.2)$$

where F_ν is the spectral flux density in the incident direction $(-\mu_0,\phi_0)$, and where δ means the Dirac Delta function, we get

$$I_\nu(0,\mu,\phi) = \frac{F_{\nu z}}{4\pi\mu\mu_0} S(\mu,\phi,\mu_0,\phi_0) = \frac{F_\nu}{4\pi\mu} S(\mu,\phi,\mu_0,\phi_0) \qquad (10.3)$$

and $F_{\nu z}$ is the vertical component of $\mathbf{F}_\nu$, i.e. downwelling power per unit horizontal area.

Comments

1. One reason for the special choice of S is the **reciprocity**:

$$S(\mu,\phi,\mu_0,\phi_0) = S(\mu_0,\phi_0,\mu,\phi) \qquad (10.4)$$

2. The definition of S is **identical** with the bistatic surface-scattering coefficient σ^0 used in microwave scattering, see Ulaby et al. (1981), p. 250.

3. **Relation to bistatic scattering cross section**: Equation (10.3) is similar to the situation in Chapter 2 for single scatterers. But here, the volume is infinite in extent; therefore, an adaptation is needed. Radiation scattered by an incident intensity $I_i = F$ does not produce a spherical wave, as in Section (2.1), but plane waves. The scattering directions for escaping radiation are limited to the upper half-space with solid angle 2π. Nevertheless, with the limitation of the illuminated surface to an area *A*, and with the assumption that scattered radiation escapes at the same place as where the incident radiation entered, a correspondence can be established between *S* and the bistatic scattering coefficient σ_{bi}:

$$S(\mu,\phi,\mu_0,\phi_0) = \sigma_{bi}(A)/A \tag{10.5}$$

4. **Emissivity and reflectivity**

The absorptivity a_1 in a given direction and thus the emissivity e_1 (reciprocal direction) of the lower half-space follows from Kirchhoff's Law with N=2: $e_1 = a_1 = 1 - r_1$, where r_1 is the reflectivity of the lower half-space (and thus the emissivity of the upper half-space). This quantity can be determined from S by computing the ratio of the scattered upwelling $F_{\nu+}(\tau = 0)$ flux to the downwelling incident flux $F_{\nu z}$:

$$r_1(\mu_0,\phi_0) = \frac{F_{\nu+}}{F_{\nu z}};\ \text{where}\ F_{\nu+} = \int_{2\pi} \mu I_\nu(0,\mu,\phi)d\Omega;\ \rightarrow\ r_1 = \frac{1}{4\pi\mu_0}\int_{2\pi} S(\mu,\phi,\mu_0,\phi_0)d\Omega \tag{10.6}$$

The normalisation by $F_{\nu z}$ (not F_ν) is required because the incident intensity is diluted over the horizontal area with respect to an area perpendicular to the beam.

5. **Polarisation**

A full treatment of polarisation requires S to be replaced by a 4x4 matrix. However, very often only one pair of orthogonal polarisation states, p and q, respectively is required. Then we need two scattering functions to describe the like- and the cross-polarised components, respectively:

$$I_{\nu,p}(0,\mu,\phi) = \frac{F_{\nu z,p}}{4\pi\mu\mu_0} S_{pp}(\mu,\phi,\mu_0,\phi_0);\quad I_{\nu,q}(0,\mu,\phi) = \frac{F_{\nu z,p}}{4\pi\mu\mu_0} S_{qp}(\mu,\phi,\mu_0,\phi_0) \tag{10.7}$$

Examples

1. **Lambert scattering** is an empirical law with complete depolarisation ($S_{pp} = S_{qp} = S/2$) found for many rough surfaces:

$$S(\mu,\phi,\mu_0,\phi_0) = S_0\mu_0\mu;\ \rightarrow\ I_\nu(0,\mu,\phi) = S_0 F_{\nu z}/4\pi \tag{10.8}$$

where S_0 is a constant. For the reflectivity we get

$$F_{\nu+} = \frac{S_0 F_{\nu z}}{4\pi} 2\pi \int_0^1 \mu d\mu = \frac{S_0 F_{\nu z}}{4};\ \text{therefore}\ r_1 = \frac{S_0}{4} \tag{10.9}$$

2. **Specular reflection**:

A perfectly flat interface can produce specular reflection where all reflected radiation is in the mirror direction. In this case there is no need for a scattering function because the azimuthal direction is conserved ($\phi = \phi_0$) and the incidence angle is equal to the reflection angle ($\mu = \mu_0$). Nevertheless it is sometimes useful to express the situation with an appropriate S function using the delta function

$$S(\mu,\phi,\mu_0,\phi_0) = 4\pi\mu_0 r_1 \delta(\mu - \mu_0)\delta(\phi - \phi_0) \tag{10.10}$$

The reflectivity r_1 is recovered by the integration according to (10.6).

3. **Blackbody**:

If S=0 we get r_1 =0, which means that there is no reflection. Then the half-space is called a blackbody. According to Kirchhoff's law this body has emissivity 1.

10.2 Scattering in and transmission through a layer

Standard Problem 2 is a scattering layer of finite thickness. Illumination is a single source from above as in Section 10.1, and emission is again neglected.

Geometry

A plane-parallel layer of finite thickness ($-z_1 \le z \le 0$) is illuminated with a parallel beam from direction ($-\mu_0,\phi_0$).

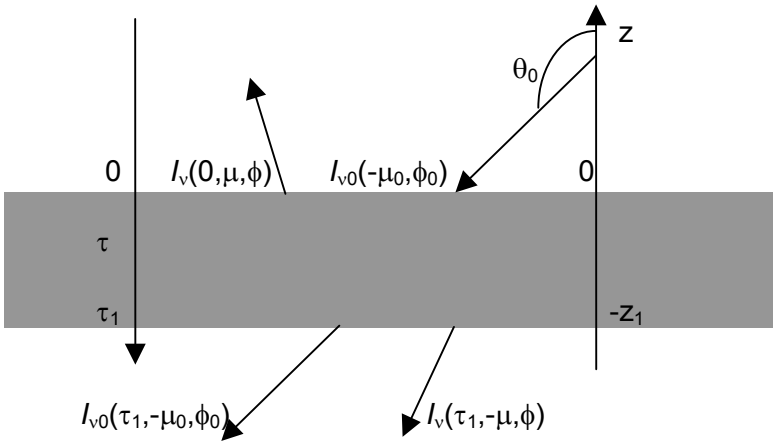

Figure 10.2: Geometry of a plane-parallel scattering layer illuminated by a beam of radiation from above showing the direct and scattered components.

Scattering and transmission functions

The **scattering function** *S* is defined as in Section 10.1. Radiation escaping at the lower boundary of the medium is split into a direct and a scattered component, the latter being described (in analogy to S) by a **transmission function** *T*. The direct component is given by

$$I_{\nu 0}(\tau_1,-\mu_0,\phi_0)= F_\nu(\tau_1)= F_\nu t_0, \text{ where } t_0=\exp(-\tau_1/\mu_0) \tag{10.11}$$

The scattered-and-transmitted radiance at $\tau=\tau_1$ is defined by

$$I_\nu(\tau_1,-\mu,\phi)= \frac{F_{\nu z}}{4\pi\mu\mu_0}\mathrm{T}(\tau_1,\mu,\phi,\mu_0,\phi_0) \tag{10.12}$$

where $\mathrm{T}(\tau_1,\mu,\phi,\mu_0,\phi_0)$ is the transmission function, and for diffuse illumination we have, in analogy to (10.1), for the scattered-and-transmitted part

$$I_\nu(\tau_1,-\mu,\phi)=\frac{1}{4\pi\mu}\int_0^1\int_0^{2\pi} T(\tau_1,\mu,\phi,\mu',\phi')\cdot I_\nu(0,-\mu',\phi')d\phi' d\mu' \tag{10.13}$$

Transmissivity and emissivity

The reflectivity is given again by Equation (10.6), and the **transmissivity**, t_1, expressing the fraction of the power transmitted through the layer, is given by (10.14), taking into account the direct beam by t_0:

$$t_1 = t_0 + \frac{1}{4\pi\mu_0}\int_{2\pi} T(\mu,\phi,\mu_0,\phi_0)d\Omega \tag{10.14}$$

Application of Kirchhoff's Law, now with *N*=3 for the three regions, gives the **layer emissivity** valid for the reciprocal direction ($\mu_0,\phi_0+\pi$): $e_1=1-t_1-r_1$.

Comments

1. **Reciprocity**, Equation (10.4), is also valid for *T*.
2. Standard Problem 1 is recovered by choosing $\tau_1 \to \infty$.
3. **Scattering layer above a Lambert surface** is called the **planetary problem**, see Chandrasekhar (1960) § 72.

10.3 Distinction between direct and scattered radiation

In connection with the standard problems, it is useful to write the radiative transfer equation in the following form (again neglecting emission)

$$\mu\frac{dI_\nu(\tau,\mu,\phi)}{d\tau} = I_\nu(\tau,\mu,\phi) - \frac{1}{4\pi}\int_{4\pi} p(\mu,\phi,\mu',\phi')I_\nu(\tau,\mu',\phi')d\Omega' - \frac{Fe^{-\tau/\mu_0}}{4\pi}p(\mu,\phi,-\mu_0,\phi_0) \quad (10.15)$$

where $I_\nu(\tau,\mu',\phi')$ consists of scattered radiation, only. The last term in (10.15) is the single-scattered radiance produced by the **reduced incident intensity** Ft_0 at position τ, where $t_0=\exp(-\tau/\mu_0)$.

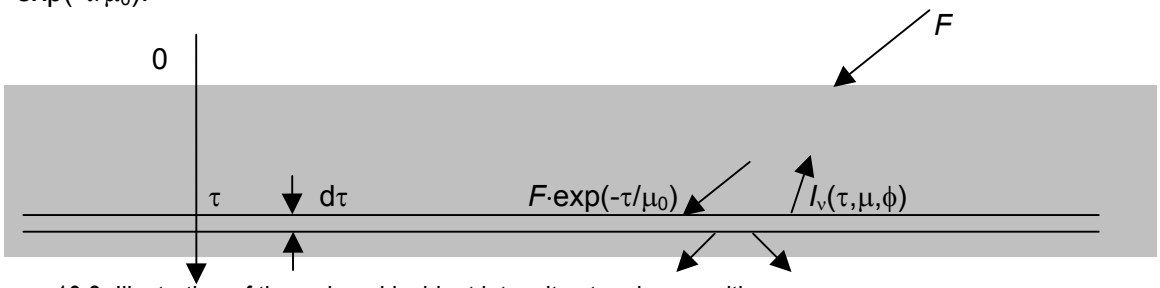

Figure 10.3: Illustration of the reduced incident intensity at a given position τ.

10.4 Axial symmetry

A further standard situation is axial symmetry, both in the phase function and in the illumination. The consequence is a simplification of the RTE (again neglecting thermal emission). By integration of the RTE over azimuth, we get (since $d\Omega' = d\phi'\,d\mu'$)

$$\mu\frac{dI_\nu(\tau,\mu)}{d\tau} = I_\nu(\tau,\mu) - \frac{1}{2}\int_{-1}^{1} p_0(\mu,\mu')\cdot I_\nu(\tau,\mu')\cdot d\mu' \quad (10.16)$$

where $p_0(\mu,\mu')$ is the phase function averaged over azimuth:

$$p_0(\mu,\mu') = \frac{1}{2\pi}\int_0^{2\pi} p(\mu,\phi,\mu',\phi')d\phi \quad (10.17)$$

Generally $p(\cos\vartheta)$, with $\cos\vartheta = \mu\mu' + \sqrt{(1-\mu^2)(1-\mu'^2)}\cos(\phi-\phi')$, see equation (8.15), is expressed by a series of **Legendre** Polynomials with coefficients g_l (Thomas and Stamnes, 1999, p. 178, Chandrasekhar, 1960, p. 7, Meador and Weaver, 1980).

$$p(x) = \varpi_0\sum_{l=0}^{\infty}(2l+1)g_l P_l(x);\ \text{where}\ x=\cos\vartheta,\ g_l = \frac{1}{2\varpi_0}\int_{-1}^{1} p(x)P_l(x)dx \quad (10.18)$$

The big advantage of this representation is that $p_0(\mu, \mu')$ of (10.17) can be expressed by the same coefficients, writing:

$$p_0(\mu,\mu') = \varpi_0\sum_{l=0}^{\infty}(2l+1)g_l P_l(\mu)P_l(\mu') \quad (10.19)$$

This representation is especially useful if the series is limited to a small number of terms. For the lowest orders we have: $P_0=1;\ P_1=x;\ P_2=0.5(3x^2-1);\ P_3=0.5(5x^3-x)$, $P_4=(35x^4-30x^2+3)/8$. Furthermore the polynomials are orthogonal with

$$\frac{2l+1}{2}\int_{-1}^{1} P_l(x)P_k(x) = \delta_{lk} = 1 \ \text{ for } \ l=k,\ \text{else}\ 0 \quad (10.20)$$

Due to the normalisation (8.13) of p we always have g_0=1, and $g_1=\langle\cos\vartheta\rangle$ is the asymmetry parameter. The g_l coefficients are determined by the last equation in (10.18). For Mie scattering, the coefficients g_l, $l=0$ to $l_{\max}$ are computed with the MATLAB function `mie_gi`, see also `mie_tetascanall`.

Examples

1. **Isotropic scattering**: $p(\tau,\mu,\mu')$ = ϖ_0 = constant; then the RTE becomes

$$\mu\frac{dI_\nu(\tau,\mu)}{d\tau} = I_\nu(\tau,\mu) - \frac{\varpi_0}{2}\int_{-1}^{1} I_\nu(\tau,\mu')\cdot d\mu' \tag{10.21}$$

There exist exact solutions for this problem (Chandrasekhar, 1960).

2. **Simplest asymmetric** case

$$p(\mu,\phi,\mu',\phi') = \varpi_0(1+a\cos\vartheta)\ ;\ p_0(\mu,\mu') = \varpi_0(1+a\mu\mu')\ ;\ g_1 = a/3 \tag{10.22}$$

and all higher-order terms are 0, giving the RTE

$$\mu\frac{dI_\nu(\tau,\mu)}{d\tau} = I_\nu(\tau,\mu) - \frac{\varpi_0}{2}\int_{-1}^{1} (1+a\mu\mu')I_\nu(\tau,\mu')\cdot d\mu' \tag{10.23}$$

3. **Rayleigh scattering**:

$$p(\mu,\phi,\mu',\phi') = \frac{3\varpi_0}{4}(1+\cos^2\vartheta)\ ;\ g_1 = 0,\ g_2 = 1/10;\ g_l = 0;\ l > 2 \tag{10.24}$$

4. **Henyey-Greenstein** phase function (Sobolev, 1975, p. 5):
This phase function is often used to mimic realistic situations for scattering in clouds:

$$p(\cos\vartheta) = \frac{\varpi_0(1-g^2)}{(1+g^2-2g\cos\vartheta)^{3/2}};\ g = g_1;\ \ g_l = g^l \tag{10.25}$$

5. **Mie scattering**:
Example: refractive index=3+0.1i, size parameter=2, highest order $l_{\max}$=7, 60 angular values.
The command line

```
>> mie_gi(3+0.1i, 2, 7, 60)
```

returns

```
    s: [60x4 double]
    Q: [1.7022 0.7237 0.9786 0.6215 0.4188]
   gi: [1.0003 0.4190 0.1564 0.0247 0.0527 0.0134 0.0143 3.7967e-04]
  giR: [0.7122 0.2472 0.0283 -0.0204 0.0306 0.0180 0.0071 -3.5325e-04]
  giL: [0.2880 0.1718 0.1280 0.0451 0.0221 -0.0046 0.0072 7.3292e-04]
```

Here the first row consists of the vectors of the scattering intensities versus scattering angle. The second row consists of the Mie efficiencies (Q_e, Q_s, Q_a, Q_b, $\langle\cos\vartheta\rangle$); the third row shows the factors $g_l;\ l = 0,\ l_{\max}$; the fourth and last rows contain the corresponding factors g_{lR} and g_{lL} for *R* and *L* polarisation.

As another example we test the situation of Rayleigh Scattering with
```
>> mie_gi(2+0.01i, 0.05, 3, 60)
```

```
    s: [60x4 double]
    Q: [6.7264e-04 4.1712e-06 6.6846e-04 6.2478e-06 6.3619e-04]
   gi: [1.0002 6.3644e-04 0.1002 3.9185e-05]
  giR: [0.7501 3.6365e-04 8.5824e-05 1.2481e-07]
  giL: [0.2501 2.7280e-04 0.1001 3.9060e-05]
```

The required values of $g_0 = 1,\ g_1 = 0,\ \ g_2 = 0.1,\ g_3 = 0$ are closely obtained. Also note that g_2 is due to the parallel polarisation $p_L = \varpi_0\cos^2\vartheta$.

11 Single Scattering

11.1 The radiative transfer equation and its solution

Situations where photons are only scattered once are called **single scattering**, or **first-order scattering**. In some situations in nature (e.g. thin fog layer, haze), scattering may be dominated by single scattering. This applies if the propagation path is < $1/\gamma_s$. However, multiple scattering cannot easily be avoided.
The single-scattering solution is important as starting point for solutions of **higher-order scattering**.
Again, as in Chapter 10, we neglect the emission term in the RTE, and we consider the situation of a plane-parallel layer with illumination from above (Figure 11.1).

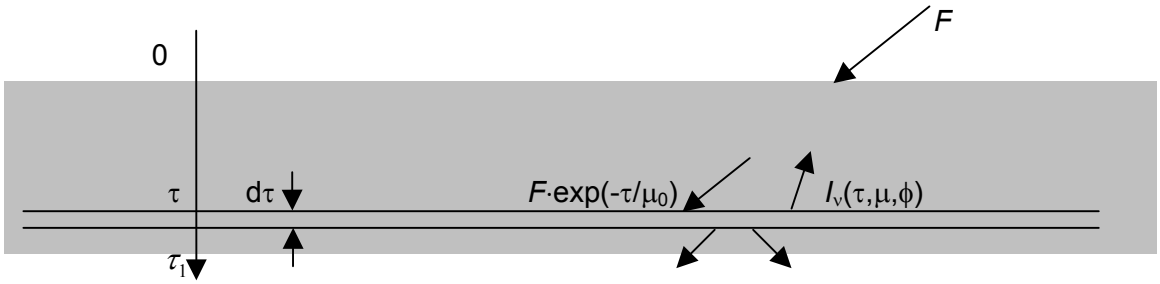

Figure 11.1: Geometry for single scattering in a plane-parallel layer.

According to (10.15) the RTE with single scattering reads for the upward radiance

$$\mu \frac{dI_\nu(\tau,\mu,\phi)}{d\tau} = I_\nu(\tau,\mu,\phi) - \frac{F_\nu}{4\pi} e^{-\tau/\mu_0} p(\tau,\mu,\phi,-\mu_0,\phi_0) \tag{11.1}$$

and for the downward radiance (with μ, μ_0 >0)

$$-\mu \frac{dI_\nu(\tau,-\mu,\phi)}{d\tau} = I_\nu(\tau,-\mu,\phi) - \frac{F_\nu}{4\pi} e^{-\tau/\mu_0} p(\tau,-\mu,\phi,-\mu_0,\phi_0) \tag{11.2}$$

The last terms in (11.1-2) are the source functions for the two situations. Inserting them into the formal solution (8.36-37) gives

$$I_\nu(0,\mu,\phi) = I_\nu(\tau_1,\mu,\phi) e^{-\tau_1/\mu} + \frac{F_\nu}{4\pi} \int_0^{\tau_1} e^{-\tau/\mu_0} e^{-\tau/\mu} p(\tau,\mu,\phi,-\mu_0,\phi_0) \frac{d\tau}{\mu} \tag{11.3}$$

$$I_\nu(\tau_1,-\mu,\phi) = I_\nu(0,-\mu,\phi) e^{-\tau_1/\mu} + \frac{F_\nu}{4\pi} \int_0^{\tau_1} e^{-\tau/\mu_0} e^{(\tau-\tau_1)/\mu} p(\tau,\mu,\phi,-\mu_0,\phi_0) \frac{d\tau}{\mu} \tag{11.4}$$

Equations (11.3-4) are the solutions of the RTE for single-scattered radiation at the upper and the lower boundary, τ=0 und τ_1, respectively, of the layer. A simplification is obtained in the standard problems where no diffuse radiation enters, see Equation (11.5) below. Then (11.3) simplifies to

$$I_\nu(0,\mu,\phi) = \frac{F_\nu}{4\pi} \int_0^{\tau_1} e^{-\tau/\mu_0} e^{-\tau/\mu} p(\tau,\mu,\phi,-\mu_0,\phi_0) \frac{d\tau}{\mu} \tag{11.3a}$$

and the same simplification applies to (11.4). Note however the product of exponentials in the integrals. A certain difficulty associated with these functions is the divergence of the arguments for grazing angles. This also means that the single-scattering approximation is hard to realise over the extremely long propagation path.

11.2 Scattering and transmission functions

In the standard problems the following boundary conditions apply (for the first one: $\tau_1=\infty$):

$$I_\nu(0,-\mu,\phi) = I_\nu(\tau_1,\mu,\phi) = 0 \tag{11.5}$$

The **scattering function** follows from identifying the upwelling radiance in the definition (10.3) for S with the radiance for single (11.3a), i.e. taking into account (11.5). If the layer is homogeneous the phase function can be extracted from the integral in (11.3), giving

$$S(\mu,\phi,\mu_0,\phi_0) = p(\mu,\phi,-\mu_0,\phi_0) I_S \tag{11.6}$$

where I_S is the integral over zenith opacity

$$I_S = \int_0^{\tau_1} e^{-\tau/\mu_0}\cdot e^{-\tau/\mu} d\tau = \int_0^{\tau_1} \exp\left(-\tau\left(\frac{\mu+\mu_0}{\mu\mu_0}\right)\right) d\tau = \frac{\mu\mu_0}{\mu+\mu_0}(1-e^{-\tau_1/\mu_0}\cdot e^{-\tau_1/\mu}) \tag{11.7}$$

and for the **transmission function** (10.12) we get in the same way

$$T(\mu,\phi,\mu_0,\phi_0) = p(-\mu,\phi,-\mu_0,\phi) I_T \tag{11.8}$$

$$I_T = \int_0^{\tau_1} e^{-\tau/\mu_0}\cdot e^{(\tau-\tau_1)/\mu} d\tau = \frac{\mu\mu_0}{\mu-\mu_0}(e^{-\tau_1/\mu} - e^{-\tau_1/\mu_0}); \quad \mu\neq\mu_0 \tag{11.9a}$$

Behaviour of (11.9a) for $\mu - \mu_0 \to 0$ (**Exercise**: Check this formula):

$$I_T \to \tau_1 e^{-\tau_1/\mu_0}; \quad \mu=\mu_0 \tag{11.9b}$$

We conclude that the scattering and transmission functions are simply related to the phase function: $S(\tau_1,\mu,\phi,\mu_0,\phi_0) \Leftrightarrow p(\mu,\phi,-\mu_0,\phi_0)$, $T(\tau_1,\mu,\phi,\mu_0,\phi_0) \Leftrightarrow p(-\mu,\phi,-\mu_0,\phi_0)$. Furthermore the reciprocity of p means reciprocity of S and T, and vice versa.

11.3 Reflectivity and transmissivity

Reflectivity

The reflectivity can be computed from (10.6) using (11.6) and (11.7) for S.

$$r(\mu_0) = \frac{1}{4\pi\mu_0}\int_0^1\int_0^{2\pi} S(\mu,\phi,\mu_0,\phi_0) d\phi d\mu = \frac{1}{2}\int_0^1 \frac{\mu p_0(\mu,-\mu_0)}{\mu+\mu_0}(1-e^{-\tau_1/\mu_0}\cdot e^{-\tau_1/\mu}) d\mu \tag{11.10}$$

Here it is helpful to express p_0 in the form of Equation (10.22), giving

$$r(\mu_0) = \frac{\varpi_0}{2}\sum_{l=0}^{\infty}(2l+1) g_l P_l(-\mu_0)\int_0^1 \frac{\mu P_l(\mu)}{\mu+\mu_0}(1-e^{-\tau_1/\mu_0}\cdot e^{-\tau_1/\mu}) d\mu \tag{11.11a}$$

If we consider the case of isotropic scattering, $p(\mu,\phi,-\mu_0,\phi_0)=\varpi_0$, we have

$$r(\mu_0) = \frac{\varpi_0}{2}\int_0^1 \frac{\mu}{\mu+\mu_0}(1-e^{-\tau_1/\mu_0}\cdot e^{-\tau_1/\mu}) d\mu = \frac{\varpi_0 F_2(\tau_1,-\mu_0)}{2\mu_0} \tag{11.11b}$$

Even this simplest situation leads to an inconvenient integral over μ. According to Tsang et al., IEEE GE-20, p. 482-485 (1982), the integral can be expressed by a special function F_2 related to the **Exponential Integral** E_n:

$$r = \frac{\varpi_0}{2}\left[1 - e^{-\tau_1/\mu_0}E_2(\tau_1) - \mu_0\ln(1+\frac{1}{\mu_0}) + \mu_0 e^{-\tau_1/\mu_0}E_1(\tau_1) - \mu_0 E_1(\tau_1+\tau_1/\mu_0)\right] \tag{11.11c}$$

$$= 0.5\varpi_0[1-\mu_0\ln(1+1/\mu_0)]\ ; \quad \text{for } \tau_1\to\infty \tag{11.11d}$$

The expression (11.11d) follows from neglecting the exponentials in (11.11b). The functions E_n are exponential integrals (Chandrasekhar (1960) Appendix1, and Abramowitz und Stegun, Handbook of Mathematical Functions (1964)):

$$E_n(z) = \int_z^\infty \frac{e^{-t}}{t^n} dt\,; \quad \text{recursion for } n \geq 1\text{: } nE_{n+1}(z) = e^{-z} - zE_n(z) \tag{11.12}$$

and for E_1 a numerical expression was given in the above references. The functions F_n (here for n=2), introduced by Chandrasekhar (1960) and by van de Hulst (1948), are defined by

$$F_n(\tau,\mu_0) = \mu_0 \int_0^1 \frac{x^{n-1}}{\mu_0 - x}\left[1 - \exp\left\{-\tau\left(\frac{1}{x} - \frac{1}{\mu_0}\right)\right\}\right] dx \tag{11.13a}$$

The equivalent representation is also used (van de Hulst, 1948) with $s = 1/\mu,\ s' = 1/x$, and it is related to the E_n function:

$$F_n(\tau,s) = \int_1^\infty \frac{1 - e^{-\tau(s'-s)}}{s'^n\,(s'-s)} ds' = \int_0^\tau e^{st} E_n(t) dt \tag{11.13b}$$

The functions were programmed in MATLAB: `E_function(n, τ)`,`F_function(n, μ, τ)`. Plots are shown in the following figures.

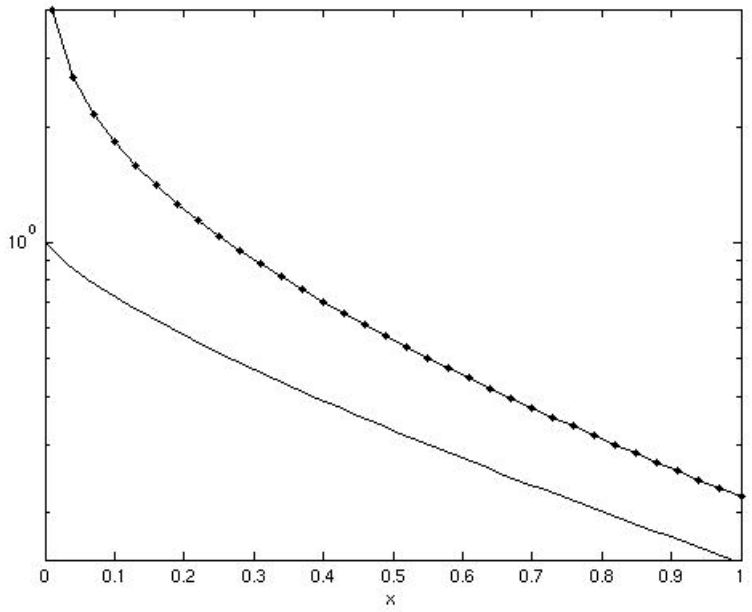

Figure 11.1: The functions E_1(x) (pointed) and E_2(x) (solid line) for 0<x<1 in semilogarithmic representation.

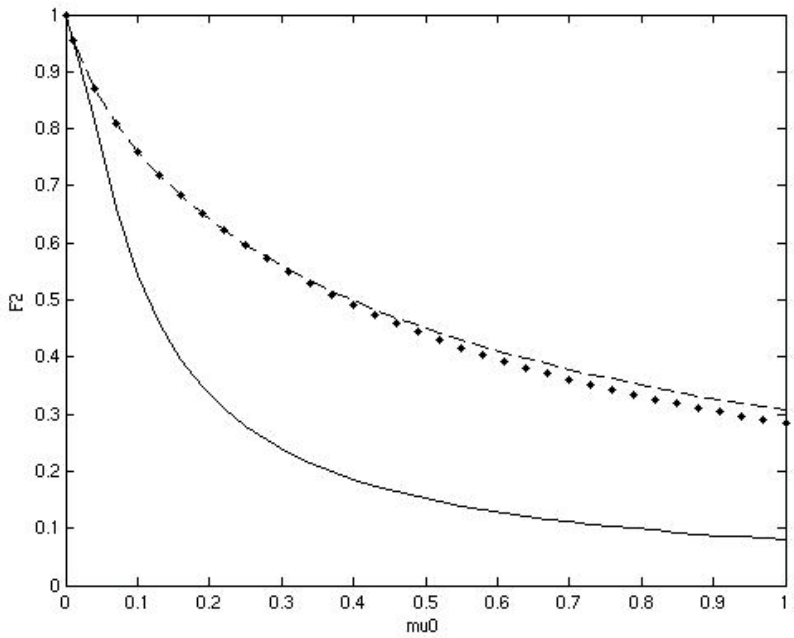

Figure 11.2: The function $F_2(\tau_1,-\mu_0)/\mu_0$ versus μ_0 for τ_1.=0.1 (solid), 1 (pointed), 10 (dashed line). Since all values are in the range (0, 1), the reflectivity is in the range (0, 0.5).

Transmissivity

The transmissivity is given by Equation (10.14), and the diffusely scattered part t_d is given by

$$t_d(\mu_0)= \frac{1}{4\pi\mu_0} \int_0^1 \int_0^{2\pi} T(\tau_1,\mu,\phi,\mu_0,\phi_0)d\phi d\mu = \frac{1}{2}\int_0^1 \frac{\mu p_0(-\mu,\mu_0)}{\mu-\mu_0}(e^{-\tau_1/\mu}-e^{-\tau_1/\mu_0})d\mu \qquad (11.14)$$

For isotropic scattering we get

$$t_d(\mu_0)= \frac{\varpi_0}{2}\int_0^1 \frac{\mu}{\mu-\mu_0}(e^{-\tau_1/\mu}-e^{-\tau_1/\mu_0})d\mu = \frac{\varpi_0 e^{-\tau_1/\mu_0}F_2(\tau_1,\mu_0)}{2\mu_0} \qquad (11.14a)$$

where the function F2 is with positive argument μ_0. Expressed in exponential integrals we get

$$t_d(\mu_0)= \frac{\varpi_0 e^{-\tau_1/\mu_0}}{2}\left[-1+e^{-\tau_1/\mu_0}E_2(\tau_1)-\mu_0\ln(\frac{1}{\mu_0}-1)+\mu_0 e^{-\tau_1/\mu_0}E_1(\tau_1)+\mu_0 E_i(\tau_1/\mu_0-\tau_1)\right] \qquad (11.14b)$$

The function Ei(x) is shown in the following figure.

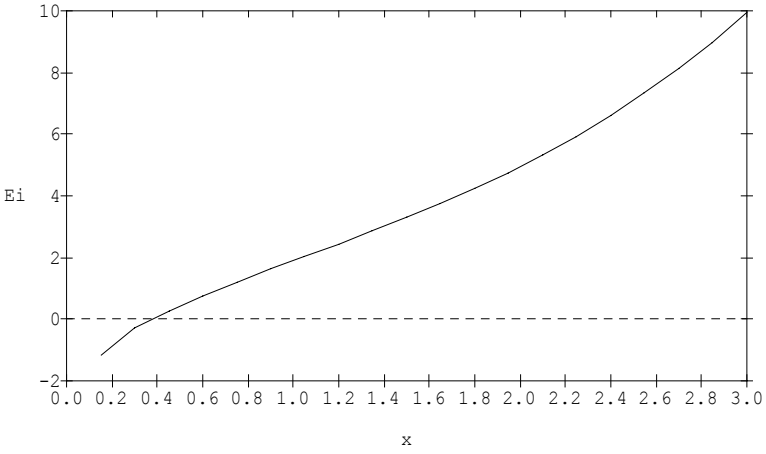

Figure 11.3: The Function

$$\text{Ei}(x)= \int_{-x}^{\infty}\frac{e^{-t}}{t}dt \quad \text{principal value}$$

$$= \gamma + \ln x + \sum_{n=1}^{\infty}\frac{x^n}{n\cdot n!} \qquad (11.15)$$

where γ=0.5772156649 is the Euler Constant.

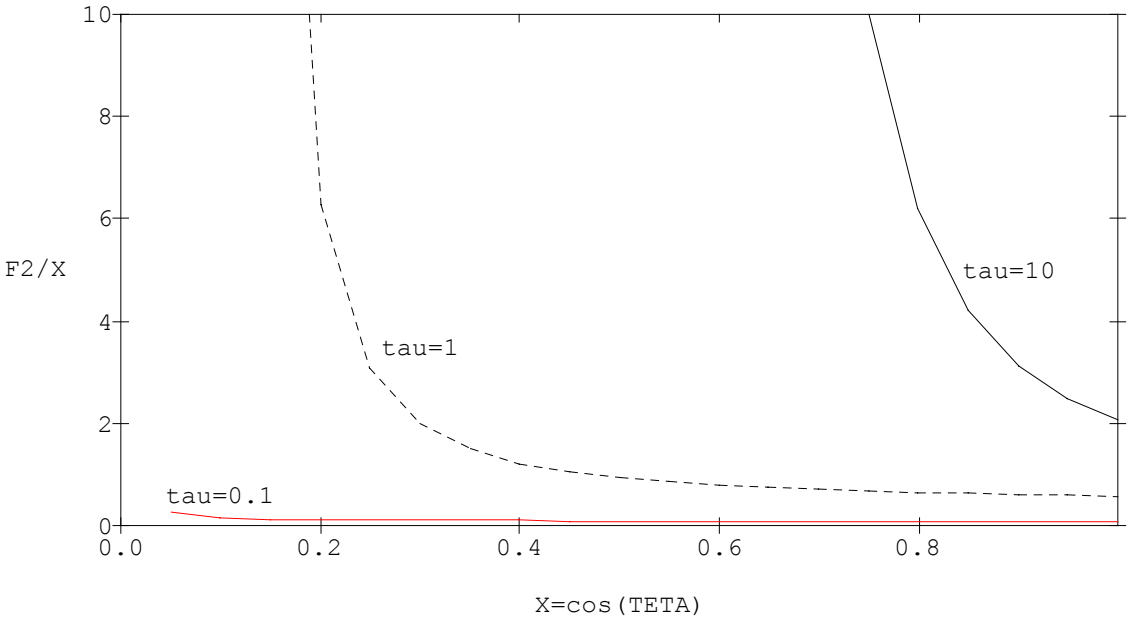

Figure 11.4: The function $F_2(\tau_1,\mu_0)/\mu_0$ for 3 values of τ_1.

The total transmissivity, $t(\mu_0,\phi_0)$, including the directly transmitted flux, is

$$t(\mu_0) = t_d(\mu_0)+t_0(\mu_0)=\left[1+\frac{\varpi_0 F_2(\tau_1,\mu_0)}{2\mu_0}\right]e^{-\tau_1/\mu_0} \qquad (11.16)$$

and the emissivity and absorptivity of the layer follow from

$$e(\mu_0) = a(\mu_0) = 1\text{-}r(\mu_0)\text{-}t(\mu_0) \tag{11.17}$$

From Figure 11.4 it is obvious that the t_d can be larger than t_0, and sometimes t_0 can even be neglected.

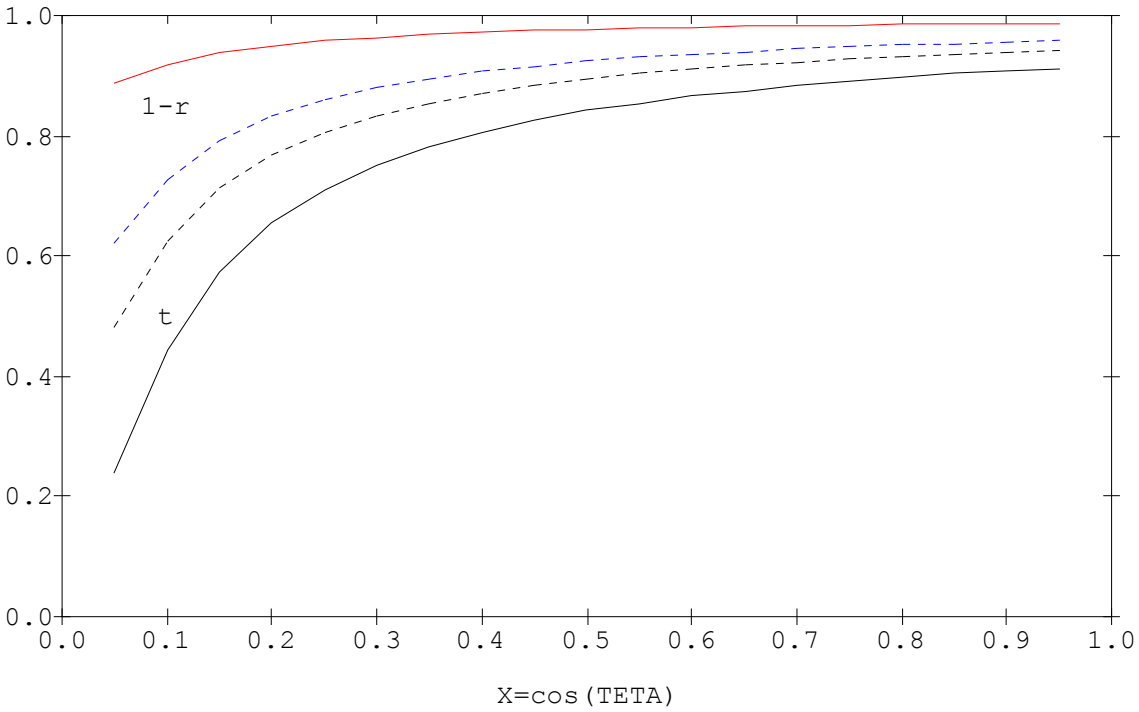

Figure 11.5: Above: The functions, 1-$r(\mu_0)$ and $t(\mu_0)$ for τ_1=0.1, ϖ_0=0.3 und (solid) und ϖ_0=1 (dotted). The emissivity is the difference. Below: same for τ_1=1.

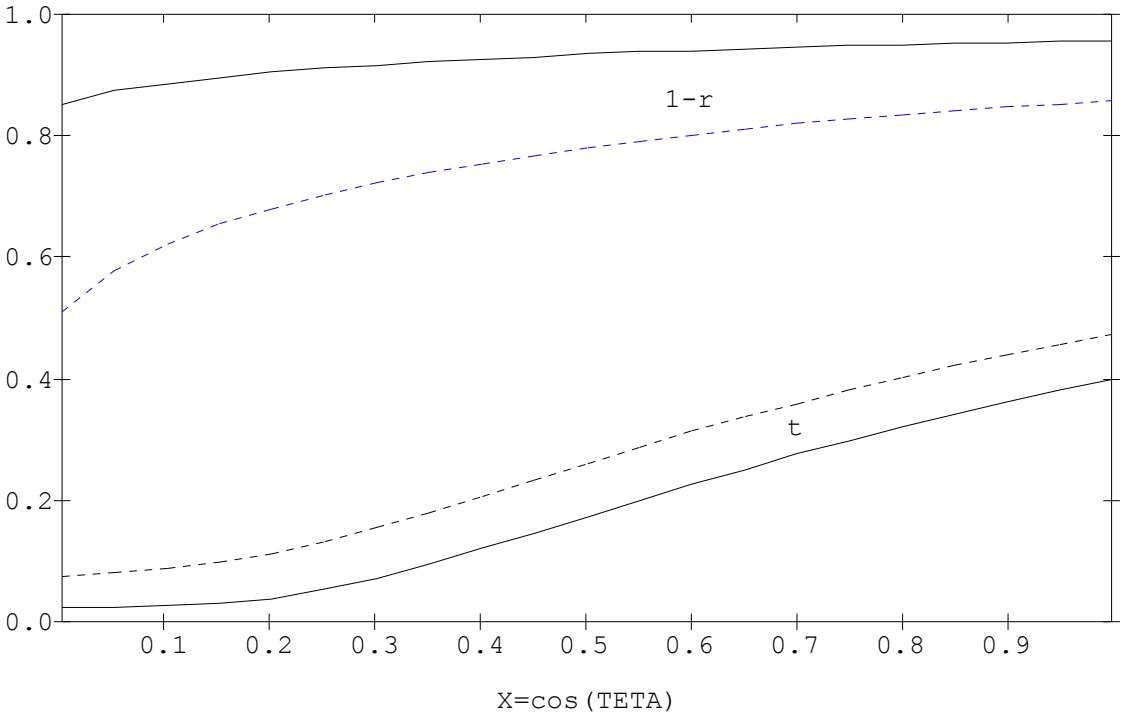

11.4 Successive orders of scattering

Single-scattering is improved by including its solution at position τ

$$I_{\nu 1}(\tau,\mu,\phi)=\frac{F_\nu}{4\pi}\int_{\tau}^{\tau_1} e^{-\tau'/\mu_0}e^{-\tau'/\mu}p(\tau',\mu,\phi,-\mu_0,\phi_0)\frac{d\tau'}{\mu}=\frac{F_\nu}{4\pi}\frac{p\mu\mu_0}{\mu+\mu_0}(e^{-\tau/\mu_0-\tau/\mu}-e^{-\tau_1/\mu_0-\tau_1/\mu}) \quad (11.18)$$

$$I_{\nu 1}(\tau,-\mu,\phi)=\frac{F_\nu}{4\pi}\int_{0}^{\tau} e^{-\tau'/\mu_0}e^{(\tau'-\tau)/\mu}p(\tau',\mu,\phi,-\mu_0,\phi_0)\frac{d\tau'}{\mu}=\frac{F_\nu}{4\pi}\frac{p\mu\mu_0}{\mu+\mu_0}(1-e^{-\tau/\mu_0}\cdot e^{-\tau/\mu}) \quad 11.19)$$

in the source term. In this way we get the solution for second-order scattering. The process can be iterated successively to higher orders, see Simmer (1994), and Thomas and Stamnes (1999) who called the method Lambda iteration. For second-order scattering, see also Chandrasekhar (1960) and van de Hulst (1948).

12 Exact Multiple Scattering

Situations with scattering usually have to deal with multiple scattering effects, i.e. a succession of at least two scattering processes. In this way, the radiation gets more and more diffuse, loosing the memory of the original direction and polarisation. The exact shape of the phase function gets less important than for single scattering. However exact solutions for multiple scattering are rare and are limited to the simplest phase functions (Chandrasekhar, 1960). Due to the reduced *p* sensitivity, these exact solutions are sometimes used as approximations for more complicated situations (Kokhanovsky, 2001).

12.1 Exact solution of Standard Problem 1 for isotropic scattering

Standard Problems 1 and 2 can be solved exactly in the case of isotropic scattering, and for a few other situations (Chandrasekhar, 1960). Here we will discuss Standard Problem 1 for the isotropic case. The solution is found through a principle of invariance, leading to an integral equation for the scattering function *S*.

Principle of invariance

Adding (or removing) a layer of the same medium to (or from) a half-space does not change the escaping radiation $I_\nu(0,\mu)$, and also the scattering function $S(\mu,\phi,\mu_0,\phi_0)$ remains the same. This is the principle of invariance (Figure 12.1).

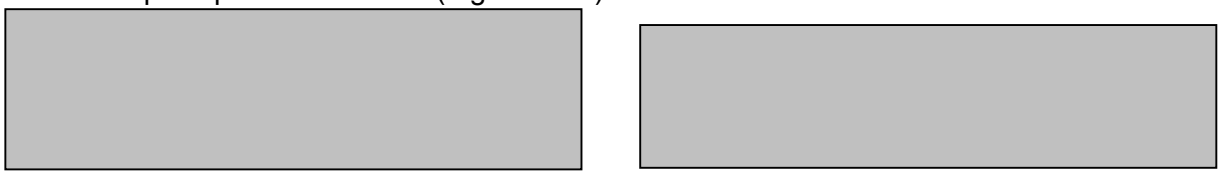

Figure 12.1: Illustration of the principle of invariance for a half-space medium.

Integral equation

The application of the principle of invariance to an infinitesimally increased half-space with isotropic scattering leads to an equation for the scattering function

$$S(\mu,\phi,\mu_0,\phi_0) = S(\mu,\mu_0) = \frac{\varpi_0 \mu \mu_0}{\mu+\mu_0} H(\mu)\cdot H(\mu_0) \tag{12.1}$$

where $H(\mu)$ is determined by either one of the two following integral equations (Chandrasekhar, 1960, § 33, 38):

$$H(\mu) = 1 + \frac{\varpi_0}{2}\mu H(\mu)\int_0^1 \frac{H(\mu')}{\mu+\mu'}d\mu' \tag{12.2}$$

$$\frac{1}{H(\mu)} = \sqrt{1-\varpi_0} + \frac{\varpi_0}{2}\int_0^1 \frac{\mu' H(\mu')}{\mu+\mu'}d\mu' \tag{12.3}$$

A derivation of Equation (12.2) is given in Section 12.4. Furthermore $H(\mu)$ has the following property (from Chandrasekhar, § 38):

$$\frac{\varpi_0}{2}\int_0^1 H(\mu')d\mu' = 1-\sqrt{1-\varpi_0} \tag{12.4}$$

The solution of (12.2) is found by iteration, starting with H=1. This value (solution for single scattering for $\tau_1\to\infty$) is inserted in the integrand of (12.2), then resolving for H gives:

$$\frac{1}{H(z)} = 1 - \frac{\varpi_0 z}{2} \int_0^1 \frac{H(\mu)}{z+\mu} d\mu \tag{12.5}$$

As a result we get an improved value of *H*(z); this improved function is again inserted in the integrand of (12.5), and the process is repeated until we get a stable solution. Results are shown in the following figure.

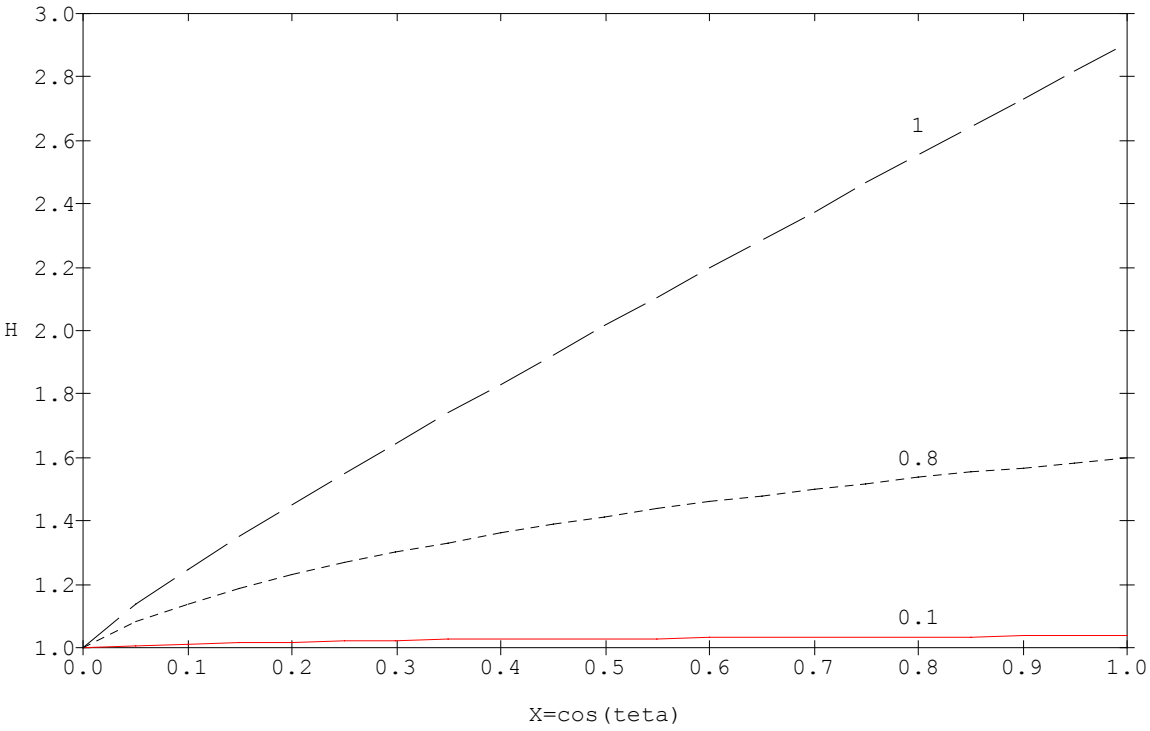

Figure 12.2: The function *H*(μ) for isotropic scattering and for 3 values of ϖ_0 = 0.1, 0.8, 1.

Improved starting functions can be found in Chandrasekhar (1960), § 22-27. All *H* values range between 1 and approximately 3. Highest values are found for vertical incidence and $\varpi_0 = 1$.

Reflectivity and emissivity

The reflectivity of the half-space can be directly expressed with the *H* function, using (12.3):

$$r(\mu_0) = \frac{1}{4\pi\mu_0} \int_0^1 \int_0^{2\pi} S(\mu,\phi,\mu_0,\phi_0) d\phi d\mu = \frac{\varpi_0 H(\mu_0)}{2} \int_0^1 \frac{\mu H(\mu)}{\mu+\mu_0} d\mu$$

$$= 1 - \sqrt{1-\varpi_0} \cdot H(\mu_0) \tag{12.6}$$

and thus the emissivity *e* =1-*r* becomes

$$e(\mu_0) = \sqrt{1-\varpi_0} \cdot H(\mu_0) \tag{12.7}$$

In contrast to the single-scattering solution (11.11d), Equation (12.6) correctly converges to 1, and (12.7) to zero, respectively, for $\varpi_0 \to 1$ (no absorption). See also Figures 12.3-5.

Backscattering

The normalised backscatter cross section (normalised by illuminated area) is simply given by

$$\sigma^0 = S(\mu_0,\mu_0) = \frac{\varpi_0 \mu_0}{2} H^2(\mu_0) \tag{12.8}$$

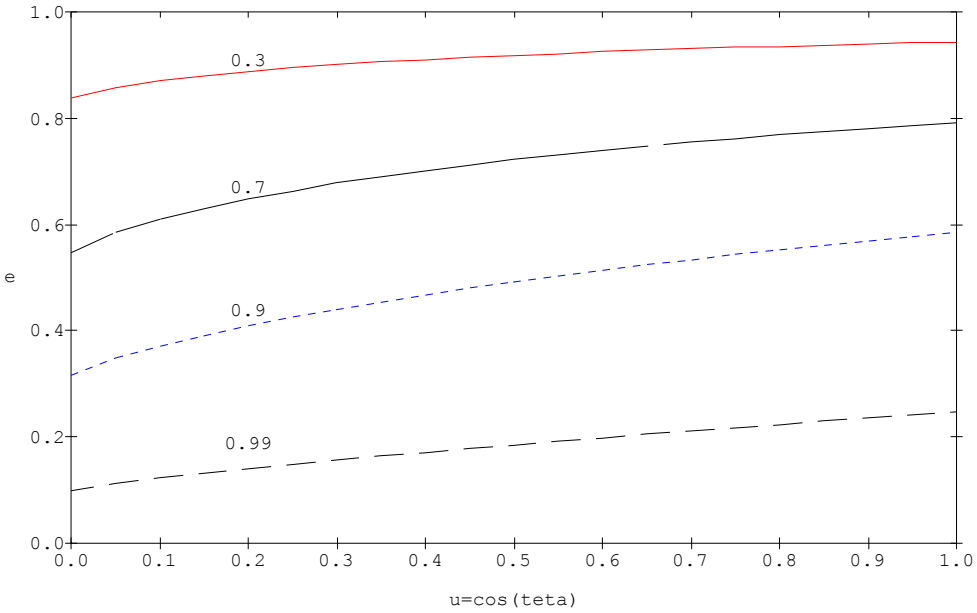

Figure 12.3: Emissivity *e* versus μ_0 for 4 different values of ϖ_0.

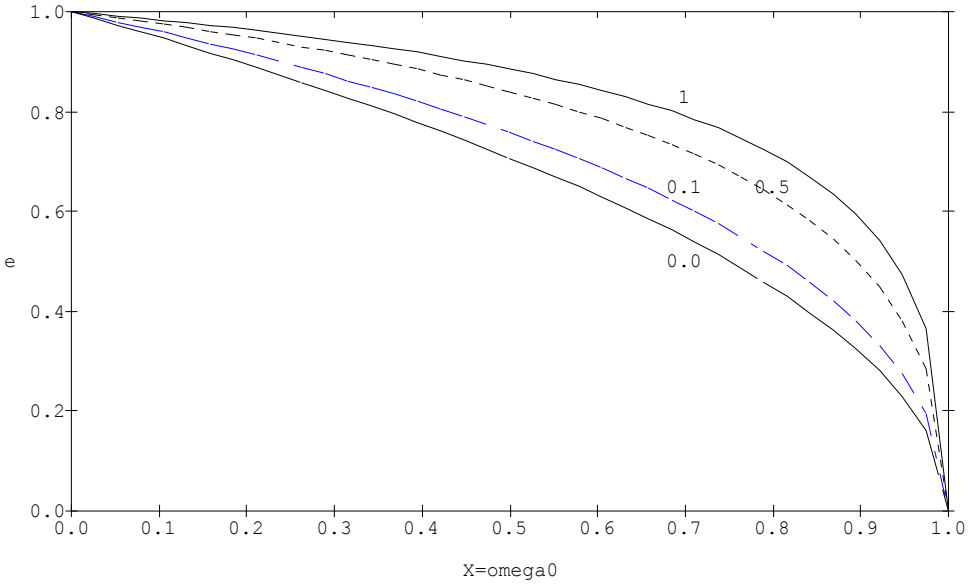

Figure 12.4: Emissivity *e* versus ϖ_0 for 4 different values of μ_0.

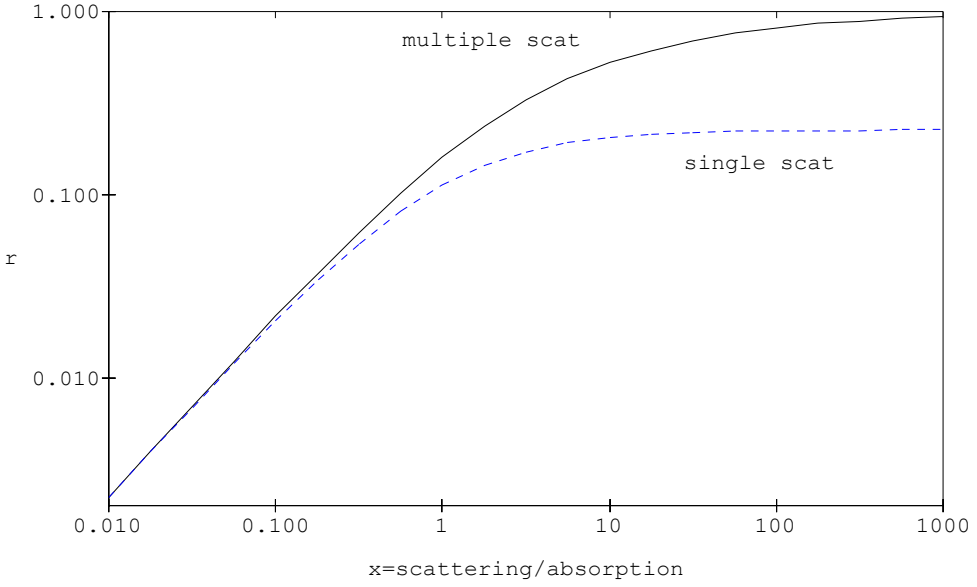

Figure 12.5: Half-space reflectivity versus $\gamma_s/\gamma_a=\varpi_0/(1+\varpi_0)$ for $\mu_0=0.5$ – exact multiple-scattering solution and for single scattering.

12.2 Exact solution of Standard Problem 2 for isotropic scattering

The S and T functions

Also Standard Problem 2 was solved exactly by Chandrasekhar (1960) using principles of invariance (§ 49-55). Here we present the solution for isotropic scattering.

$$S(\tau_1,\mu,\phi,\mu_0,\phi_0) = S(\tau_1,\mu,\mu_0) = \frac{\varpi_0\mu\mu_0}{\mu+\mu_0}\left[X(\mu)X(\mu_0) - Y(\mu)Y(\mu_0)\right] \tag{12.9}$$

$$T(\tau_1,\mu,\phi,\mu_0,\phi_0) = T(\tau_1,\mu,\mu_0) = \frac{\varpi_0\mu\mu_0}{\mu-\mu_0}\left[Y(\mu)X(\mu_0) - X(\mu)Y(\mu_0)\right] \tag{12.10}$$

The functions $X(\mu)$ and $Y(\mu)$ are obtained from the coupled integral equations:

$$X(\mu) = 1 + \frac{\varpi_0\mu}{2}\int_0^1 \frac{X(\mu)X(\mu') - Y(\mu)Y(\mu')}{\mu+\mu'}d\mu' = 1 + \frac{1}{2}\int_0^1 S(\tau_1,\mu,\mu')\frac{d\mu'}{\mu'} \tag{12.11}$$

$$Y(\mu) = e^{-\tau_1/\mu} + \frac{\varpi_0\mu}{2}\int_0^1 \frac{Y(\mu)X(\mu') - X(\mu)Y(\mu')}{\mu-\mu'}d\mu' = e^{-\tau_1/\mu} + \frac{1}{2}\int_0^1 T(\tau_1,\mu,\mu')\frac{d\mu'}{\mu'} \tag{12.12}$$

Comparison with single scattering gives a first approximation to $X(\mu)$ and $Y(\mu)$:

$$X(\mu)=1,\ Y(\mu)=\exp(-\tau_1/\mu) \tag{12.13}$$

and if with inclusion of second-order scattering (Chandrasekhar, p. 216)

$$X(\mu)=1+0.5\varpi_0 F_1(\tau_1,-\mu),\ Y(\mu)=\exp(-\tau_1/\mu)[1+0.5\varpi_0 F_1(\tau_1,\mu)] \tag{12.14}$$

On the other hand, for $\tau_1\to\infty$, we have $X(\mu) \to H(\mu)$, $Y(\mu) \to 0$.

Integral properties

$$\frac{\varpi_0}{2}\int_0^1 X(\mu)d\mu = 1 - \sqrt{1-\varpi_0 + \left[\frac{\varpi_0}{2}\int_0^1 Y(\mu)d\mu\right]^2} \tag{12.15}$$

used to test the functions $X(\mu)$ und $Y(\mu)$.

Reflectivity and transmissivity

The reflectivity $r(\tau_1,\mu)$ of the layer follows from (10.6) and (12.9)

$$r(\tau_1,\mu) = \frac{\varpi_0}{2}\int_0^1 \frac{X(\mu)X(\mu') - Y(\mu)Y(\mu')}{\mu+\mu'}\mu'\cdot d\mu' = 1\text{-}[(1\text{-}x_0)X(\mu)+y_0Y(\mu)] \tag{12.16}$$

and the transmissivity, $t(\mu_0,\phi_0)=t_0(\mu_0,\phi_0)+t_d(\mu_0,\phi_0)$, follows from (10.14) and (12.10)

$$t(\tau_1,\mu) = e^{-\tau_1/\mu} + \frac{\varpi_0}{2}\int_0^1 \frac{Y(\mu)X(\mu') - X(\mu)Y(\mu')}{\mu-\mu'}\mu'\cdot d\mu' = y_0X(\mu) + (1\text{-}x_0)Y(\mu) \tag{12.17}$$

The last expressions in (10.16) and (10.17) are from Chandrasekhar (1960), p. 184, where x_0 and y_0 are the zero-order moments of $\varpi_0 X$ and $\varpi_0 Y$:

$$x_0 = \frac{\varpi_0}{2}\int_0^1 X(\mu)d\mu\ ;\ y_0 = \frac{\varpi_0}{2}\int_0^1 Y(\mu)d\mu \tag{12.18}$$

and finally the emissivity is given by:

$$e(\tau_1,\mu) = 1 - r - t = (1\text{-}x_0\text{-}y_0)\cdot[X(\mu)\text{-}Y(\mu)] \tag{12.19}$$

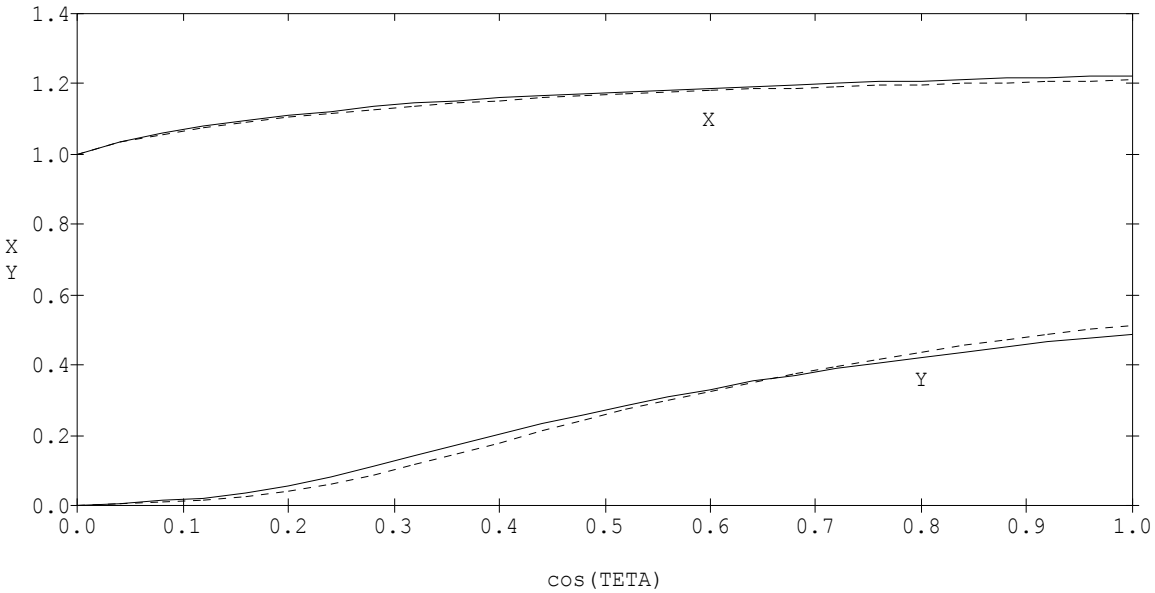

Figure 12.6: The functions $X(\mu)$ and $Y(\mu)$ for τ_1 =1 and ϖ_0 = 0.5. The pointed lines show the results after the first iteration, starting with (12.13), and the solid lines are results after the third iteration.

0 XY	2 X1	3 Y1	4 X2	5 Y2	6 X3	7 Y3
27 x0,y0	0.2878	0.0618	0.2894	0.0639	0.2898	0.0628
28 x0test	0.2902		0.2900		0.2901	

Table 12.1: x_0, y_0 and x_{0test} of Eq. (12.15) for the first 3 iterations of $X(\mu)$ and $Y(\mu)$ for $\tau_1 = 1$ and $\varpi_0 = 0.5$

Figures 12.6-7 show the example with $\tau_1 = 1$ and $\varpi_0 = 0.5$ with values x_0=0.290, y_0=0.063 as shown in Table 12.1. From Equations (12.15-18) we get *r, t* for τ_1 =1, ϖ_0 = 0.5, as shown in the following Figure 12.7. As a general observation it is noted that *r* and *t* increase whereas *e* decreases from the single- to the multiple-scattering solution.

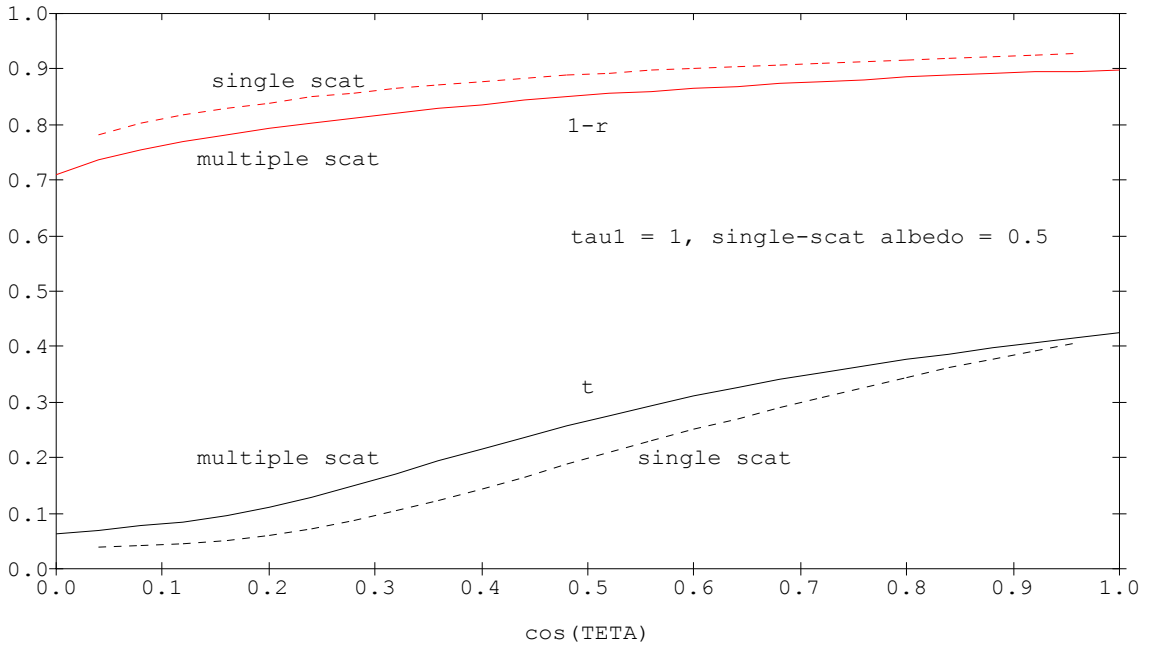

Figure 12.7: Transmissivity and 1- reflectivity versus cosine of incidence angle for a layer with isotropic scattering, $\tau_1 = 1$ and $\varpi_0 = 0.5$ for single and multiple scattering.

12.3 Discussion

For isotropic scattering the exact solution is simple, especially for a half-space. The results show the most important behaviour of multiple scattering, especially the "late" convergence toward a **white body** for $\varpi_0 \to 1$ (Figures 12.4 and 12.5). Unfortunately the results are not directly applicable to scattering problems with strongly anisotropic phase functions. With efforts it is possible to transform an anisotropic scattering problem to a more isotropic one. The Delta-Eddington Approximation is an example (Joseph et al. 1976, Meador and Weaver, 1980, Thomas and Stamnes, 1999). Such transformations improve the applicability of the exact theory.

The computation of the *X* and *Y* functions is more delicate than computing the *H* function. Get your own experience!

12.4 Appendix: Derivation of Equation (12.2)

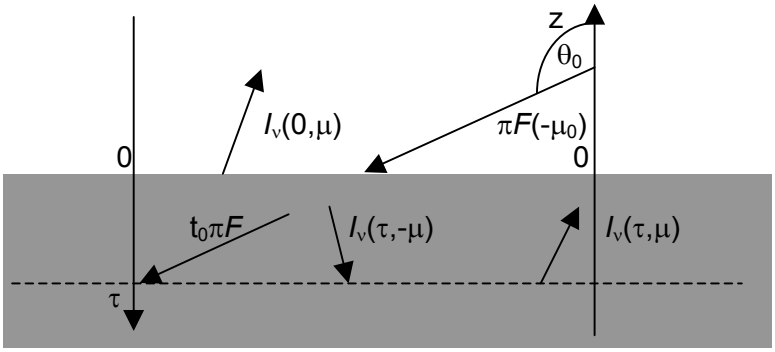

Boundary condition:

$$I_\nu(0,-\mu)=0 \qquad \text{(A1)}$$

Principle of invariance: Adding a layer (0, τ) to a half-space with the same properties does not change the scattering function $S(\mu,\mu_0)$.
First we have at the surface of the half-space

$$I_\nu(0,\mu) = \frac{F}{4\pi\mu} S(\mu,\mu_0) \qquad \text{(A2a)}$$

and after addition of a layer of optical thickness τ, the radiance, now at depth τ must still be expressible by S , but now also including diffuse incident radiation:

$$I_\nu(\tau,\mu)=\frac{Fe^{-\tau/\mu_0}}{4\pi\mu} S(\mu,\mu_0)+\frac{1}{2\mu}\int_0^1 S(\mu,\mu')\cdot I_\nu(\tau,-\mu')d\mu' \qquad \text{(A2b)}$$

where the first term is due to scattering by the medium below level τ of the reduced direct beam, and the second term is due to scattering, again by the half-space below level τ of the diffuse incident radiation. On the other hand, the RTE also describes the radiance at level τ, and if averaged over azimuth (without emission), for $p=p_0=\varpi_0$, we get:

$$\mu\frac{dI_\nu(\tau,\mu)}{d\tau}=\mu\frac{\partial I_\nu(\tau,\mu)}{\partial\tau}=I_\nu(\tau,\mu)-J_\nu(\tau,\mu) \qquad \text{(A3)}$$

$$J_\nu(\tau,\mu)=\frac{\varpi_0}{2}\int_{-1}^1 I_\nu(\tau,\mu')\cdot d\mu'+\frac{F\varpi_0}{4\pi}e^{-\tau/\mu_0} \qquad \text{(A4)}$$

Multiplication of (A2b) with μ, and taking the derivative with respect to τ at τ=0 (where $I_\nu(0,-\mu)$= 0) gives an equation similar to the RTE:

$$\mu\frac{\partial I_\nu(0,\mu)}{\partial\tau}=-\frac{F}{4\mu_0}S(\mu,\mu_0)+\frac{1}{2}\int_0^1 S(\mu,\mu')\cdot\frac{\partial I_\nu(0,-\mu')}{\partial\tau}d\mu' \qquad \text{(A5)}$$

If we eliminate the derivatives in (A5) we get an equation for the *S* function. To this end we use Equations (A3) and (A4):
a) Left-hand side of (A5):

$$\mu\frac{\partial I_\nu(0,\mu)}{\partial\tau} = I_\nu(0,\mu) - J_\nu(0,\mu) = \frac{F}{4\pi\mu}S(\mu,\mu_0) - \frac{F\varpi_0}{4\pi} - \frac{\varpi_0}{2}\int_0^1 I_\nu(0,\mu'')\cdot d\mu'' =$$

$$= \frac{F}{4\pi\mu}S(\mu,\mu_0) - \frac{F\varpi_0}{4\pi} - \frac{F\varpi_0}{8\pi}\int_0^1 S(\mu'',\mu_0)\cdot\frac{d\mu''}{\mu''} \qquad \text{(A6)}$$

b) Right-hand side of (A5), derivative in the integrand:

$$\frac{\partial I_\nu(0,-\mu')}{\partial\tau} = \frac{I_\nu(0,-\mu') - J_\nu(0,-\mu')}{-\mu'} = \frac{J_\nu(0,-\mu')}{\mu'} = \frac{F\varpi_0}{4\pi\mu'} + \frac{F\varpi_0}{8\pi\mu'}\int_0^1 S(\mu'',\mu_0)\cdot\frac{d\mu''}{\mu''} \qquad \text{(A7)}$$

Equations (A6) and (A7) inserted in (A5) leads to

$$\left[\frac{1}{\mu}+\frac{1}{\mu_0}\right]\frac{F}{4}S(\mu,\mu_0) = \frac{F\varpi_0}{4} + \frac{F\varpi_0}{8}\int_0^1 S(\mu'',\mu_0)\cdot\frac{d\mu''}{\mu''} +$$

$$\frac{1}{2}\int_0^1 S(\mu,\mu')\left[\frac{F\varpi_0}{4\mu'} + \frac{F\varpi_0}{8\mu'}\int_0^1 S(\mu'',\mu_0)\cdot\frac{d\mu''}{\mu''}\right]d\mu'$$

Division by $\frac{F}{4\pi}\frac{\mu+\mu_0}{\mu\mu_0}$ gives

$$S(\mu,\mu_0) = \frac{\varpi_0\mu\mu_0}{\mu+\mu_0}\left\{\left(1+\frac{1}{2}\int_0^1 S(\mu'',\mu_0)\cdot\frac{d\mu''}{\mu''}\right) + \frac{1}{2}\int_0^1 S(\mu,\mu')\left[1+\frac{1}{2}\int_0^1 S(\mu'',\mu_0)\cdot\frac{d\mu''}{\mu''}\right]\frac{d\mu'}{\mu'}\right\}$$

$$= \frac{\varpi_0\mu\mu_0}{\mu+\mu_0}H(\mu_0)\cdot H(\mu) \qquad \text{(A8)}$$

where $H(\mu)$

$$H(\mu) = \varpi_0\left(1+\frac{1}{2}\int_0^1 S(\mu',\mu)\cdot\frac{d\mu'}{\mu'}\right) = \varpi_0\left(1+\frac{1}{2}\int_0^1 S(\mu,\mu')\cdot\frac{d\mu'}{\mu'}\right) \qquad \text{(A9)}$$

Insertion of *S* of (A8) in (A9) leads to the Integral equation (12.2):

$$H(\mu) = 1 + \frac{\varpi_0}{2}\mu H(\mu)\int_0^1 \frac{H(\mu')}{\mu+\mu'}d\mu' \qquad \text{(A10)}$$

13 Approximate Solutions for Multiple Scattering

Approximate solutions of the RTE are obtained if the number of propagation directions is limited. In this way the radiative transfer equation is replaced by a system of linear differential equations (Chandrasekhar, 1960, starting with §20). Most popular are the Two-Stream (or Two-Flux) Models going back to Schuster (1905) and Kubelka and Munk (1931). A good overview was given by Meador and Weaver (1980), and these models are also well described in Thomas and Stamnes (1999) and in a different way by Ishimaru (1978).

In certain situations, the scattering is indeed limited to two directions, e.g. if the medium consists of plane-parallel slabs of a dielectric material. Then the two-stream model is an exact one. This situation will be discussed here as a primitive snowpack scattering model.

13.1 A simple snowpack/cloud reflectance and transmittance model from microwaves to ultraviolet: The ice-lamella pack

From: C. Mätzler, Journal of Glaciology, J. Glaciology, Vol. 46, No. 152, pp. 20-24 (2000).

Abstract

Modelling the reflectance (reflectivity) and transmittance (transmissivity) of volume scatterers is delicate. Slightly different approaches can lead to different results, thus making comparisons difficult. Here a simple, analytic multiple-scattering model is presented as a possible reference for comparisons and also for better understanding the physics involved. The model quantifies the transmittance and reflectance of homogeneously distributed scatterers within slabs of any thickness. The simplicity of the model is given by the one-dimensional geometry, a system consisting of freely arranged ice lamellae in air. Although direct applications will be limited, the model gives a spectral description of ice clouds and snowpacks over a very broad spectral range from microwaves to the ultraviolet. In addition to the transmittance and reflectance the model also gives the emittance through Kirchhoff's law. Comparison with other models shows, on one hand, agreement in the spectral description when compared with current snow models, and on the other, some quantitative inconsistencies between all of them. It appears that the lamella pack produces the same optical spectra as an average snow model with spherical ice grains whose radius corresponds to about the lamella thickness whereas microwave spectra appear to be slightly different.

The model

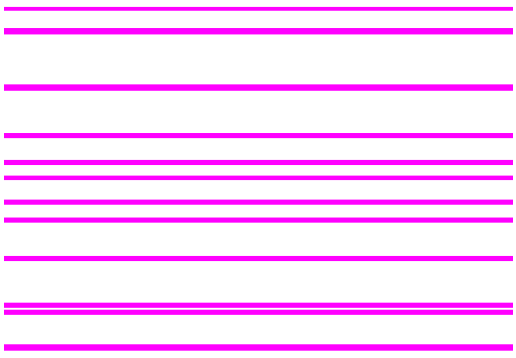

Figure 1: Pack of freely arranged ice lamellae of thickness *d* packed to a volume fraction *v* (0<*v*<1), on average there are *N* lamellae per meter depth, representing a model of a cloud or of a snowpack. Freely arranged lamellae can be in direct contact (second from bottom), thus increasing the average thickness.

Expressing the number *N* of lamellae per meter depth by the volume fraction *v* and by the lamella thickness *d* we have

$$N = v/d \qquad (1)$$

Reflection at a single ice lamella:

For a dielectric lamella with negligible losses, the reflectivity is given by the **Airy formula** (Born and Wolf, 1980)

$$r = 2r_1 \frac{1-\cos(2P)}{1+r_1^2-2r_1\cos(2P)} \tag{2}$$

r_1 Fresnel reflectivity (air-ice), P one-way phase through the lamella. For vertical incidence

$$r_1 = \left|\frac{n-1}{n+1}\right|^2 \tag{3}$$

and

$$P = n'kd \tag{4}$$

where $n = n' + i\cdot n''$ is the complex refractive index of ice and k the vacuum wave number.

The average reflectivity of a lamella:

Now, since d is assumed to be slightly different for different lamellae, the phase terms in (2) are smeared out when averaged over many lamellae, except for very small values of P. Coherent superpositions of reflections at different lamellae disappear due to the variable distance between them, i.e. by the *free arrangement* of the lamellae. Noting that $r_1 << 1$, the denominator of (2) can be approximated by 1. The average lamella reflectivity r_{av} can then be written as

$$r_{av} = \begin{cases} 4r_1 \sin^2 P; & P < 3\pi/4 = 2.356 \\ 2r_1\ ; & P \geq 2.356 \end{cases} \tag{5}$$

For a small phase, Equation (5) gives the coherent reflectivity of the lamella through the first maximum at one quarter wavelength, and it provides a continuous transition from the coherent to the incoherent situation at larger thickness.

The Two-Flux scattering coefficient:

The radiative transfer equation decays into a pair of first-order differential equations identical to the ones used in the two- flux model. The up- and downwelling intensities, $I_1(z)$ and $I_2(z)$, respectively, can be described by (emission being omitted here, but later included)

$$\frac{dI_{1,2}}{dz} = \mp\gamma_a I_{1,2} + \gamma_s (I_2 - I_1) \tag{6}$$

For N lamellae per meter depth the scattering coefficient γ_s is given by $\gamma_s = Nr_{av}$. However, due to the free arrangement, this quantity is reduced by the probability $(1-v)$ of two adjacent lamellae being in contact, thus γ_s is given by

$$\gamma_s = N(1-v)r_{av} = \begin{cases} \dfrac{4v(1-v)r_1 \sin^2 P}{d}; & P = n'kd < 3\pi/4 = 2.356 \\ \dfrac{2v(1-v)r_1}{d}; & P \geq 2.356 \end{cases} \tag{7}$$

The contacting lamellae have an increased thickness, therefore we can introduce the average thickness as $d_{av} = d/(1-v)$. Thus (7) can also be expressed by

$$\gamma_s = \begin{cases} \dfrac{4vr_1 \sin^2 P}{d_{av}}; & P = n'kd_{av}(1-v) < 3\pi/4 = 2.356 \\ \dfrac{2vr_1}{d_{av}}; & P \geq 2.356 \end{cases} \tag{7'}$$

The reason why *d* was introduced is the fact that *d* is the correlation length of the medium. With increasing *v* more and more lamellae touch adjacent ones until *v* approaches 1 when the medium consists of thick ice plates, separated by a few thin air gaps of thickness *d*.

The two-flux absorption coefficient:

Small dielectric losses can be included by the absorption coefficients of ice $\gamma_{a,ice}$ and air $\gamma_{a,air}$. The absorption coefficient γ_a of the lamella model is

$$\gamma_a = v\,\gamma_{a,ice} + (1\text{-}v)\,\gamma_{a,air} \tag{8}$$

In case of high dielectric losses, absorption happens locally within the topmost lamella (9').

Reflectance, transmittance and emittance of the slab:

Without atmospheric absorption, slab height *h* above a non-reflecting background. The reflectivity *r*, and the transmissivity *t* of the slab are (using the reflectivity r_0 for infinite thickness, the transmission function t_0 and the damping coefficient γ_2)

$$r = r_0\,\frac{1-t_0^2}{1-r_0^2 t_0^2};\ \text{and} \qquad t = t_0\,\frac{1-r_0^2}{1-r_0^2 t_0^2}; \qquad \gamma_{a,ice} d < 1 \tag{9}$$

where

$$t_0 = \exp(-\gamma_2 h); \quad r_0 = \frac{\gamma_s}{\gamma_s + \gamma_a + \gamma_2}\ ; \quad \gamma_2 = \sqrt{\gamma_a^2 + 2\gamma_a\gamma_s} \tag{10}$$

Exception for opaque lamellae; only incoherent reflections at the 3 topmost air-ice interfaces (without multiple scattering):

$$r = r_1(1+2\exp(-2\gamma_{a,ice} d)); \quad t = 0; \qquad \gamma_{a,ice} d > 1 \tag{9'}$$

Finally, the emissivity *e* of the slab is obtained from Kirchhoff's law, for absorptivity *a*:

$$a = e = 1\text{-}t\text{-}r \tag{11}$$

and the last equation follows from energy conservation. Note that the emissivity of the whole (slab and background) system is given by $e_0 = 1 - r = e + t$.

Results and Discussion

For a sufficiently deep pack, the reflectivity is only a function of the ratio $x = \gamma_s/\gamma_a$:

$$r = r_0 = \frac{x}{x + 1 + \sqrt{1+2x}} \tag{12}$$

$$r_0 \cong 1\text{-}\sqrt{\frac{2}{x}} \tag{13}$$

The often used Approximation (13) is approached for large values of *x*, e.g. for snow at visible wavelengths. Inserting *x* from (7') and (8) for $\gamma_{a,air} = 0$ and for large *P* we get

$$x = \frac{2r_1}{\gamma_{a,ice} d_{av}} \tag{14}$$

and thus from (13) we find

$$r_0 \cong 1 - K\sqrt{\gamma_{a,ice} d_{av}} \tag{15}$$

a well-known approximation for strong volume-scatterers (e.g. Bohren, 1987). Here, *K* is given by $r_1^{-1/2}$; thus for lossless ice we get from (3):

$$K = \frac{n'+1}{n'-1} \tag{16}$$

For n'=1.33 we get r_1=0.020 and K=7.06. According to an early snowpack model (Bohren and Barkstrom, 1974), the reflectance of a deep snowpack can be written as

$$r_0 \cong 1 - 5.96\sqrt{\gamma_{a,ice} D_{BB}} \tag{17}$$

where D_{BB} is the sphere diameter of the Bohren and Barkstrom Model. This result agrees with (15) by choosing

$$d_{av} = 0.61 D_{BB} \tag{18a}$$

Another comparison can be made using the snow model of Wiscombe and Warren (1980). Reflectivities of thick snowpacks computed with this model for different grain diameters D_{WW} were taken from Marshall (1989) and from Sergeant et al. (1993) at a wavelength of 1μm, and the results are shown by the data on the upper curve of Figure 2. The curve represents Equation (12) for x=4.915mm/D_{WW}. Comparing this result with (14) for r_1=0.0171 (n'=1.301) and $\gamma_{a,ice}$=0.024/mm we find x=1.42/d_{av}, thus agreement is achieved with the lamella model if

$$d_{av} = 0.29 D_{WW} \tag{18b}$$

The lower curve in Figure 2 represents the model of De Haan et al. (1987), with x =2.69mm/D_{DH}. Agreement with the lamella model is achieved if the De Haan grain diameter D_{DH} is given by

$$d_{av} = 0.53 D_{DH} \tag{18c}$$

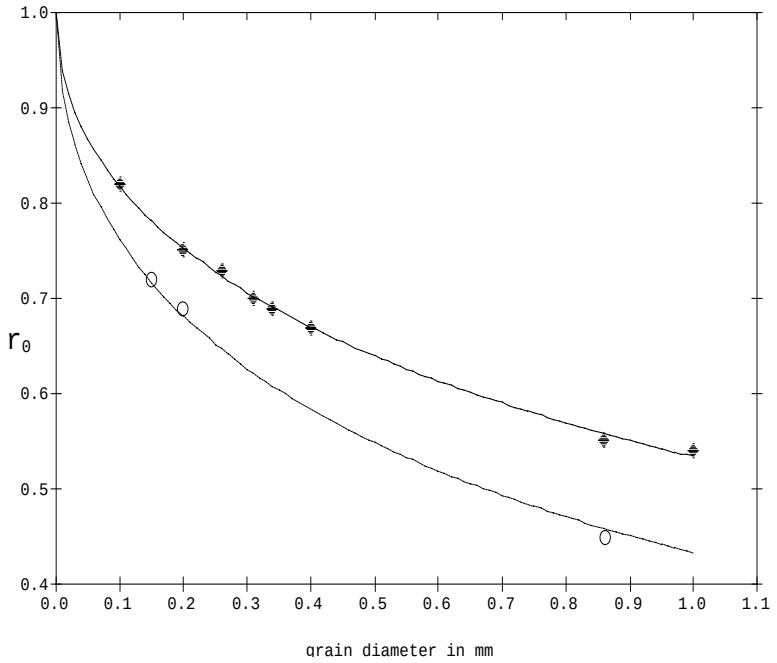

Figure 2: Decrease of the reflectance r_0 of pure snow (wavelength = 1 μm) with increasing grain diameter D (in mm) of spherical ice grains. Data points (diamonds) along the upper curve are computed with the model of Wiscombe and Warren (1980), the curve represents Equation (13) with x = 4.915mm/D. The lower curve represents (13) with x =2.69mm/D, the data points were computed by Sergeant et al. (1998), using the model of De Haan et al. (1987).

Comparison of the three equations (18a,b,c) indicates that different snow reflectance models lead to slightly different results (all within about a factor of 2) with respect to the grain diameter. On average the lamella thickness is about equal to the grain radius.

Another comparison was made with data of the NASA-ASTER spectral library (http://asterweb.jpl.nasa.gov). The results are shown in Figure 3 for three different effective grain sizes D_{AS}=0.024, 0.082 and 0.174 mm, respectively. The lamella thickness, d, was assumed to be equal to D_{AS}, and a constant ice-volume fraction v=0.1 was assumed. The spectral ice data were taken from Warren (1984). According to the description of the ASTER library, the ASTER spectra were modelled based on broadband measurements made by Salisbury et al. (1994) at the John Hopkins University IR Laboratory (2-14μm). The agreement between the spectra of lamella-pack and the ASTER snowpack is excellent. Especially at wavelengths below 1.4μm, the ASTER data and the lamella-pack model give almost indistinguishable results. From this coincidence it can be concluded that the ASTER grain size corresponds to d for v=0.1. In terms of d_{av} we have

$$d_{av} = 1.1\, D_{AS} \qquad (18d)$$

Unfortunately, in the ASTER library the *grain size* D_{AS} is not clearly defined. After discussion with the authors of the database it is probable that ASTER *grain size* means radius. In fact, Wald (1994) used *radius* and *grain size* as synonyms.

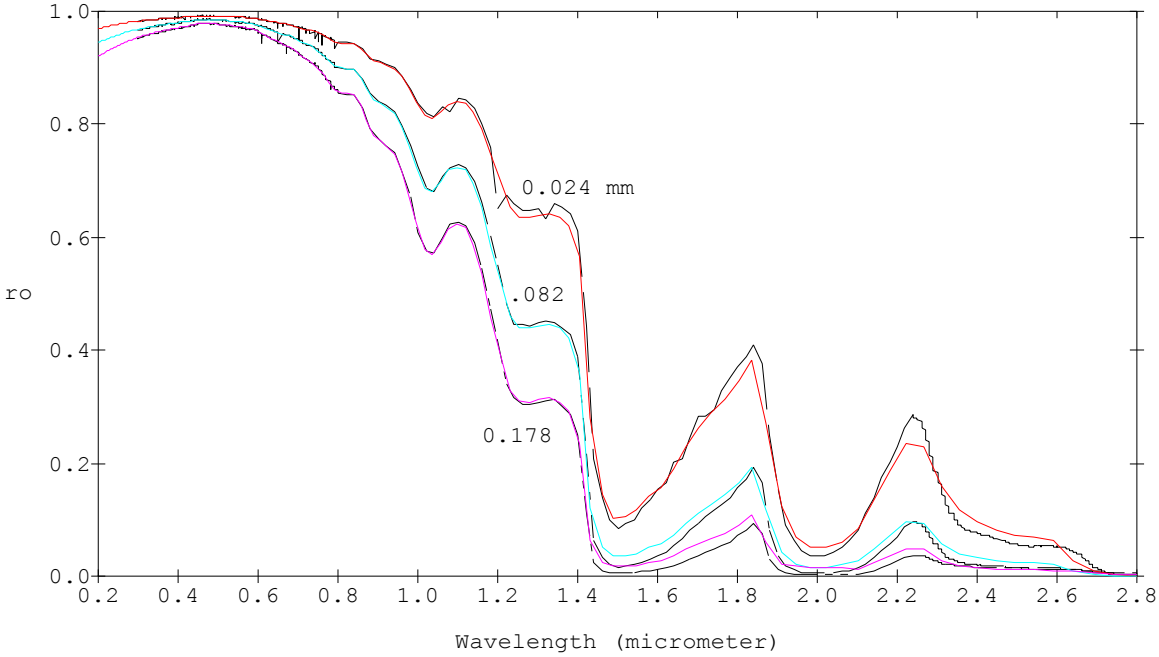

Figure 3: Reflectance of thick snowpacks versus wavelength between 0.2 and 2.8 μm for 3 effective grain sizes: 0.024 mm (uppermost pair of curves), 0.082 mm (middle pair), and 0.174 mm (lowest pair). The smoother curves represent the lamella-pack model with the lamella thickness equal to the grain size for v=0.1, and the noisier curves represent data from the ASTER spectral library.

From updated spectral information on the complex refractive index of pure water ice (Warren, 1984; Mätzler, 1998b), microwave to ultraviolet reflectivity and transmissivity spectra were computed for given packs. Examples of reflectance and transmittance data of two 10 cm thick snowpacks at a temperature of 266K are shown in Figures 4 and 5, and Figure 6 shows the spectra of an ice cloud (shortest wavelength is 200nm). The corresponding reflectivity spectra for infinite thickness are shown as well. The computations are based on Equations (9), (9') and (10). Note that at lower frequencies where the phase P is small, we obtain a reflectivity which increases with increasing k^2d, i.e. with frequency, thus the emissivity decreases as is observed for dry snow in the microwave range.

In Figures 4 and 5 the reflectivity in the 2 to 100 GHz range is compared with the results of the recent Microwave Emission Model of Layered Snowpacks, MEMLS, (Wiesmann et al. 1998, Wiesmann and Mätzler 1999) for the same thickness, density, temperature and for correlation lengths p_{MEMLS} of the isotropic heterogeneity fitted to the present data. It is found that p_{MEMLS} is significantly larger than d, and its influence on the scattering coefficient is stronger than for d. Indeed, three-dimensional Rayleigh scattering increases with $k^4(p_{MEMLS})^3$, whereas in the one-dimensional geometry scattering increases with k^2d. Also the shape of the MEMLS spectra (Figures 4 and 5) are slightly steeper than in the present model. Thus there is a functional difference between scattering in one- and 3-dimensional heterogeneity at microwave frequencies, whereas at optical frequencies both types of heterogeneity produce coincident spectra and coincident grain-size dependence.

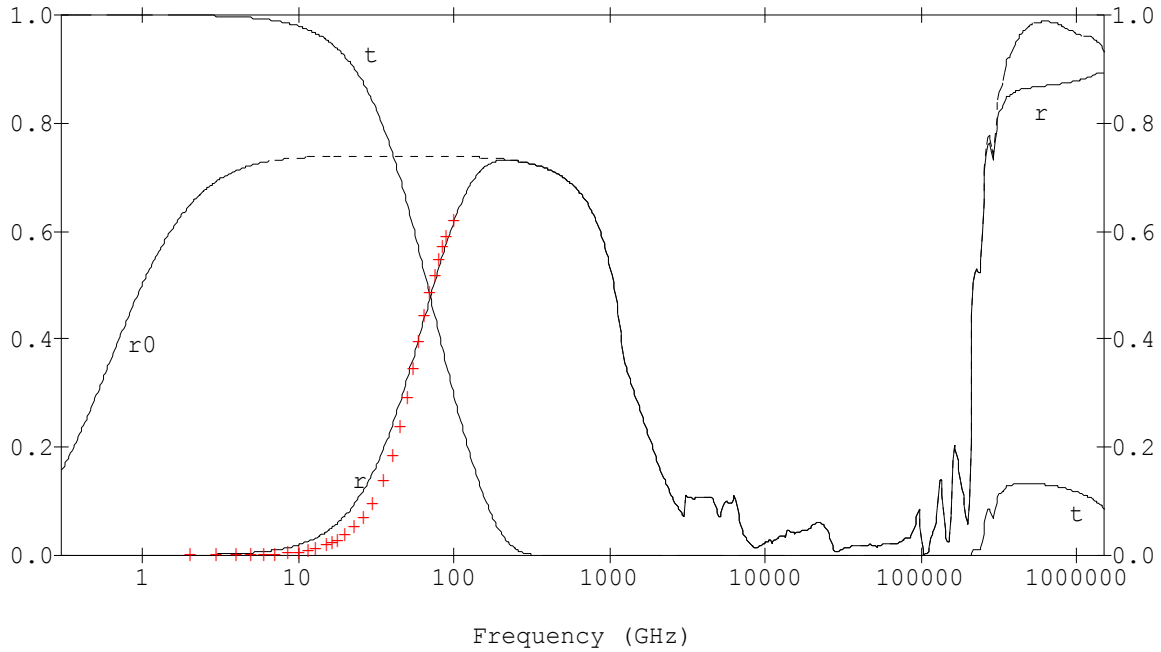

Figure 4: Radio to UV spectra of transmissivity *t* and reflectivity *r* of a thin snowpack consisting of a 10 cm deep ice-lamella pack with *d*=0.05mm, *v*=0.1. Also shown is the reflectivity r_0 of the same snow, but at infinite thickness. The data points labelled + are MEMLS results of *r* for the same snow density, thickness and temperature (266K), but with p_{MEMLS} = 0.2 mm.

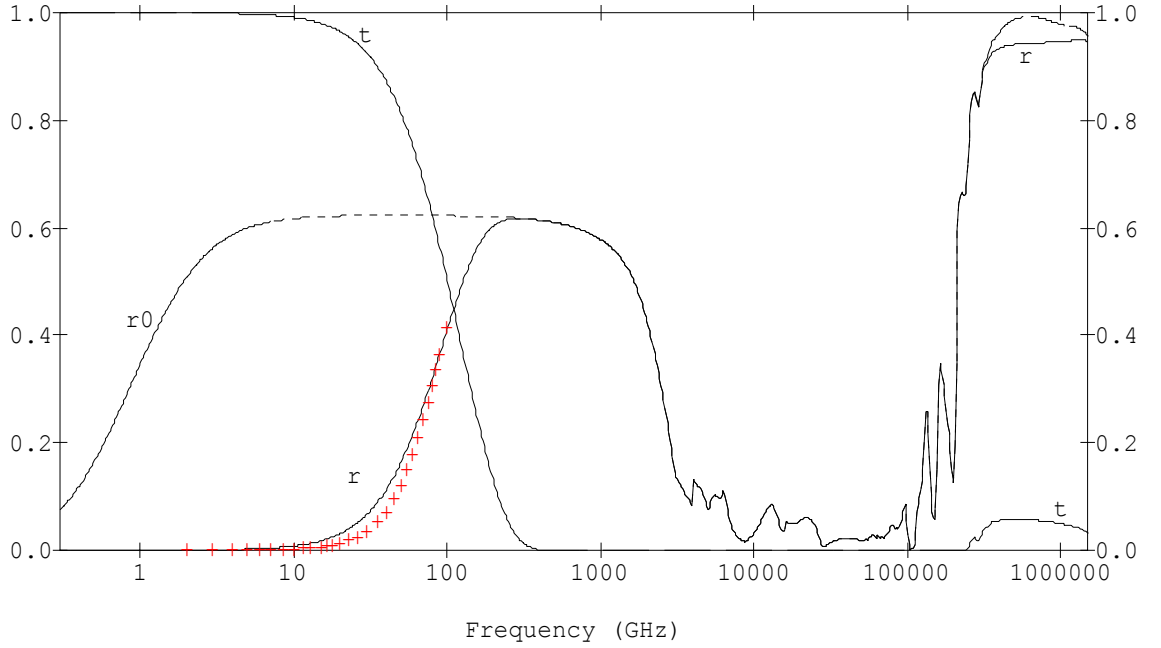

Figure 5: Radio to UV spectra of transmissivity *t* and reflectivity *r* of a thin snowpack consisting of a 10 cm deep ice-lamella pack with *d*=0.02mm, *v*=0.1. Also shown is the reflectivity r_0 of the snow at infinite thickness. The data points labelled + are MEMLS results of *r* for the same snow density, thickness and temperature (266K), but with p_{MEMLS} = 0.12mm.

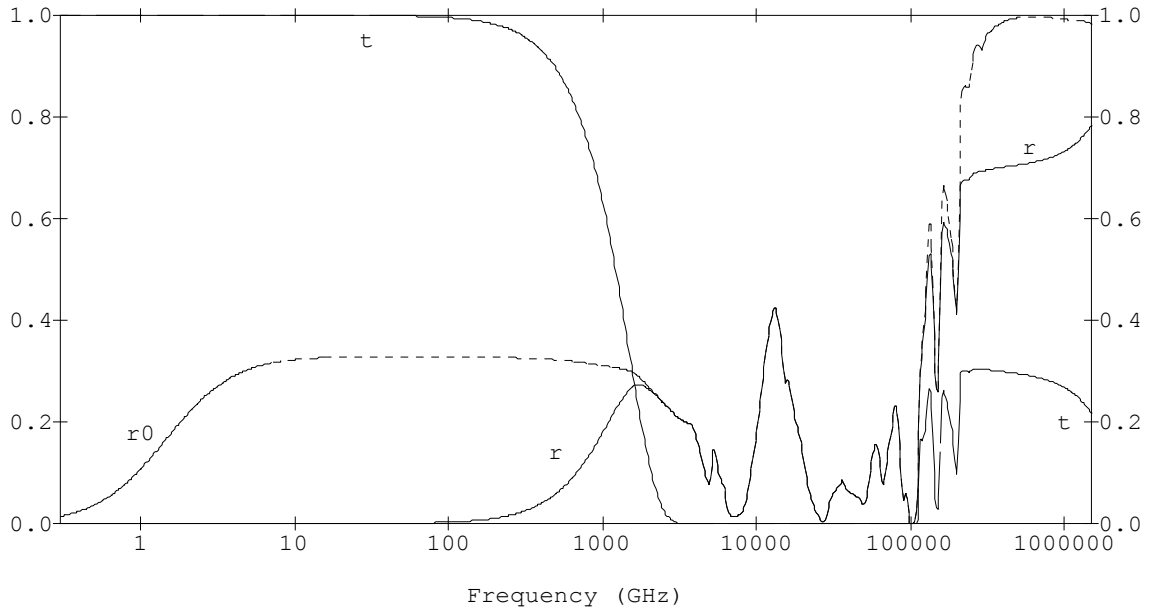

Figure 6: Radio to UV spectra of transmissivity *t* and reflectivity *r* of an ice cloud consisting of a 100 m deep ice-lamella pack with d=3μm, v=2·10^{-6}. Also shown is the reflectivity r_0 of the same cloud, but at infinite thickness. Absorption in moist air was neglected.

A comparison between the two correlation lengths d and p_{MEMLS} follows from geometrical considerations, referring to the specific surface $s=S/V$ of a granular medium where S is the total surface of particles within volume V. In the 3-dimensional case, the equation of Debye et al. (1957) applies:

$$s = 4v(1-v) / p_{MEMLS} \tag{19}$$

whereas in the one-dimensional case of Figure 1, s is given by

$$s = 2v(1-v) / d \tag{20}$$

Comparing (19) and (20) gives

$$p_{MEMLS}=2d \tag{21}$$

In view of Equation (21) the discrepancy in Figures 4 and 5 between p_{MEMLS} and d is not too severe.

For the general behaviour of the model as seen in Figures 4 to 6, the following can be noted: There is a broad maximum of the infinite reflectivity r_0 in the 10 to 1000 GHz range. This maximum decreases with decreasing d whereas the maxima increase at short wavelengths. This property is intrinsic to volume scattering when the wavelength changes from larger to smaller than the characteristic size of the scatterers. The reason why the maximum of r_0 is so flat over the 10 to 1000 GHz range is the common behaviour of γ_a and γ_s in this frequency range, both increasing with the square of frequency. The behaviour is different below 10 GHz where γ_a converges to a frequency independent value, thus leading to an increase of r_0 with frequency squared.

The transmissivity shows a high-frequency cut-off near 100 GHz for the 10 cm snowpacks and near 1000 GHz for the ice cloud. The difference is mainly due to the different water-equivalent depth decreasing from 10 mm for the snowpack to 0.2 mm for the cloud. The transition from Equation (9) to (9'), from transparent to opaque lamellae, takes place deep within the cut-off region, at frequencies above 4000 GHz, and returns to (9) again at a wavelength below 3μm (f >10^5 GHz). At the transition point the reflectivity (9') is larger than for (9), leading to visible jumps in the spectra. The transition from incoherent to coherent lamella reflections, as expressed by P=3π/4 in Equation (7), occurs in the decreasing part of r, close to 1000 GHz in Figure 4 and near 3000 GHz in Figure 5 (see the slight change in slope).

Conclusions

A simple, physical, multiple-scattering model was presented for describing the reflectance and the transmittance (Equations 9 and 10) over a very large frequency range in a volume-scattering medium,

such as snowpacks and clouds, consisting of ice and air. The one-dimensional geometry consists of a slab of freely arranged, horizontally aligned ice lamellae of a given original thickness d. Due to occasional contacts between adjacent lamellae, the average lamella thickness d_{av} is slightly larger than d. Either one of these parameters describes the structure together with the ice-volume fraction v. It was shown that the short-wave reflectance spectra up to a wavelength of 2.8μm coincide with snow spectra modelled for spherical ice grains using Mie theory for grain radii being about equal to d_{av}. Also the decrease of the reflectance with increasing grain size is the same in both types of models. A certain discrepancy between different snow reflectance models was observed (Equations 18a-d).
Concerning the microwave range there is no general agreement between the ice-lamella model and scattering in a 3-dimensional heterogeneity. Nevertheless the present one-dimensional geometry gives an approximate agreement with reflectivities computed with a snow-emission model if the correlation length p_{MEMLS} of the 3-dimensional medium is properly adjusted to d. By using the information available on the complex refractive index of ice, very broad-band spectra for snowpacks and clouds can be constructed from the formulae presented here. Due to the simplicity of the ice-lamella pack, this model could work as a reference in the development, validation and improvement of more elaborate ones.

References

Bohren C.F. and B.R. Barkstrom, "Theory of the optical properties of snow", J. Geophys. Res., Vol. 79, pp. 4527-4535 (1974).

Bohren C.F., "Multiple scattering of light and some of its observable consequences", Amer. J. Phys. Vol. 55, pp. 524-533 (1987).

Born M. and E. Wolf, "Principles of Optics", 6th Edition, Cambridge (1980).

Debye P., H.R. Anderson, and H. Brumberger, "Scattering by an inhomogeneous solid II. The correlation function and its application", J. Appl. Phys., 28, 679-683 (1957).

De Haan, J.F., P.B. Bosma and J.W. Hovenier, "The adding method for multiple scattering calculations of polarized light", Astron. Astrophys. Vol. 183, pp. 371-391 (1987).

Ishimaru, A. "Wave propagation and scattering in random media", Vol. 1 and 2, Academic Press, Orlando (1978).

Marshall S.E. "A physical parameterization of snow albedo for use in climate models", NCAR-University of Colorado, Cooperative Thesis No. 123 (NCAR/CT-123), Boulder, Colorado (1989)

Mätzler C., "Applications of the Interaction of Microwaves with the Natural Snow Cover", Remote Sensing Reviews, Vol. 2, pp. 259-392 (1987).

Mätzler C., "Autocorrelation functions of granular media with free arrangement of spheres, spherical shells or ellipsoids", J. Applied Physics, Vol. 81 (3), pp.1509-1517 (1997).

Mätzler C., "Improved Born Approximation for scattering in a granular medium", J. Appl. Phys., Vol. 83, No. 11, pp. 6111-6117 (1998a).

Mätzler C., "Microwave properties of ice and snow", in B. Schmitt et al. (eds.) "Solar System Ices", Astrophys. and Space Sci. Library, Vol. 227, Kluwer Acad. Publ., Dordrecht, pp. 241-257 (1998b).

Meador W.E. and W.R. Weaver, "Two-stream approximations to radiative transfer in planetary atmospheres: A unified description of existing methods and a new improvement", J. Atmosph. Sci. Vol. 37, pp. 630-643 (1980).

Salisbury J.W., D.M. D'Aria and A. Wald, "Measurements of thermal infrared spectral reflectance of frost, snow and ice", J. Geophys. Res. Vol. 99, pp. 24,235-24,240 (1994).

Sergeant C., E. Pougatch, M. Sudul and B. Bourdelles, "Experimental investigation of optical snow properties", Annals of Glaciology, Vol. 17, pp. 281-287 (1993).

Sergeant C., C. Leroux, E. Pougatch and F. Guirado, "Hemispherical-directional reflectance measurements of natural snow in the 0.9-1.45 μm spectral range: comparison with adding-doubling modelling", Annals of Glaciology, Vol. 26, pp. 59-63 (1998).

Wald, A. E., "Modeling thermal infrared (2-14 μm) reflectance of frost and snow", J. Geophys. Res., Vol. 99, p. 24,241-24,250 (1994).

Warren S.G., "Optical constants of ice from the ultraviolet to the microwave", Appl. Optics, Vol. 23, p. 1206-1225 (1984).

Wiesmann, A., C. Mätzler and T. Weise, "Radiometric and structural measurements of snow samples", Radio Science, Vol. 33, pp. 273-289 (1998).

Wiesmann, A. and C. Mätzler, "Documentation for MEMLS 98.1, Microwave Emission Model of Layered Snowpacks", Research Report No. 98-2, Microwave Dept., Institute of Applied Physics, University of Bern (1998), and Remote Sensing of Environment, Vol. 70, No. 3, pp. 307-316 (1999).

Wiscombe W.J. and S.G. Warren, "A model for the spectral albedo of snow, Pure snow", J. Atmos. Sci. Vol. 37, pp. 2712-2733 (1980).

13.2 Comparison of lamella pack with spherical scatterers

The following comparison of optical snow spectra is from:

C. Mätzler, "Relation between grain size and correlation length of snow", Session C04 Cryosphere: The role of microstructure and layering on the physical properties, metamorphosis, and deformation of snowpacks, AGU Fall Meeting, San Francisco, CA, Dec. 2002.

Different shapes of scatterers in Figures 1a and 1b with the same specific surface show similar reflectance and transmittance spectra, see Figures 2a and 2b.

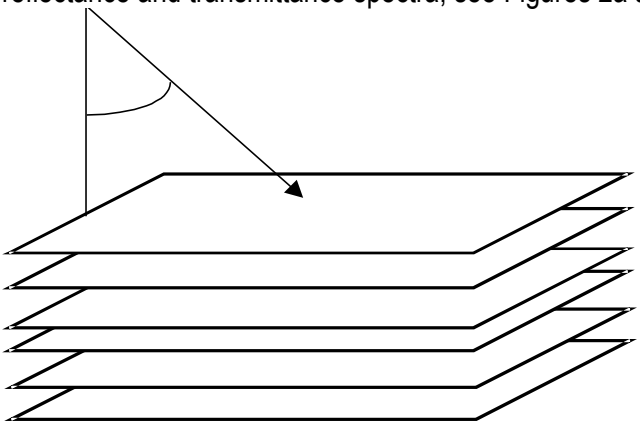

Fig. 1a: Stack of irregularly spaced ice lamellae

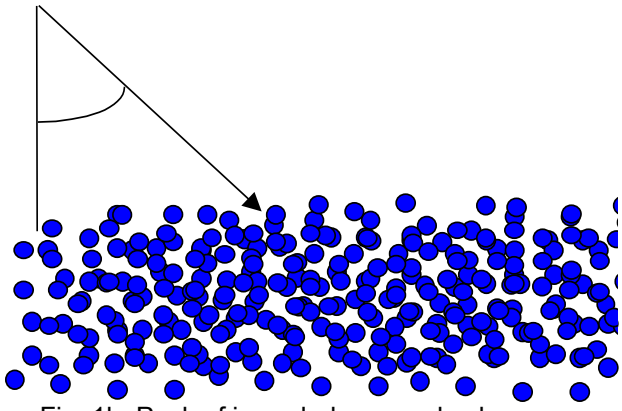

Fig. 1b: Pack of irregularly spaced spheres.

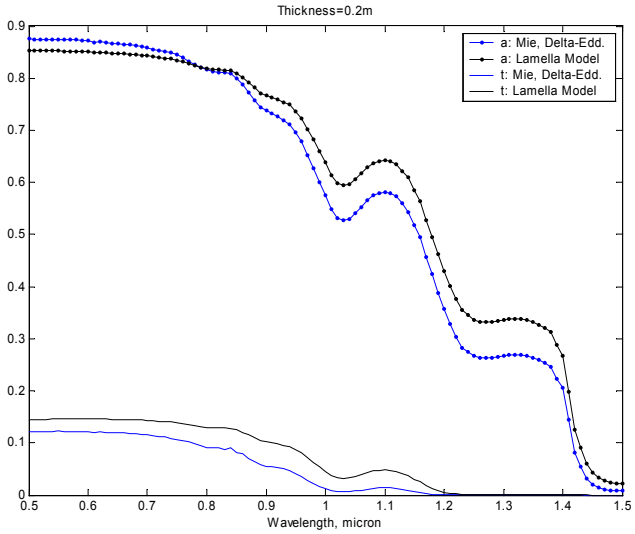

Figure 2a: Albedo (reflectivity) a and transmittance (transmissivity) t versus wavelength (μm) of a 20 cm deep snowpack, density 100kg/m^3, incidence angle 53°. Comparison of spheres (D=0.8mm) with lamella pack for lamella thickness $d=D/3$; blue: Mie-Delta-Eddington model of Wiscombe and Warren (1980), black: lamella model of Mätzler (2000).

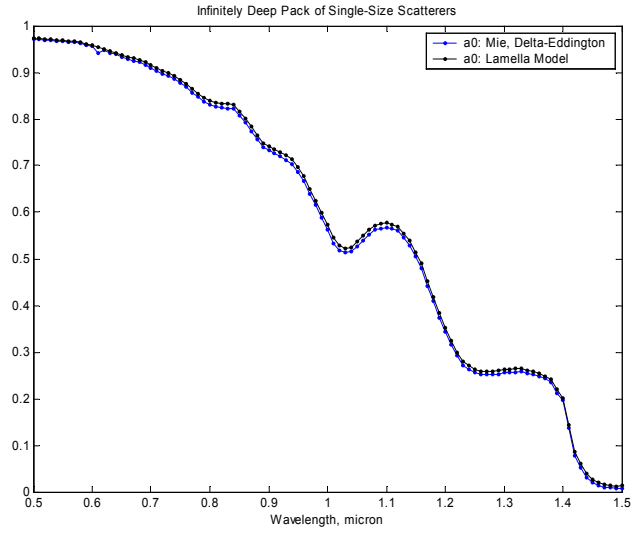

Figure 2b: As Figure 2a, but for a deep snowpack with illumination adapted to the respective geometry: vertical incidence for lamella pack, diffuse illumination for pack of spheres. The spectral albedos of the two situations agree almost perfectly.

Literature

Abreu, L. W., G. P. Anderson, "The MODTRAN 2/3 Report and Lowtran 7 Model", Technical Report, Phillips Laboratory, Geophysics Directorate, Hanscom, Massachusetts (1996), see also: http://www.ontar.com/Software/pub_ModtranFascod_Documentation.htm

Bekefi B., "Radiation Processes in Plasmas", John Wiley, New York (1966). ExWi Library: TLF 111

Bracewell, R., "The Fourier Transform and its Applications", McGraw Hill, New York (1965). ExWi Library: GQE 119

Bohren C.F. and D.R. Huffman, “Absorption and Scattering of Light by Small Particles”, John Wiley, New York, NY (1983). ExWi Library: TDD 122

Chandrasekhar S., "Radiative Transfer", Dover Publication (1960). ExWi Library: TDD 211

Clebsch A. "Über die Reflexion an einer Kugelfläche". Journal für Mathematik, Vol. 61, Heft 3, pp. 195-262 (1863).

Debye, P. "Polar Molecules", first published by Chemical Catalog Company, New York (1929), reprinted by Dover Publications, New York (1945), German Edition: "Polare Molekeln", Leipzig (1929).

Debye, P.J.W., H.R. Anderson, and H. Brumberger. 1957. "Scattering by an inhomogeneous solid II. The correlation function and its application", J. Appl. Phys., 28, 679-683.

Deirmendjian, D. “Electromagnetic Scattering on Spherical Polydispersions”, American Elsevier, New York, NY (1969). ExWi Library: TDD 124

Dicke R.H. "The measurement of thermal radiation at microwave frequencies", Rev. Sci. Instr., Vol. 17, pp. 268-275 (1946).

Dicke R H, Beringer R, Kuhl R L & Vane A B. "Atmospheric absorption measurements with a microwave radiometer", *Phys. Rev.* Vol. 70, pp. 340-348 (1946).

Eder G. "Elektrodynamik", BI Hochschultaschenbücher 233, Mannheim, (1967).

Goody R.M. and Y.L. Yung, "Atmospheric Radiation – Theoretical Basis", 2nd Ed. Oxford University Press, Oxford UK, (1989). ExWi Library: XJA 160

Ishimaru A. “Wave Propagation and Scattering in Random Media“, Vol. 1, 2, Academic Press, New York (1978), ExWi Library: TDD 186.

Hilbert D. Begründung der elementaren Strahlungstheorie, Physik. Zeitschrift, Vol. XIII, pp. 1056-1064, (1912).

van de Hulst H.C., "Scattering in a planetary atmosphere ", Astrophys. J. Vol. 107, p. 220-246 (1948).

van de Hulst H.C., "Light Scattering by Small Particles", Dover Publication (1957).

van de Hulst H.C. "Multiple Light Scattering: Tables, Formulae and Applications" Academic Press, New York (1980).

von Hippel A.R. "Dielectrics and Waves", M.I.T. Press, Cambridge Mass. (1954). ExWi Library: TEA 149

Janssen M.A. (ed.) "Atmospheric Remote Sensing by Microwave Radiometry", Wiley Series in Remote Sensing, New York (1993).

Joseph, J.H, W.J. Wiscombe and J.G. Weinman, “The Delta-Eddington Approximation for radiative flux transfer”, J. Atmosph. Sci. 33, 2452-2459 (1976).

Kirchhoff G., "Über das Verhältnis zwischen dem Emissionsvermögen und dem Absorptionsvermögen der Körper für Wärme und Licht", Poggendorfs Annalen der Physik und Chemie, Bd. 109, S. 275-301 (1860), s. auch Schöpf (1978), ExWi: CGK 120.

Kokhanovsky A.A. "Light Scattering Media Optics: Problems and Solutions", Berlin, Springer (2001): ExWi TDD 215.

Kong J.A. “Electromagnetic Wave Theory”, John Wiley, New York (1986). ExWi Library: TEA 150

Kraus J.D., "Radio Astronomy", McGraw Hill, New York (1966). ExWi Library: YMD 128

Kubelka P. and F. Munk, "Ein Beitrag zur Optik der Farbanstriche", Zeitschrift Tech. Phys. Vol. 12, 593 (1931).

H.J. Liebe, G.A. Hufford, and M.G. Cotton: Propagation Modeling of Moist Air and Suspended Water/Ice Particles at Frequencies Below 1000 GHz, AGARD 52nd Specialist Meeting of the Electromagnetic Wave Propagation Panel, Mallorca, Spain (1993).

Lorenz L. V., "Lysbevaegelsen i og uden for en af plane Lysbolger belyst Kugle" (Upon the light reflected and refracted by a transparent sphere), Kongelige Danske Vidensk. Selskabs Shrifter 6, 1-62 (1890).

Martin L., "Microwave Transmision and Emission Measurements for Tropspheric Monitoring", Inauguraldissertation, Phil.nat. Fakultät, Universität Bern, Bern, Mai (2003).

Mätzler C., "Improved Born Approximation for scattering in a granular medium", J. Appl. Phys., Vol. 83, No. 11, pp. 6111-6117 (1998).

Mätzler C. and A. Wiesmann, "Extension of the Microwave Emission Model of Layered Snowpacks to Coarse-Grained Snow", Remote Sensing of Environment, Vol. 70, No. 3, pp. 317-325 (1999).
Mätzler C., “MATLAB Functions for Mie Scattering and Absorption”, IAP Res. Rep. No. 02-08, Institute of Applied Physics, University of Bern, June (2002a).
Mätzler C., “MATLAB Functions for Mie Scattering and Absorption, Version 2”, IAP Res. Rep. No. 02-11, Institute of Applied Physics, University of Bern, August (2002b).
Mätzler C., “Mie Scattering With and Without Diffraction”, IAP Res. Rep. 2004-02, April (2004).
Mätzler C., “Drop-Size Distributions and Mie Computations for Rain”, IAP Res. Rep. No. 02-16, August (2002).
Mätzler C. and L. Martin, “Advanced Model of Extinction by Rain and Measurements at 38 and 94 GHz and in the Visible Range”, IAP Res. Rep. No. 2003-1, February (2003).
Mätzler C., "On the determination of surface emissivity from satellite observations", IEEE Geoscience and Remote Sensing Letters, Vol.2, No. 2, pp. 160-163 (2005).
Maxwell Garnett, J.C., "Colors in metal glasses and metal films", Trans. Royal Soc. (London), CCIII, pp. 385-420 (1904).
Meador W.E. and W.R. Weaver, “Two-stream approximations to radiative transfer in planetary atmospheres: A unified description of existing methods and a new improvement”, J. Atmosph. Sci. Vol. 37, pp. 630-643 (1980).
Mie G., "Beiträge zur Optik trüber Medien, speziell kolloidaler Metallösungen (Considerations on the optics of turbid media, especially colloidal metal solutions)", Ann. Phys. 25, 377-442 (1908).
Mishchenko M.I., J.W. Hovenier, and L.D. Travis (eds.), "Light scattering by non-spherical particles", Academic Press (2000), ExWi: TDD 208.
Mobley C.D., "Light and water", Academic Press (1994), ExWi: TDD 209.
Planck M., "Zur Theorie der Energieverteilung im Normalspektrum", Verhandlungen der DPG, Teil 2, S. 237-245 (1900).
Planck M. "Theorie der Wärmestrahlung (The Theory of Heat Radiation)", Lectures, 6th Edition, Stuttgart (1966), English transl. by Dover Publications.
Rosenkranz, P. W., Water vapor microwave continuum absorption: A comparison of measurements and models, Radio Science, **33**, pp. 919-928 (1998). Correction, Radio Science, **34**, p. 1025 (1999).
Schuster A., "Radiation through a foggy atmosphere", Astrophys. J., Vol. 21, p. 1-22 (1905).
Sihvola, A. "Electromagnetic mixing formulas and applications", Electromagnetic Waves Series 47, IEE, London, UK (1999).
Simmer C. "Satellitenfernerkundung hydrologischer Parameter der Atmosphäre mit Mikrowellen", Verlag Dr. Kovac, Hamburg (1994).
Sobolev V.V. "Light Scattering in Planetary Atmospheres", Transl. from Russian by W.M. Irvine, Pergamon Press New York (1975).
Thomas G.E. and K. Stamnes, "Radiative Transfer in the Atmosphere and Ocean", Cambridge University Press, Cambridge, UK, (1999), ExWi Libr. TDD 212.
Ulaby F.T., R. Moore, and A.K. Fung: "Microwave Remote Sensing, Active and Passive", Vol. I, Microwave Remote Sensing Fundamentals and Radiometry" (1981), Vol. II, Radar Remote Sensing and Surface Scattering and Emission Theory (1982); Vol. III, From Theory to Applications, Artech House Inc., Norwood, MA 02062 (1986). ExWi Libr. XKA 115, 129, 130.
Townes C.H. and A.L. Schawlow, "Microwave Spectroscopy", McGraw Hill, New York (1955), Dover (1975). ExWi Library: SFZ 128
Tsang L., J.A. Kong, and R.T. Shin, "Theory of Microwave Remote Sensing", Wiley, New York (1985). ExWi Library: XKA 136
Tsang L., J.A. Kong, and K.H. Ding, "Scattering of Electromagnetic Waves" - (Vol. 1) Theories and Applications, (Vol. 2) Numerical Simulations, (Vol. 3) Advanced Topics, Wiley, New York (2000), ExWi: OGG 201.
Warnick, K.F., "Computational Electromagnetics, Lecture Notes, Brigham Young University, Provo, UT, USA, Download from internet, March (2005).
Wiener O., "Zur Theorie der Refraktionskontanten", Ber. Verh. Königl. Sächs. Ges. Bd. 62, 256-277 (1910).
Wiesmann A., C. Mätzler and T. Weise, "Radiometric and structural measurements of snow samples", Radio Science, Vol. 33, pp. 273-289 (1998).
Wyatt, C.L. "Radiometric calibration: Theory and Methods", Academic Press, New York (1978).
Zege, E.P., A.P. Ivanov and I.L. Katsev, "Image Transfer Through a Scattering Atmosphere", Springer (1991).
Zhou, X.S., "Vector-Wave Functions in Electromagnetic Theory", Aracne Edition, Rome, Italy (1994). ExWi Library: OGF 201